

1 Identification of highly oxygenated organic molecules and their role in 2 aerosol formation in the reaction of limonene with nitrate radical

3 Yindong Guo¹, Hongru Shen¹, Iida Pullinen^{2, a}, Hao Luo^{1,3}, Sungah Kang², Luc Vereecken², Hendrik Fuchs², Mattias
4 Hallquist⁴, Ismail-Hakki Acir^{2, b}, Ralf Tillmann², Franz Rohrer², Jürgen Wildt², Astrid Kiendler-Scharr², Andreas
5 Wahner², Defeng Zhao^{1,5,6*}, Thomas F. Mentel^{2*}

6 ¹Department of Atmospheric and Oceanic Sciences & Institute of Atmospheric Sciences, Fudan University, 200438,
7 Shanghai, China

8 ²Institute of Energy and Climate Research, IEK-8: Troposphere, Forschungszentrum Jülich [GmbH](#), 52425, Jülich,
9 Germany

10 ³IRDR ICoE on Risk Interconnectivity and Governance on Weather/Climate Extremes Impact and Public Health,
11 Fudan University, Shanghai 200438, China

12 ⁴Department of Chemistry and Molecular biology, University of Gothenburg, Göteborg, 41258, Sweden

13 ⁵Shanghai Frontiers Science Center of Atmosphere-Ocean Interaction, Fudan University, Shanghai 200438, China

14 ⁶Institute of Eco-Chongming (IEC), 20 Cuiniao Rd., Chongming, Shanghai, 202162, China

15 ^a Now at: Department of Applied Physics, University of Eastern Finland, Kuopio, 70210, Finland.

16 ^b Now at: Institute of Nutrition and Food Sciences, University of Bonn, Bonn, 53115, Germany.

17 *Correspondence to:* Defeng Zhao (dfzhao@fudan.edu.cn), Thomas F. Mentel (t.mentel@fz-juelich.de)

18
19 **Abstract.** Nighttime ~~nitrate radical~~(NO₃)-initiated oxidation of biogenic volatile organic compounds (BVOC) such
20 as monoterpenes is important for the atmospheric formation and growth of secondary organic aerosol (SOA), which
21 has significant impact on climate, air quality and human health. In such SOA formation and growth ~~from the oxidation~~
22 ~~of monoterpenes by NO₃~~, highly oxygenated organic molecules (HOM) may be crucial, but their formation pathways
23 and role in aerosol formation have yet to be clarified. Among monoterpenes, limonene is of research particular interest
24 for its high emission globally and high SOA yield. In this work, HOM formation in the reaction of limonene with
25 nitrate radical (NO₃) was investigated in the SAPHIR chamber (Simulation of Atmospheric PHotochemistry In a
26 large Reaction chamber). About 280 HOM products were identified, grouped into 619 monomer series (each
27 including 3 families) and one family, 11 dimer families and 3 trimer families. Both closed-shell products and open-
28 shell peroxy radicals (RO₂•) were observed, and many of them have not been reported previously. Monomers and
29 dimers accounted for ~~over 90~~47 % and 47 % of HOM concentrations, respectively, with trimers making up the
30 remaining 6%. In the most abundant monomer series—families, C₁₀H₁₅₋₁₇NO₆₋₁₄, carbonyl products outnumbered
31 hydroxyl products, indicating the importance of ~~the unimolecular~~-RO₂• termination pathway by unimolecular
32 dissociation. Both RO₂• autoxidation and alkoxy-peroxy pathways were found to be important processes leading to
33 HOM. Time-dependent concentration profiles of monomer products containing nitrogen showed mainly second-
34 generation formation patterns. Dimers were likely formed via the accretion reaction of two monomer RO₂•, and

35 HOM-trimers via the accretion reaction between monomer RO_2^\bullet and dimer RO_2^\bullet . Trimers are suggested to play an
36 important role in new particle formation (NPF) observed in our experiment. A HOM yield of 1.5 % (~~+0.7 %~~/~~-0.7 %~~)
37 % was estimated considering only first-generation products. SOA mass growth could be reasonably explained by
38 HOM condensation on particles assuming irreversible uptake of ultra-low volatility organic compounds (ULVOC),
39 extremely low volatility organic compounds (ELVOC) and low volatility organic compounds (LVOC). This work
40 provides evidence for the important role of HOM formed via the limonene + NO_3 reaction in NPF and SOA-growth
41 of SOA particles.

42

43 1 Introduction

44 The nitrate radical (NO_3) is an important nighttime oxidant in tropospheric chemistry, and can reach mixing ratios of
45 several hundred pptv during nighttime (Seinfeld and Pandis, 2006). It can react with volatile organic compounds
46 (VOC) and is especially reactive to alkenes, where ~~at the~~ nitrate ~~group~~radical can ~~be added~~undergo an addition reaction
47 to ~~the~~ C=C double bond ~~through addition reaction~~ (Finlayson-Pitts and Pitts, 1997; Seinfeld and Pandis, 2006).
48 Biogenic ~~monoterpenes~~monoterpenes ($\text{C}_{10}\text{H}_{16}$) ~~is~~are a large ~~source of~~contribution to the alkenes in the atmosphere
49 (Klinger et al., 2002; Guenther et al., 2012), and ~~it's~~their major nighttime loss pathway is ~~reacting~~reaction with NO_3
50 (Beaver et al., 2012; Rollins et al., 2012; Ayres et al., 2015; Fry et al., 2013). The chemistry of monoterpenes with
51 NO_3 has implications on the cycle of reactive nitrogen and thus on ozone formation (Brown and Stutz, 2012).
52 Furthermore, since the NO_3 radical is formed through the reaction of NO_2 with O_3 , it is considered to be of
53 anthropogenic origin, and reactions of NO_3 with biogenic VOC (BVOC) thus represent ~~a typical~~an important
54 interaction between biogenic emissions and anthropogenic emissions.

55 The reaction of NO_3 with monoterpenes can ~~also~~ form secondary organic aerosols (SOA), which can have a
56 large impact on global climate, air quality and human health (Hallquist et al., 2009; Shrivastava et al., 2017).
57 Laboratory studies showed that monoterpenes have high SOA yields in the reaction with NO_3 due to the low volatility
58 of oxidation products (Ng et al., 2008; Rollins et al., 2009; Fry et al., 2013; Fry et al., 2014; Ayres et al., 2015; Jokinen
59 et al., 2015; Zhou et al., 2015; Boyd et al., 2015; Nah et al., 2016; Boyd et al., 2017; Slade et al., 2017; Claffin and
60 Ziemann, 2018; Bates et al., 2022; Dam et al., 2022). Field studies also showed that nighttime NO_3 -initiated oxidation
61 of monoterpenes contributes significantly to SOA in forested regions influenced by anthropogenic emissions (Pye et
62 al., 2010; Rollins et al., 2012; Fry et al., 2013; Ayres et al., 2015; Zhou et al., 2015; Xu et al., 2015; Lee et al., 2016;
63 Zhang et al., 2018; Chen et al., 2020) and potentially in urban areas due to the extensive usage of so-called volatile
64 chemical products (VCP) (Nazaroff and Weschler, 2004; McDonald et al., 2018). For example, the Southern Oxidant
65 and Aerosol Study (SOAS) showed that the BVOC + NO_3 reactions were a substantial source of SOA (Ayres et al.,
66 2015; Xu et al., 2015; Lee et al., 2016; Massoli et al., 2018). Therefore, accurate predictions and evaluations of SOA
67 concentration and thus its climate and environmental effects require a comprehensive understanding of the reactions
68 of monoterpenes with NO_3 .

69 Recently, a class of organic compounds named highly oxygenated-organic molecules (HOM) have been shown

70 to be critical substances in the SOA formation from BVOC oxidation, particularly monoterpenes, featuring high
71 ~~oxidation degree, high~~ O/C ratio and low to extremely low volatility (Ehn et al., 2014; Tröstl et al., 2016; Kirkby et
72 al., 2016; Bianchi et al., 2019). HOM here refers to ~~organic~~ compounds ~~which are~~ formed in the gas phase via
73 ~~autoxidation and which~~ contain at least six oxygen atoms (Bianchi et al., 2019). ~~Donahue et al. (2012) divided~~ Most
74 HOM are classified as ULVOC/ELVOC or LVOC (Bianchi et al., 2019) according to the classification of
75 atmospheric organics ~~into five categories~~ based on their volatility (saturation concentration, C^*) by Donahue et al.
76 (2012)⁸ ~~:-~~ (extremely low volatility organic compounds (ELVOC), low volatility organic compounds (LVOC), semi-
77 volatile organic compounds (SVOC), intermediate volatility organic compounds (IVOC) ~~and~~), volatile organic
78 compounds (VOC). ~~Most HOM are classified as ELVOC or LVOC (Bianchi et al., 2019),~~ and a recent update by
79 Schervish and Donahue (2020) (ultra-low volatility organic compounds (ULVOC)). And thus, HOM can be a
80 ~~substantial source for SOA contribution to growth of SOA particles through gas-particle partitioning.~~

81 ~~The clarification~~ A better description of the HOM -formation chemistry in ~~limonene +~~ the oxidation of
82 monoterpenes by NO_3 ~~system~~ will improve ~~the our~~ understanding of the role of HOM ~~for in~~ SOA formation, as well
83 as the relationship between oxidation products, SOA formation and reaction systems. Field ~~observations~~
84 ~~and observation campaigns as well as laboratory simulation~~ experiments have proven the important contribution of
85 HOM in monoterpene + NO_3 SOA (Lee et al., 2016; Faxon et al., 2018). In the SOAS campaign, HOM-ONs (organic
86 nitrates) were identified in both gas and particle phase, ~~including~~ using a NO_3^- -Chemical Ionization time-of-flight
87 Mass Spectrometer (CI-APi-TOF) and a High Resolution Time-of-Flight Chemical Ionization Mass Spectrometer
88 (HR-ToF-CIMS) coupled to a Filter Inlet for Gases and AEROsols (FIGAERO). ~~Species with the sum formula~~
89 $\text{C}_{10}\text{H}_{15,17,19}\text{NO}_{4-11}$ ~~were observed~~ which are formed through the oxidation of monoterpenes by NO_3 (Lee et al., 2016;
90 Massoli et al., 2018). In a campaign in a boreal forest in Hyytiälä, measurement using a NO_3^- -CI-APi-TOF and
91 positive matrix factor (PMF) analysis showed a nighttime factor of HOM-ON formed via NO_3 oxidation of
92 monoterpenes (Yan et al., 2016). Besides the observations at forested regions, monoterpene-derived HOM via NO_3
93 oxidation also contribute to organic aerosols in urban regions. For example, Liu et al. (2021) and Nie et al. (2022)
94 have found that HOM derived from monoterpene nighttime chemistry are important in megacities in China, especially
95 during summertime. A number of laboratory studies have reported HOM formation by the oxidation of monoterpenes
96 with NO_3 . Boyd et al. (2015) observed $\text{C}_{10}\text{H}_{17}\text{NO}_{4/5}$ and $\text{C}_{10}\text{H}_{15}\text{NO}_{5/6}$ in the gas phase in β -pinene + NO_3 experiments
97 ~~and using~~ a quadrupole chemical ionization mass spectrometer with I^- as the reagent ion (I^- -CIMS). They proposed
98 possible formation schemes of these ONs. Nah et al. (2016) further detected 5 and 41 HOM-ONs in the NO_3 oxidation
99 of α -pinene and β -pinene, respectively, such as $\text{C}_{10}\text{H}_{15/17/19}\text{NO}_{4-9}$ in the gas- and particle-phase, using I^- -FIGAERO
100 HR-ToF-CIMS. Claffin and Ziemann (2018) provided formation mechanisms for HOM-ONs via gas-phase and
101 particle-phase reactions in the β -pinene + NO_3 ~~experiment~~-reaction system, where particle-phase products were
102 analyzed using reversed-phase high-performance liquid chromatography equipped with a UV-vis photodiode array
103 detector (HPLC-UV), Electron-Ionization Thermal Desorption Particle Beam Mass Spectrometer (EI-TDPBMS),
104 Chemical Ionization Finnigan PolarisQ Ion Trap Mass Spectrometer (CI-ITMS), and Electrospray-Ionization Mass

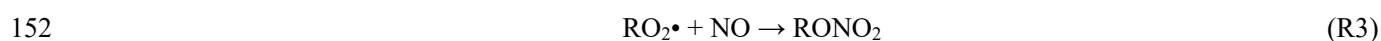
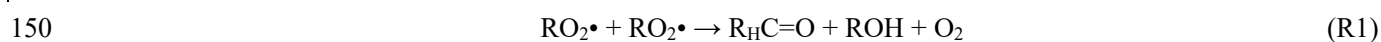
105 Spectrometer (ESI-MS). Recently, Shen et al. (2021) found a large number of HOM (>150 species) in the β -pinene
106 + NO_3 reaction; using NO_3^- -CI-API-TOF. HOM formed in the reaction of four monoterpenes (α -pinene, β -pinene,
107 Δ -3-carene, and α -thujene) with NO_3 were also detected using NO_3^- -CI-API-TOF by Dam et al. (2022). Bell et al.
108 (2021) found that dimer dinitrates ($\text{C}_{20}\text{H}_{32}\text{N}_2\text{O}_{8-13}$) contribute a large portion of SOA from α -pinene + NO_3 and also
109 detected monomer ON such as $\text{C}_{10}\text{H}_{15}\text{NO}_{5-10}$ and $\text{C}_{10}\text{H}_{14,16}\text{N}_2\text{O}_{7-11}$), although using FIGAERO-CIMS and an
110 Extractive ElectroSpray Ionization time-of-flight mass spectrometer (EESI-ToF-MS). The detailed speciation
111 depends on analytical method to some extent. And, though. Moreover, the HOM composition in the particle-phase
112 was found to depend on aging time and reaction conditions such as dark versus light (Bell et al., 2021; Wu et al.,
113 2021a).

114 Among ~~all species of~~ the monoterpenes, understanding the reaction system of limonene with NO_3 is of special
115 importance. The emission of limonene makes the 4th largest contribution with an estimated global emission of 11.4
116 Tg annually, preceded only by α -pinene, ~~trans~~- β -ocimene and β -pinene (Guenther et al., 2012). Besides its biogenic
117 origin, limonene is also a common additive in cleaning products (Nazaroff and Weschler, 2004) and can even be used
118 as a tracer for fragrances in some places (Gkatzelis et al., 2021). Several studies have shown adverse health effects
119 due to indoor pollution caused by the ozonolysis of limonene (Clausen et al., 2001; Fan et al., 2003; Carslaw et al.,
120 2012; Pagonis et al., 2019). Moreover, limonene stands out with its high reactivity towards the NO_3 radical (with a
121 lifetime of 3 min at 298 K at 20 pptv NO_3) (Ziemann and Atkinson, 2012), and NO_3 oxidation of limonene has high
122 SOA yield (SOA mass yield 15 to 231 %) (Hallquist et al., 1999; Spittler et al., 2006; Fry et al., 2011; Fry et al., 2014;
123 Boyd et al., 2017; Berkemeier et al., 2020; Mutzel et al., 2021). A number of earlier studies have provided valuable
124 insights into the reaction of limonene with NO_3 regarding its ~~SOA yield~~, main products and their formation pathways
125 ~~as well as~~, the SOA yield, and the SOA physicochemical properties ~~of SOA (Peng et al., 2018)~~. For example,
126 Hallquist et al. (1999) measured the SOA mass yield and revealed the dominance of organic nitrates (ON) and
127 carbonyl compounds in the products. Fry et al. (2011) determined the organic nitrate yield and proposed a reaction
128 scheme leading to the formation of organic nitrates ON and carbonyls, and Fry et al. (2014) compared the SOA and
129 ON yields from the NO_3 oxidation of α -pinene, β -pinene, and limonene, and demonstrated why limonene + NO_3
130 leads to more SOA and ON than α -pinene from a structural perspective. Boyd et al. (2017) found a higher N:C ratio
131 ~~for~~ limonene + NO_3 SOA than for β -pinene + NO_3 SOA. Finally, Peng et al. (2018) studied the optical properties
132 of the limonene + NO_3 SOA.

133 Regarding the HOM formation in the reaction of limonene with NO_3 , Faxon et al. (2018) reported a series of
134 HOM in the particle phase, including C_{7-10} monomers with 3-11 oxygen atoms and C_{11-20} dimers with 5-19 oxygen
135 atoms; using I-FIGAERO HR-ToF-CIMS. However, identification of gas-phase HOM products in the limonene +
136 NO_3 reaction is still lacking and their formation mechanisms remain unclear. Theoretical investigations have revealed
137 that NO_3 addition on the endocyclic C=C double bond is more favorable than the exocyclic one due to a lower energy
138 barrier (Jiang et al., 2009). Typically, in the limonene + NO_3 reaction, the, and this endocyclic double bond of
139 limonene thus tends to be attacked by NO_3 and leads to products including hydroxy-substituted ON or diketone

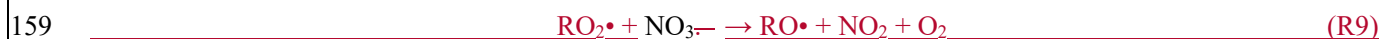
140 products. The remaining exocyclic double bond can also be attacked by NO₃ in secondary chemistry, leading to more
141 functionalized products (Fry et al., 2011)).

142 The formation of HOM via autoxidation involves a sequence of multiple intramolecular H-shift and O₂ addition
143 reactions, and results in highly oxygenated peroxy radicals (HOM-RO₂•) (Ehn et al., 2014)). ~~Analogous to “traditional”~~
144 ~~RO₂•. These~~ HOM-RO₂• can ~~be involved in similar reactions~~ react similarly to traditional RO₂• (Bianchi et al.,
145 2019)). The bimolecular reactions of HOM-RO₂• with RO₂•, HO₂• and NO lead to highly oxidized closed shell
146 products including carbonyls, hydroperoxides, alcohols, or organic nitrates as termination groups, (R1 to R3), or form
147 accretion products, ~~as shown in R1 to~~ (R4) (Ehn et al., 2014; Mentel et al., 2015). Unimolecular termination
148 reactions of HOM-RO₂• lead to carbonyls or epoxides (R5 to R6) (Crouse et al., 2013). On the other hand, reactions
149 of HOM-RO₂• with NO, RO₂•, NO₃ at nighttime can lead to alkoxy radicals as chain propagating steps (R7 to R9):



154 ~~Unimolecular termination reactions of HOM-RO₂• lead to carbonyls or epoxides (→ R=O + OH (R5)~~

155 ~~In addition, HOM-RO₂• can also be converted to alkoxy radicals (HOM-RO•) through reactions with NO, other →~~
156 ~~epoxide + OH~~ (R6)



160 If ~~these~~ the reactive HOM-RO• products undergo an H-migration reaction, they will again form HOM-RO₂ radicals
161 (“alkoxy-peroxy” pathway) (Mentel et al., 2015)), continuing the autoxidation chain. Finally, the HOM-RO• may
162 also fragment leading to small RO₂ radicals, isomerize leading to carbonyls (Bianchi et al., 2019) or react with O₂ to
163 form carbonyls (Ziemann and Atkinson, 2012).

164 In this study, HOM formation in the NO₃ oxidation of limonene was investigated. We report the identification
165 of gas-phase HOM products, including monomers, dimers and trimers. The formation pathways of dominant products
166 in each category are proposed based on their time profiles in response ~~of~~ multiple additions of limonene in the
167 experiment and on the information in literature. Based on this analysis, we estimated HOM yields and discuss the
168 role of HOM in nucleation and ~~SOA~~ growth of SOA particles.

169

170 2 Experimental and Methods

171 2.1 Experimental setup

172 The limonene + NO₃ experiment was performed in the atmospheric simulation chamber SAPHIR (Simulation of
173 Atmospheric PHotochemistry In a large Reaction chamber) at the Forschungszentrum Jülich, Germany. SAPHIR is
174 a 270 m³ double-wall cylindrical Teflon chamber with a surface-to-volume ratio of ~1 m² m⁻³. Details of SAPHIR

175 have been described before (Rohrer et al., 2005; Zhao et al., 2015a; Zhao et al., 2015b; Zhao et al., 2018). and are
176 only summarized here. Detailed experimental procedures can be found in Fig. 1a. Before each experiment, SAPHIR
177 was flushed for about 4 h at a flow rate of 370 m³ h⁻¹ with high-purity synthetic air (purity >99.9999 % O₂ and N₂)
178 in order to clean the chamber. To simulate nighttime conditions for the NO₃ chemistry the chamber roof remained
179 closed throughout the experiment. The experiment was performed under dry conditions (RH <2 %) at a temperature
180 of 302 ± 3 K. No seed aerosols were used in the experiments. A fan was used for active mixing in the chamber,
181 leading to a typical mixing time of ~1 min (Fuchs et al., 2013).

182 NO₃ radicals were generated via the reaction of ozone with nitrogen dioxide:



187 Therefore, O₃ and NO₂ were first added to the chamber to form N₂O₅ and NO₃ with mixing ratios of ~2 ppbv
188 and ~0.15 ppbv, respectively. About 20 min later, 65 ppbv of limonene was added to start the organic chemistry. Five
189 more additions of limonene followed, with added concentrations of about 4 ppbv, 4 ppbv, 3 ppbv, 3 ppbv, 2 ppbv, 2
190 ppbv, and finally 108 ppbv (Fig. 1a), which divided the experiment into six periods (P1 to P6) (Fig. 1a). For period
191 P3 and P5, NO₂ and O₃ were also added to compensate for the loss of NO₃ and N₂O₅ (Fig. 1a). The concentrations of
192 NO₂ and O₃ were maintained around 20 to 70 ppbv throughout the experiment, ensuring at the major loss of limonene
193 was by reaction with NO₃ rather than with O₃ (Fig. S1 in the SI). In the first ten min of reaction (named period P1a
194 hereafter, Fig. 1a), NO₃ accounted for 86 % of the chemical loss of limonene.

195 2.2 Instrumentation

196 Gas-phase HOM were detected by a Chemical Ionization time-of-flight Mass Spectrometer (CI-API-TOF, Aerodyne
197 Research Inc., USA) with a resolution (m/z)/($\Delta m/z$) of ~3800 using ¹⁵NO₃⁻ as the reagent ion, which is capable of
198 detecting organic molecules with high oxygen content (Eisele and Tanner, 1993; Jokinen et al., 2012). The mass
199 spectra were analyzed using the software Tofware (Tofwerk/Aerodyne) in Igor Pro (WaveMetrics, Inc.). Peak
200 identification was conducted by a high-resolution analysis. (examples shown in Fig. S2). We observed several peaks
201 which were obviously products from the isoprene + NO₃ reaction, such as C₅H₁₀N₂O₈·¹⁵NO₃⁻ at m/z 289. Such peaks
202 were present before the limonene oxidation reaction started, suggesting that these compounds preexisted in the
203 chamber. They These isoprene oxidation products were likely released from the chamber wall as residue species
204 formed in an isoprene + NO₃ experiment performed two days before (Zhao et al., 2021) and released slowly
205 from chamber walls due to their semi-volatile character. Their total concentration is less than 1 ppt. All the isoprene-
206 HOM observed (C₅H₉NO_{7,10}, C₅H₈N₂O₈₋₁₀, C₅H₁₀N₂O₈, C₅H₉N₃O_{9,10}) are saturated and do not contain C=C double
207 bond. The isoprene-HOM will not influence the reaction of limonene with NO₃ in this study. Therefore, they are not
208 discussed as products from the limonene oxidation in our experiment. (However, we cannot exclude that they were
209 partly generated from fragmentation in the limonene + NO₃ reaction.)

210 A set of instruments were used to measure other gas-phase species, including VOC, NO_x, O₃, NO₃ and N₂O₅
 211 (Shen et al., 2021). Concentrations of NO₃ and N₂O₅ were measured in-situ using a home-built diode laser-based,
 212 cavity ring-down spectrometer similar to the instrument described in the work by Wagner et al. (2011). The
 213 concentrations of limonene were measured using a Proton Transfer Reaction Time-of-Flight Mass Spectrometer
 214 (PTR-TOF-MS, Ionicon Analytik, Austria). The SOA number concentration, surface concentration and size
 215 distribution were detected by an SMPS (TSI DMA3081/TSI ~~CPC3785~~),CPC3786) and a CPC (TSI 3785).
 216 Temperature and relative humidity were continuously monitored throughout the experiment.

217 2.3 Determination of HOM concentration and “primary” HOM yield

218 HOM concentrations were obtained from the normalized signals to the total signals of the mass spectra (nc,
 219 normalized counts) by applying a calibration coefficient (C) of 2.5×10^{10} molecule cm⁻³ nc⁻¹. C was determined using
 220 H₂SO₄ as the charging efficiency of HOM and H₂SO₄ are considered to be equal (Ehn et al., 2014; Pullinen et al.,
 221 2020; Shen et al., 2021). The details of determination of the calibration coefficient are shown in the supplement S1.
 222 A mass-independent transmission efficiency was used according to our previous study, which causes an additional
 223 uncertainty of 14 % (Pullinen et al., 2020). In this previous study, the transmission efficiency curve of nitrate CI-API-
 224 TOF was determined and found to monotonously decrease with increasing mass of ions but only slightly depend on
 225 the mass range (14 % change). As we used the same setting as our previous study, we have included the slight
 226 dependence of transmission on m/z in the uncertainties. The concentrations of HOM were corrected for chamber wall
 227 losses, which were determined for a number of HOM similar to our previous study (Zhao et al., 2018)The
 228 concentrations of HOM were corrected for a chamber wall loss, with details described in the supplement. When the
 229 chamber is actively mixed, the wall loss was determined to be $(2.2 \pm 0.2) \times 10^{-3}$ s⁻¹. As the HOM yield was determined
 230 during the first 3 min of the experiment, we considered the wall loss rate to be constant (62.2×10^{-43} s⁻¹) during this
 231 period. Sensitivity analysis ~~proved~~showed that the HOM yield in this study is not very sensitive to the wall loss rate
 232 and is changing by only +0.2488 % and -0.1244 % if the wall loss rate is varied by +100 % or -50 %.

233 The HOM yield was calculated as:

$$234 \quad Y = \frac{[HOM]}{[VOC]_r} = \frac{I(HOM) \cdot C}{[N_2O_5]_r} \quad (\text{Eq. 1})$$

$$235 \quad Y = \frac{[HOM]}{[VOC]_r} = \frac{I(HOM) \cdot C}{[N_2O_5]_r} \quad (\text{Eq. 1})$$

236 where ~~[HOM]~~[HOM] is the concentration of HOM, $I(HOM)$ is the total signal intensity of HOM, C is the
 237 calibration factor, and ~~[VOC]~~[VOC]_r and ~~[N₂O₅]~~[N₂O₅]_r stand for the concentrations of limonene and N₂O₅
 238 reacted, respectively. We used the reacted concentration of N₂O₅ rather than the measured reacted limonene
 239 concentration as a large fraction of limonene was already reacting away during the VOC injection before it was
 240 homogeneously mixed in the chamber. During this part of the experiment, the high limonene concentration resulted
 241 in a rapid loss of NO₃, such that every NO₃ formed from the decomposition of N₂O₅ reacted with limonene:



244 The initial NO₃ concentration before the limonene injection was small compared to the time-integrated loss of N₂O₅,
 245 and other NO₃ loss processes were negligible right after the limonene injection, so that the observed decrease in the
 246 N₂O₅ concentration equals indeed the consumption of limonene. The wall loss rate constant of N₂O₅ in the SAPHIR
 247 chamber is 7.2×10⁻⁵ s⁻¹ (Fry et al., 2009). As the HOM yield determination is based on the first 3 min, the wall loss
 248 of N₂O₅ can be ignored compared to the loss via the reaction of NO₃ with limonene.

249 The uncertainty of the HOM yield was estimated to be -55 %/ +117 % based on the combined uncertainties of
 250 the HOM-ON peak intensities (~10 %), the limonene concentration (~15 %), the transmission efficiency (-0 %/+14 %)
 251 and the calibration factor (-52 %/ +101 %) using error propagation (Zhao et al., 2021). The first 3 min after the
 252 injection of limonene were used to calculate the HOM yield, when most of the first-generation oxidation products
 253 were produced and negligible particles were yet formed. The HOM yield thus reflects the “primary” HOM yield.

254 2.4 Determination of HOM condensation on SOA

255 The SOA mass from the condensation of HOM was calculated to evaluate the role of HOM for the SOA mass growth.
 256 Detailed estimation methods are described in the supplement, including the determination of particle wall loss and
 257 dilution loss rate (Sect. S2). In brief, the growth rate of SOA through HOM vapor condensation is based on the
 258 collision rate of vapor molecules with aerosols in the kinetic regime. The Fuchs-Sutugin approach is applied to
 259 describe the correction for transition from the kinetic to the diffusion regime (Fuchs and Sutugin, 1971; Ehn et al.,
 260 2014). Based on the volatility of HOM, we considered two scenarios for HOM condensation. In Scenario 1, all HOM
 261 were assumed to irreversibly condense on the surface of particles leading to particle mass growth. In Scenario 2, only
 262 the irreversible uptake of LVOC and ULVOC/ELVOC compounds were considered to contribute to the SOA growth
 263 of SOA particles in order to examine the role of LVOC and ELVOC while IVOC and SVOC were not included. The
 264 classification of ELVOC, LVOC, IVOC and SVOC was based on the work by-, although they may also contribute
 265 to SOA. The calculation of saturation concentration C^* (in µg/m³) of each HOM was done based on their
 266 molecular compositions using two different parameterizations considering the uncertainties in estimating volatility
 267 (Wu et al., 2021b):

- 268 1. an updated version of the parameterization of Donahue et al. (2011) by Mohr et al. (2019)
 269 (Scenario 2a):

$$270 \log_{10}(C^*) = (25 - n_C) \log_{10}(C) = (25 - n_C) \times 0.475 - (n_O - 3n_N) \times 0.2 - 2 \frac{(n_O - 3n_N)n_C}{(n_C + n_O - 3n_N)} \times 0.9 - n_N \times 2.5$$

271 (Eq. 2)

272 where n_C , n_O , n_N and n_H are the number of carbon, oxygen, nitrogen and hydrogen atoms of the compound,
 273 respectively.

- 274 2. a parameterization based on HOM from α -pinene ozonolysis by Peräkylä et al. (2020) (Scenario 2b):

$$275 \log_{10}(C^*) = n_C \log_{10}(C) = n_C \times 0.18 - n_H \times 0.14 - n_O \times 0.38 + n_N \times 0.80 + 3.1 \quad (\text{Eq. 3})$$

276 where n_C , n_O , n_N and n_H are the number of carbon, oxygen, nitrogen and hydrogen atoms of the compound,
 277 respectively.

278 [with similar parameter notation.](#)

279 **2.5 Simulations of the RO₂• loss pathway based on the Master Chemical Mechanism (MCM)**

280 The RO₂• loss pathways were estimated based on MCM simulations (<http://mcm.york.ac.uk/>). The gas-phase
281 reactions of limonene + NO₃ under dark condition were simulated using iChamber, an open-source program
282 (<https://sites.google.com/view/wangsiyuan/models?authuser=0>
283 ~~(<https://sites.google.com/view/wangsiyuan/models?authuser=0>)~~) (Wang and Pratt, 2017). The default chemistry of limonene + NO₃ in the MCM was applied in this study
284 (Saunders et al., 2003b). Photolysis reactions were excluded by setting the zenith angle to 90°. Concentrations of O₃,
285 NO₃, NO₂ and N₂O₅ as well as temperature and relative humidity were constrained to the experimental data with a
286 time resolution of 1 min. The chamber dilution rate of 1.5×10⁻⁵ s⁻¹ was applied to all species. The P1 period was
287 simulated using the above conditions and the initial concentrations of limonene were added in the model according
288 to the experimental procedures. The sum of all 140 RO₂• in the limonene subset of MCM v3.3.1 were used in the
289 usual way to estimate the loss rates of RO₂• bimolecular reactions. The reaction rate constants are provided in Table
290 S3, and calculated loss rates are shown in Fig. S3. [We note that the MCM reaction schemes do not include the](#)
291 [accretion reactions between HOM-RO₂•.](#) Berndt et al. (2018a) [determined the rate constant of accretion reaction of](#)
292 [C₁₀H₁₅O₄• formed via α-pinene ozonolysis to be ~1×10⁻¹¹ cm³ molecule⁻¹ s⁻¹, which is of the same order as the upper](#)
293 [limit for RO₂• + RO₂• reactions used in the MCM schemes for functionalized peroxy radicals such as acyl peroxy](#)
294 [radicals](#) (Jenkin et al., 1997; Saunders et al., 2003a) [S2](#). [However, currently we do not see a reliable updated set of](#)
295 [rate coefficients that are applicable to the reaction system in this study. If the rate constants of some RO₂• + RO₂•](#)
296 [reactions were higher than those used in MCM, the concentrations of RO₂• would be lower and relative importance](#)
297 [of RO₂• + RO₂• in RO₂• fate would increase. Several simulation results are shown in Fig. S4, including NO₃, N₂O₅,](#)
298 [limonene, RO₂•, reaction rate of limonene with NO₃ \(k×limonene×NO₃\), and examples of 1st and 2nd-generation RO₂•.](#)

299 In the early stage of each period, RO₂• mainly reacted with RO₂• and NO₃, although in the later stage the reaction
300 with NO₂ also contributed to a significant fraction of RO₂• loss (Fig. S2S3, showing period P1 as an example). During
301 the period P1a when our peak assignment was based on, the RO₂• loss was dominated by RO₂• + RO₂• and RO₂• +
302 NO₃.

303

304 **3 Results and discussion**

305 **3.1 Experiment overview and observed HOM**

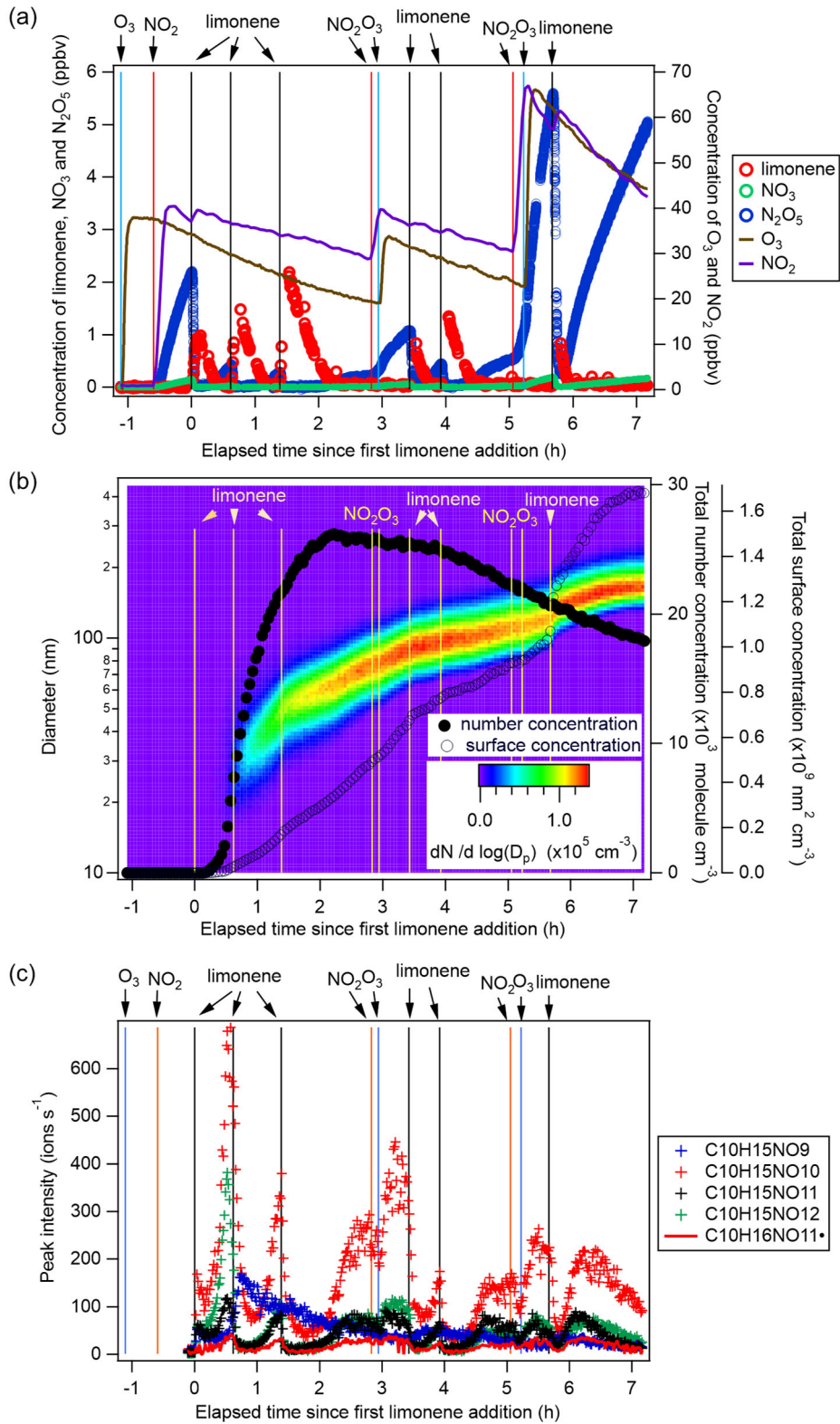
306 After each limonene addition, the concentration of limonene rose first and then rapidly declined, while the
307 concentrations of NO₃ and N₂O₅ rapidly decreased due to the fast reaction between limonene and NO₃ and gradually
308 increased when limonene had been consumed (Fig. 1a). About 10 min after the first limonene addition, new particles
309 [were had already](#) formed and quickly grew in size (Fig. 1b). Therefore, we used the first 10 min reaction time (period
310 P1a) to identify gas-phase HOM products, and the whole experiment to examine the contribution of HOM to SOA.

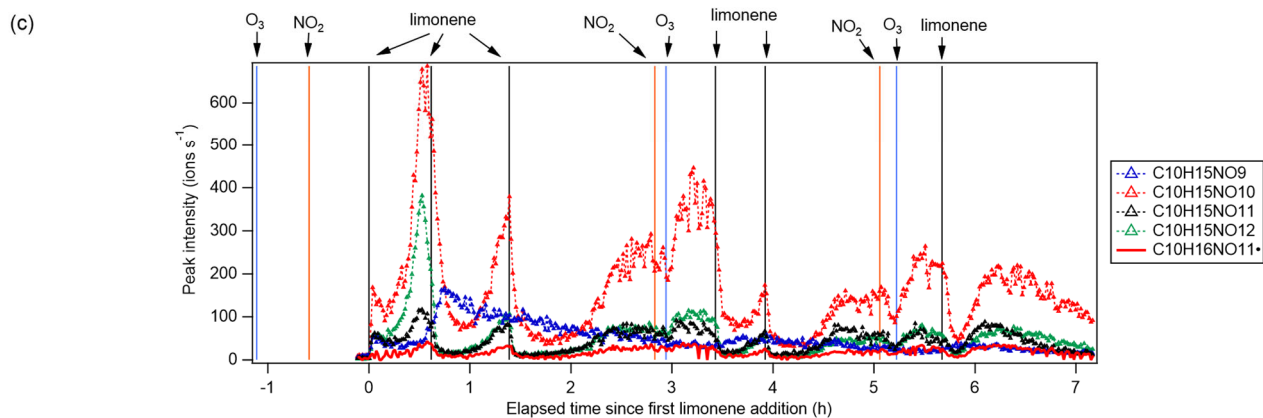
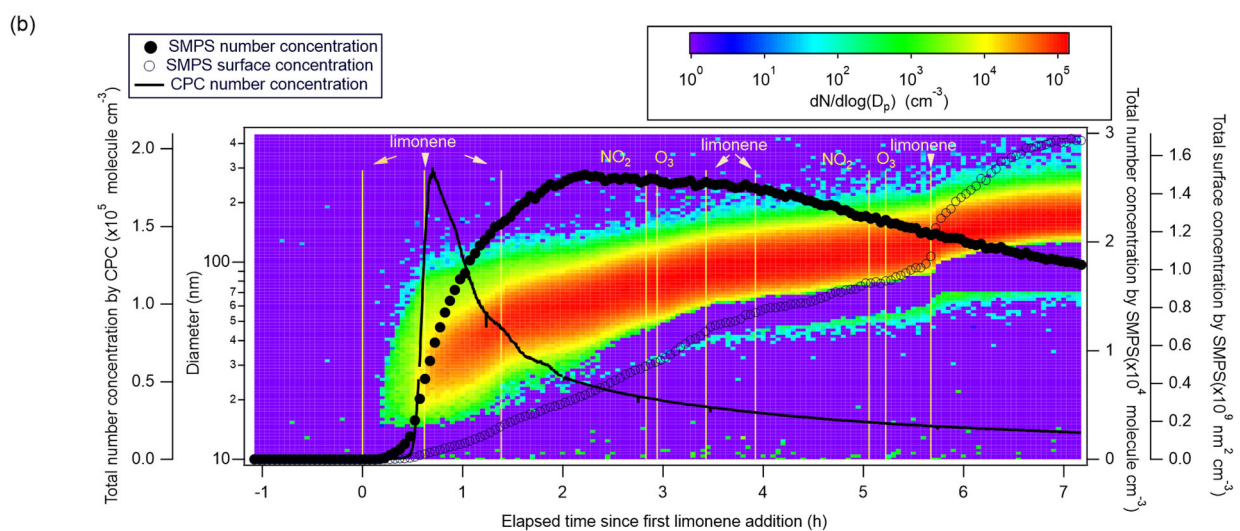
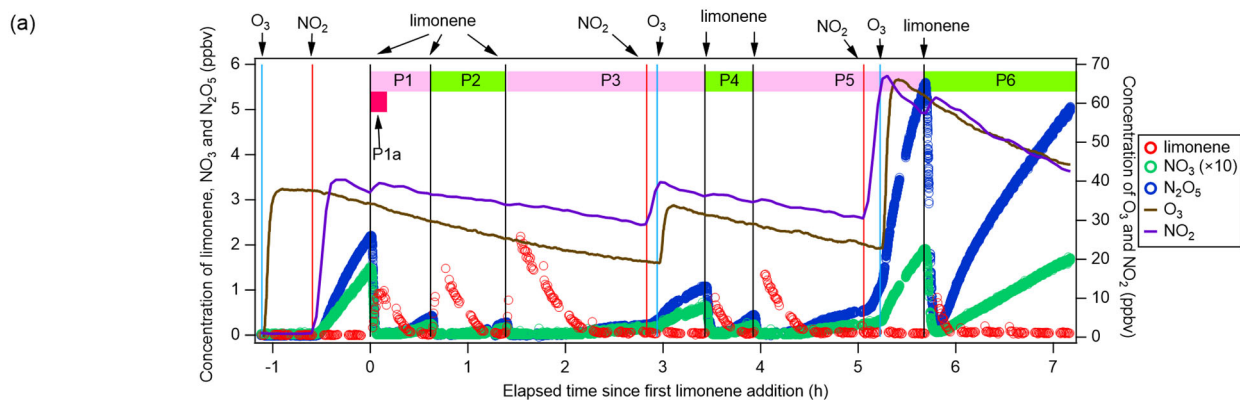
311 During period P1, HOM were quickly formed. We identified about 280 HOM compounds, including monomers
312 (C₇-C₁₀, ~280-460 Th), dimers (C₁₇-C₂₀, ~490-700 Th), and trimers (C₂₆-C₃₀, ~720-960 Th) (Fig. 2a). Their detailed

313 formulas can be found in Table S1. HOM on the horizontal lines of the Kendrick mass defect plot (O-based) (Fig. 3
314 and Fig ~~S8, S12S5, S6~~) share the same number of C, N and H atoms, with the number of oxygen atoms increasing
315 from left to right. Such HOM compounds are defined as a family. We notice that most monomer peroxy radical
316 families are each related to two monomer closed-shell product families, with one H atom more or one H atom less,
317 which are the expected termination products of $RO_2\cdot + RO_2\cdot$ reactions, or if $HO_2\cdot$ is present, $RO_2\cdot + HO_2\cdot$ termination
318 products. These three related families are defined as a "series", with the same number of C and N number, such as
319 $C_{10}H_{15-17}NO_{6-14}$. In total, we identified 6 monomer series ($C_{10}H_{15-17}NO_{6-14}$, $C_{10}H_{14-16}N_2O_{9-15}$, $C_{10}H_{14-16}O_{7-12}$, $C_9H_{13-15}NO_{7-14}$,
320 $C_8H_{11-13}NO_{6-13}$ and $C_7H_{9-11}NO_{7-11}$) and 1 monomer family ($C_{10}H_{17}N_3O_{12-16}$), 11 dimer families ($C_{20}H_{31}NO_{10-15}$,
321 $C_{20}H_{33}NO_{12-16}$, $C_{20}H_{32}N_2O_{9-20}$, $C_{20}H_{31}N_3O_{14-20}$, $C_{20}H_{33}N_3O_{12-20}$, $C_{20}H_{34}N_4O_{15-20}$, $C_{20}H_{32}O_{13-16}$, $C_{19}H_{29}NO_{10-13}$,
322 $C_{19}H_{31}NO_{10-15}$, $C_{19}H_{30}N_2O_{10-18}$ and $C_{19}H_{31}N_3O_{15-19}$), and 3 trimer families ($C_{30}H_{47}N_3O_{18-24}$, $C_{30}H_{48}N_4O_{16-24}$ and
323 $C_{29}H_{46}N_4O_{19-24}$). The monomer family $C_{10}H_{17}N_3O_{12-16}$ are not classified as series because the supposedly relevant
324 families are not clearly identified. Compounds containing at least one nitrogen atom accounted for more than 90 %
325 of the identified HOM products ~~while the remaining fraction were non-nitrated products.~~ We assume that compounds
326 containing nitrogen atoms are organic nitrates, because other N-containing species such as amines or nitro compounds
327 are very unlikely to be formed from the reaction of limonene with NO_3 . Organic nitrates formed in this study could
328 be alkylnitrates, or (acyl)peroxynitrates formed via the reaction of $RO_2\cdot$ with NO_2 .

329 During period P1a, in the absence of particles, both HOM monomers and oligomers were observed, including
330 monomers (47 %), dimers (47 %) and trimers (6 %) (Fig. 2a). Concentrations of gas-phase dimers and trimers
331 decreased evidently after particle formation (Fig. 2b, 5, 6), indicating a fast gas-particle condensation and strong
332 tendency of oligomers to condense on particles.

333



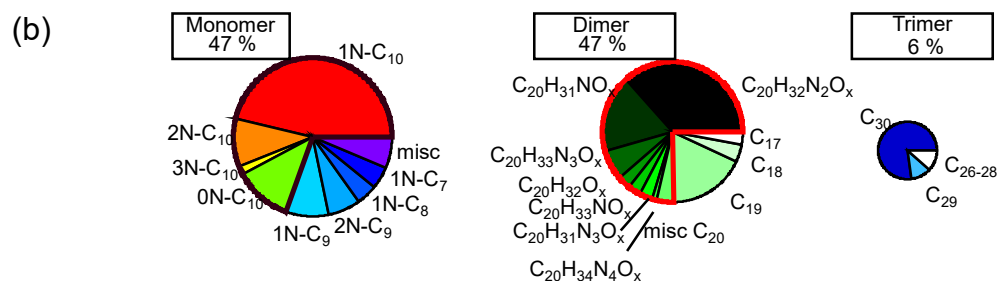
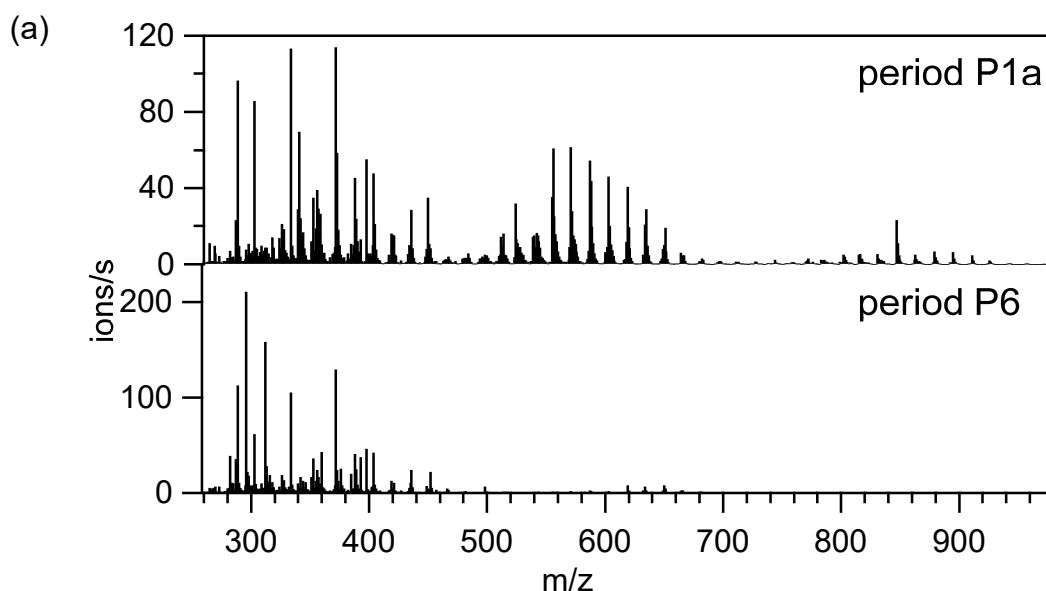


335
 336 Figure 1. (a) Time series of the concentrations of limonene, NO_3 , N_2O_5 (left panel, the concentrations of NO_3 are
 337 magnified by a factor of 10 for clarity), as well as O_3 and NO_2 (right panel). The time periods P1 to P6 as well as
 338 P1a are also marked. (b) Total particle concentration and its size distribution during the whole period of experiment
 339 detected by SMPS and CPC. The solid and hollow black circles refer to total number concentration and total
 340 surface concentration detected by SMPS, respectively. Colors represent particle number concentration distribution
 341 based on $\log(D_p)$. The solid black line refers to total number concentration detected by CPC. (c) Time series of peak
 342 intensity of typical products of the $\text{C}_{10}\text{H}_{15}\text{NO}_x$ family and $\text{C}_{10}\text{H}_{16}\text{NO}_{11}\bullet$ as a representative of the $\text{C}_{10}\text{H}_{16}\text{NO}_x\bullet$

343 family. Vertical lines indicate the time of O₃ and NO₂ ~~addition~~ additions, as well as six limonene injections.

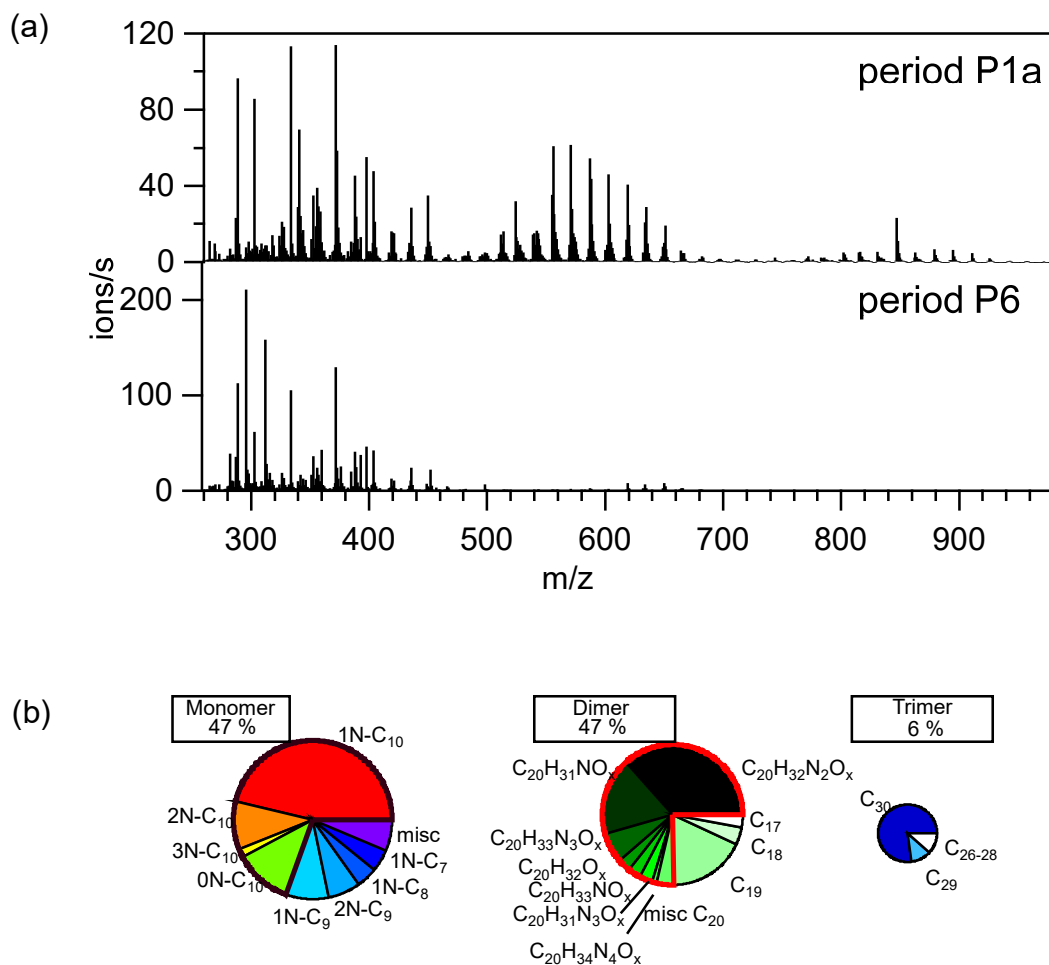
344

345 Based on their typical time series, (Fig. 1c), products can be classified as first-generation or second-generation
346 products (Fig. 1e). Generally, the concentrations of first-generation products, which result from the direct reaction
347 of limonene with NO₃, are expected to quickly increase after the limonene addition, followed by a steady decline due
348 to wall loss or chemical reactions. Concentrations of typical second-generation products, which result from further
349 reactions of first-generation products, are expected to show a gradually increasing concentration pattern after a
350 limonene addition and reach their maximum contribution concentration later than first-generation products. These
351 general expectations are modified in our case, since the particle concentration increased in our experiment (Fig. 1b)
352 and the condensational sink of HOM products became stronger over time. Thus, an increase in concentration suggests
353 ~~an overcome of that~~ the increasing condensational sink was exceeded by increasing production with time, i.e. from
354 second-generation pathways.



355

356 To sum up, gas-phase HOM formed in the limonene + NO₃ system were dominated by HOM monomers and
357 dimers. Time series patterns of the products indicate multiple generations of reaction pathways.



358

359 Figure 2. (a) Average mass spectra of the first 10 min reaction time after the first addition of limonene (period P1a,
 360 upper panel) and the last limonene addition period till particles reached maximum mass concentration (period P6,
 361 lower panel). (b) Pie charts (from left to right: rainbow, green, and blue colors) representing the relative contributions
 362 of identified series/families to HOM monomers, dimers, and trimers, respectively, during the P1a period. The area of
 363 each pie is in proportion to their concentrations during the P1a period.

364

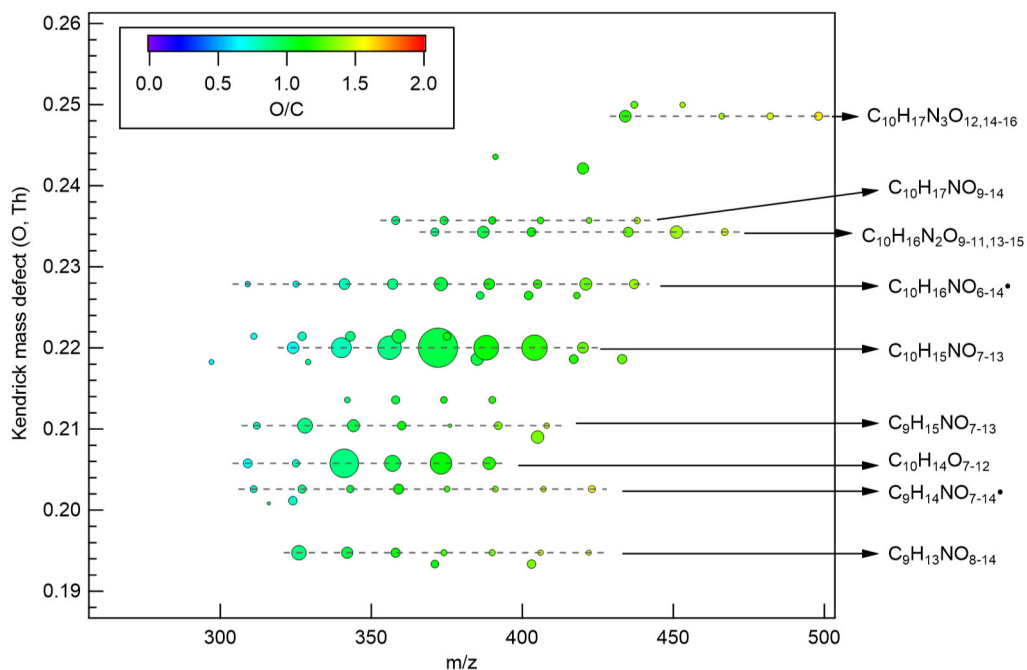
365 3.2 Monomers and their formation pathways

366 3.2.1 Overview of HOM monomers

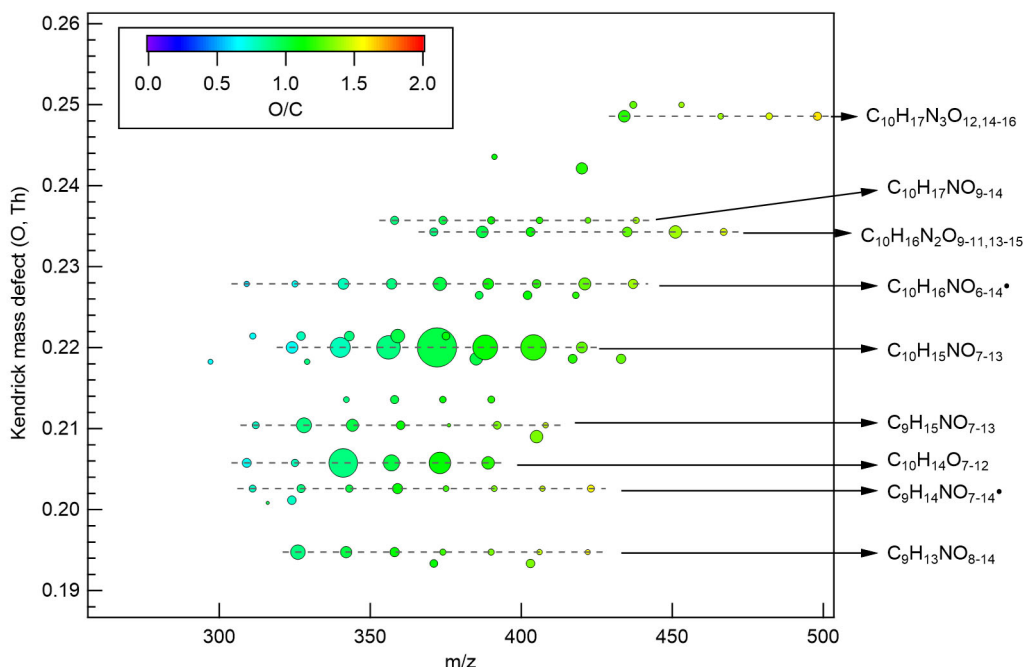
367 A number of HOM monomer families were detected with an increasing oxygenation pattern at 16 Th intervals (Fig.
 368 3). Such a pattern is attributed to autoxidation of RO₂• (with 32 Th interval for each O₂ addition) plus the alkoxy-
 369 peroxy pathway (shifted by 16 Th compared with exclusive autoxidation) as discussed below. During period P1a, the
 370 most abundant HOM monomers are C₁₀ compounds (64 %), such as peroxy radicals C₁₀H₁₆NO_x• and closed-shell
 371 products C₁₀H₁₅NO_x and C₁₀H₁₇NO_x, which are carbonyl compounds and hydroxyl or hydroperoxy compounds from
 372 the termination reactions of C₁₀H₁₆NO_x•, respectively-- (R14).



374 According to the nitrogen atoms contained, C₁₀-HOM monomers can be classified into 1N-, 2N-, 3N-monomers,
 375 and monomers without nitrogen atoms. While 1N-C₁₀ HOM monomers were likely formed by direct NO₃ addition
 376 to limonene, C₁₀-HOM monomers containing multiple N atoms were likely formed via multiple reaction steps.
 377 Besides C₁₀ HOM monomers, C₆₋₉ HOM monomers were also observed. These C₆₋₁₀ families are discussed below in
 378 the order of their contributions to HOM monomers.



379



380

381 Figure 3. Kendrick mass defect plot (O-atom-based) of major monomer products. The area of the circles is
 382 proportional to the average intensity of each compound during the P1a period with the largest circle representing
 383 C₁₀H₁₅NO₁₀. The color denotes O/C ratios. Dashed lines indicate major product families. For clarity, the reagent ions

384 $^{15}\text{NO}_3^-$ is omitted from molecular formula. The calculation of O-atom-based Kendrick mass defect includes two steps.
385 First, the IUPAC mass scale (based on the ^{12}C atomic mass as exactly 12 Da) is rescaled to Kendrick mass: Kendrick
386 mass = IUPAC mass \times (16/15.9949), which converts the mass of O from 15.9949 to exactly 16. Then, Kendrick mass
387 defect is given by: Kendrick mass defect = nominal Kendrick mass – exact Kendrick mass. Thus, compounds with
388 the same number of each kind of atom except for O have equal O-atom-based Kendrick mass defect, and are shown
389 in a horizontal line in the O-atom-based Kendrick mass defect plot.

390

391 3.2.2 1N-C₁₀ monomers

392 Among C₁₀ HOM monomers, the 1N-C₁₀ families were most abundant and included stable closed-shell products
393 C₁₀H₁₅NO_x (x=7-13) and C₁₀H₁₇NO_x (x=9-14) and peroxy radicals C₁₀H₁₆NO_x• (x=6-14). The concentration of
394 C₁₀H₁₆NO₁₁• increased in the later phase of each limonene addition period (Fig. 1c), showing mostly a time profile
395 of a second-generation product, similar as most of the other radicals in the C₁₀H₁₆NO_x• family (Fig. S3S7). However,
396 the time series of C₁₀H₁₅NO_x compounds showed an overlaying pattern of first- and second-generation products
397 dominated by a second-generation time profile with the exception of C₁₀H₁₅NO₉ (Fig. 1c). ~~Given that RO₂• are~~
398 ~~chemically active, it is likely that C₁₀H₁₆NO_x• radicals converted immediately after their formation, so that their~~
399 ~~concentrations did not exhibit a first-generation time profile. At this time, we do not have a reasonable explanation~~
400 ~~for the trend of C₁₀H₁₅NO₉.~~ Due to sensitivity restrictions of CIMS, the primary peroxy radical C₁₀H₁₆NO₅• was not
401 detected, which was supposed to show 1st-generation pattern. The absence of first-generation characteristics of the
402 time profile of most HOM peroxy radicals C₁₀H₁₆NO_{x(x>6)}• may be attributed to two possible reasons. They either did
403 not undergo efficient autoxidation, or they underwent immediate conversion including autoxidation and/or
404 bimolecular reactions with other RO₂• or NO₃ forming closed-shell products such as dimers or continuing the radical
405 chain forming RO•. The instantaneous increase of 2N-dimers and trimers after the first limonene addition shown
406 below suggests that C₁₀H₁₆NO_{x(x>6)}• were indeed formed efficiently via autoxidation. Therefore, the latter reason is
407 more likely. At this time, we do not have a reasonable explanation for the trend of C₁₀H₁₅NO₉, though we should
408 consider that there are many isomers at play, which may have very different chemical pathways (un)available.

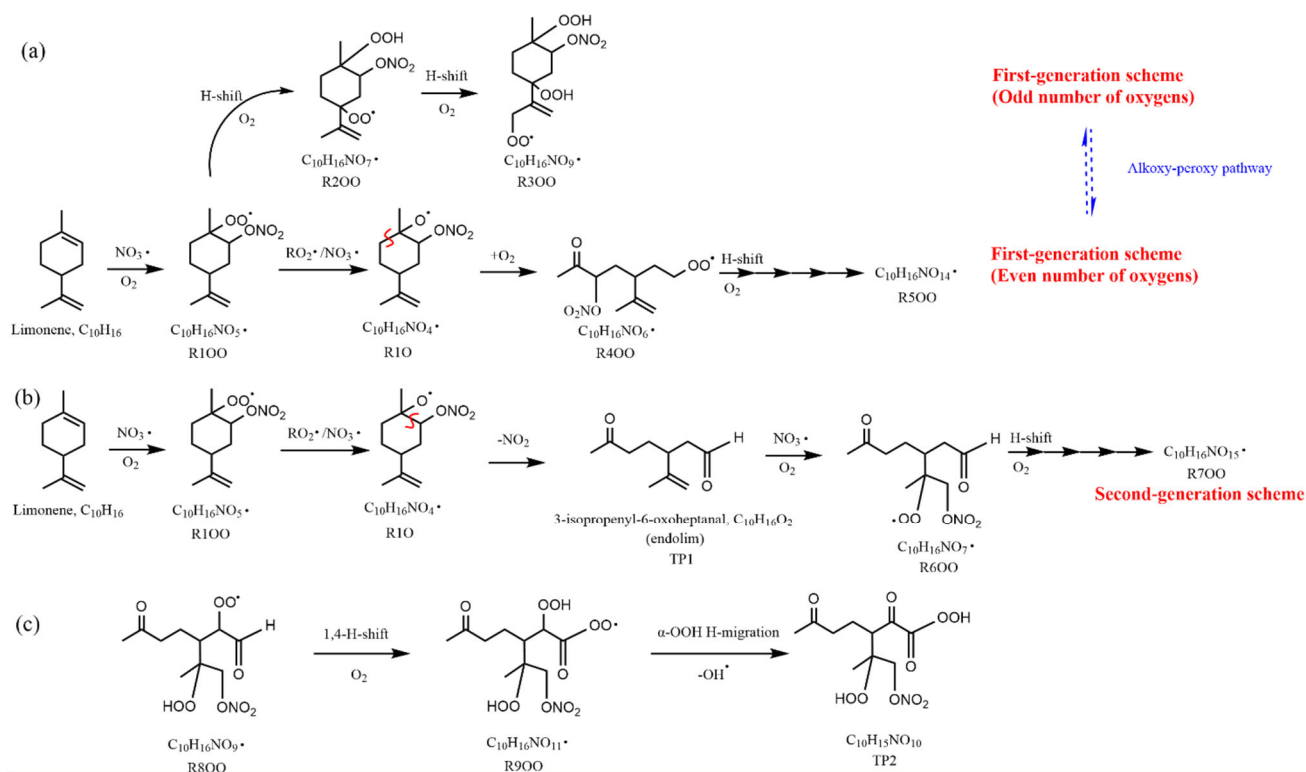
409 Since the C₁₀H₁₅NO_x family showed an overlaying pattern of the first-generation and second-generation
410 products, they likely contained multiple isobaric substances produced through different pathways. Based on the
411 literature, possible formation pathways of these products were tentatively proposed (Seinfeld and Pandis, 2006;
412 Vereecken and Peeters, 2010; Mentel et al., 2015; Vereecken and Nozière, 2020). As an example of the pathways to
413 form first-generation products, C₁₀H₁₆NO_{2x-1}• (with an odd number of oxygen atom) and their corresponding
414 termination products can be formed via autoxidation of the first peroxy radical C₁₀H₁₆NO₅• (R1OO), showing
415 C₁₀H₁₆NO₉• (R3OO) as an example (Scheme 1a, first-generation products). C₁₀H₁₆NO_{2x}• (with an even number of
416 oxygen atom) can be formed via alkoxy-peroxy channels. For example, the ring-opening of the alkoxy radical
417 C₁₀H₁₆NO₄• (R1O), which was formed via the reaction of C₁₀H₁₆NO₅• (R1OO) with another RO₂• or NO₃ radical or
418 NO₃- (Scheme 1a, first-generation products). Ring-opening of R1O ~~lead~~leads to C₁₀H₁₆NO₆• (R4OO), which can

419 undergo autoxidation forming $C_{10}H_{16}NO_{2x}\cdot$. In addition, the alkoxy radical $C_{10}H_{16}NO_4\cdot$ (R1O) is susceptible to ring-
 420 opening reactions (Novelli et al., 2021), which can lead to a first-generation stable product 3-isopropenyl-6-
 421 oxoheptanal (endolim, TP1) after C-C bond cleavage followed by the elimination of a NO_2 fragment (Scheme 1b,
 422 second-generation products). Endolim (TP1) has been detected as a major product in previous limonene + NO_3
 423 studies (Hallquist et al., 1999; Spittler et al., 2006).

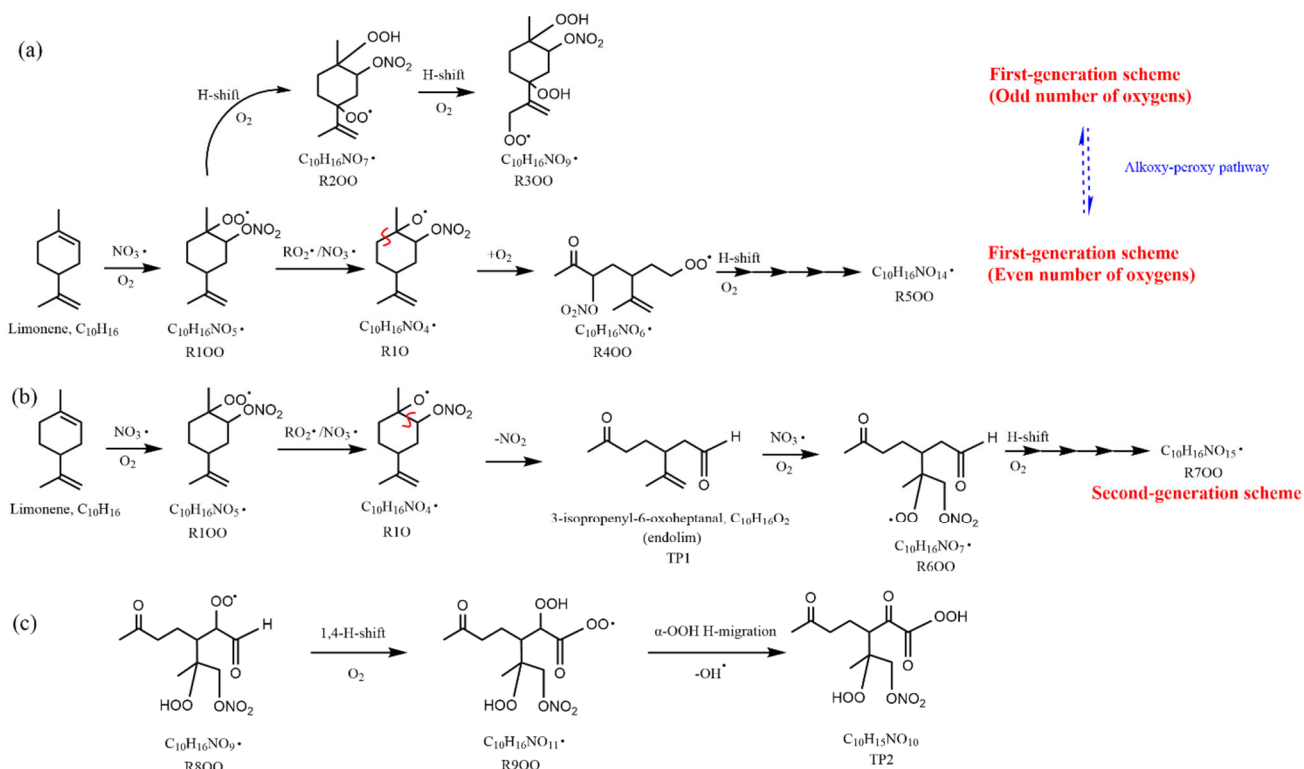
424 As an example of second-generation chemistry, the remaining double bond of endolim could react with NO_3 to
 425 form $RO_2\cdot$, followed by the autoxidation to form second-generation $C_{10}H_{16}NO_x\cdot$ (with odd number of oxygen atoms).
 426 Similar to first-generation pathways, second-generation $C_{10}H_{16}NO_x\cdot$ with even number of oxygen atoms can be
 427 formed via alkoxy-peroxy channel. From the time profile of $C_{10}H_{15}NO_x$, the second-generation pathway (Scheme 1b)
 428 was expected to play a more important role, in agreement with the theoretical result by Kurtén et al. (2017), in which
 429 the two bond-cleavage pathways of limonene-derived $RO\cdot$ radical were considered. It is worth mentioning that the
 430 reaction products of limonene with O_3 may also react with NO_3 , forming $C_{10}H_{16}NO_x\cdot$ (Scheme S1). However, as
 431 shown above, this was a minor pathway in our experiment (Sect. 2.1). We would like to note that to simplify the
 432 scheme, only the reaction of NO_3 with the endocyclic double bond is presented, since this reaction is faster than that
 433 with the exocyclic double bond (Jiang et al., 2009; Fry et al., 2011).

434 $C_{10}H_{16}NO_x\cdot$ with both even and odd number of oxygen atoms as well as their termination products had
 435 comparable abundance, which suggests that the alkoxy-peroxy pathway was important for $RO_2\cdot$ formation in this
 436 reaction. This finding is analogous to the findings in the reaction of a number of alkenes with O_3 and in the reaction
 437 of isoprene and β -pinene with NO_3 (Mentel et al., 2015; Zhao et al., 2021; Shen et al., 2021).

438



439



440

441 Scheme 1. Illustrative scheme for HOM formation in the limonene + NO₃ reaction. (a) Example formation pathways
 442 leading to first-generation 1N-C₁₀ HOM-RO₂ radicals (C₁₀H₁₆NO_x• with even or odd numbers of O-atoms). (b)
 443 Second-generation scheme involving the formation of endolim. (c) Scheme of intramolecular termination of RO₂•
 444 radicals forming carbonyl products taking the C₁₀H₁₆NO₉• radical as an example. Note that the depicted reactions
 445 may not be the dominant pathways.

446

447 Among 1N-C₁₀ monomers, concentrations of carbonyl compounds were much higher than the sum of hydroxy-
 448 and hydroperoxy-substituted compounds (Table 1). According to Hyttinen et al. (2015), for nitrate CI-API-TOF,
 449 HOM containing two hydrogen bond donors (such as -OOH and -OH group) have strong binding energy with NO₃⁻.
 450 Additional hydrogen bond donors only enhance the binding energy marginally. If we compare HOM carbonyl product
 451 (such as C₁₀H₁₅NO₁₀) with the corresponding hydroxy product (C₁₀H₁₇NO₁₀), they only differ in one functional group.
 452 As both are highly functionalized, it is likely that HOM carbonyl have a quite similar sensitivity with HOM alcohol.
 453 If the sensitivity of carbonyl HOM were lower, this would result in even more dominance of carbonyl HOM over
 454 hydroxyl HOM. Thus, we conclude that carbonylnitrates are more abundant than hydroxynitrates or
 455 hydroperoxynitrates. This finding is likely attributed to unimolecular termination reactions of RO₂•, although reaction
 456 paths via RO• also cannot be excluded. Smaller unbranched RO• tend to react with O₂ forming carbonyl compounds
 457 while for larger or branched RO•, isomerization can also form carbonyl compounds and is a more energetically
 458 favorable and thus faster pathway compared with the reaction with O₂ (Ziemann and Atkinson, 2012)~~This finding is~~
 459 ~~likely attributed to unimolecular termination reactions of RO₂•.~~ The importance of unimolecular termination
 460 reactions of HOM-RO₂• and the resulting high ratio of carbonyl compounds to hydroxyl/hydroperoxyl compounds

461 has also been found in the reaction system of β -pinene + NO_3 (Shen et al., 2021; Dam et al., 2022). This high ratio is
 462 also consistent with findings in the ozonolysis of alkenes (Mentel et al., 2015), where unimolecular termination
 463 reactions were also proposed to be the likely explanation (Crouse et al., 2013; Rissanen et al., 2014). As discussed
 464 in our previous study by Shen et al. (2021), this higher abundance of carbonylnitrates is not likely to be explained by
 465 the reaction of alkoxy $\text{RO}\cdot + \text{O}_2$ forming carbonyls and $\text{HO}_2\cdot$, decomposition of β -nitrooxyperoxynitrate or self-
 466 reactions of $\text{RO}_2\cdot$ via the Bennett and Summers mechanism forming carbonyls and H_2O_2 . Reactions between $\text{RO}_2\cdot$
 467 in general should produce overall equal amounts of carbonyl and hydroxyl compounds. The decomposition of β -
 468 nitrooxyperoxynitrate is slow in the gas-phase. The reaction of alkoxy $\text{RO}\cdot$ with O_2 for large $\text{RO}\cdot$ is generally slower
 469 than isomerization and decomposition (Vereecken and Peeters, 2009, 2010). Thus, the higher abundance of
 470 carbonylnitrates compared to hydroxynitrates may be attributed to unimolecular termination of $\text{HOM-RO}_2\cdot$. In
 471 addition, isomerization of $\text{RO}\cdot$ forming carbonyl compounds may also contribute to this finding. Our result thus
 472 further emphasizes that unimolecular termination reactions of RO_2 radicals are important pathways in the formation
 473 of HOM monomers derived from the reactions of monoterpenes with NO_3 (Shen et al., 2021). Scheme 1c shows this
 474 ~~intramolecular~~unimolecular termination process using a $\text{C}_{10}\text{H}_{16}\text{NO}_9\cdot$ radical as an example. $\text{C}_{10}\text{H}_{16}\text{NO}_9\cdot$ undergoes
 475 a 1,4-H-shift and O_2 addition to form a $\text{C}_{10}\text{H}_{16}\text{NO}_{11}\cdot$ radical. The $\text{C}_{10}\text{H}_{16}\text{NO}_{11}\cdot$ radical further undergoes an H-shift
 476 of the α -OOH H-atom, which produces a carbonyl closed-shell product as well as an $\text{OH}\cdot$ radical.

477 For 1N- C_{10} HOM monomers, the products detected in this study generally agree with previous laboratory and
 478 field studies on the reaction of limonene and other monoterpenes. Faxon et al. (2018) also observed $\text{C}_{10}\text{H}_{15}\text{NO}_x$ as
 479 the most prevalent products in the particle phase from limonene + NO_3 . In the SOAS campaign, both $\text{C}_{10}\text{H}_{15}\text{NO}_x$ and
 480 $\text{C}_{10}\text{H}_{17}\text{NO}_x$ products were detected and were believed to be products of nighttime chemistry (Lee et al., 2016). The
 481 high abundance of 1N- C_{10} HOM monomers is consistent with the finding that $\text{C}_{10}\text{H}_{15}\text{NO}_x$ and $\text{C}_{10}\text{H}_{17}\text{NO}_x$ dominate
 482 the chemical composition of SOA formed via NO_3 oxidation of α -pinene and β -pinene, as shown in previous chamber
 483 studies (Takeuchi and Ng, 2019).

484 In summary, 1N- C_{10} HOM monomers are mainly formed via second-generation pathways, and unimolecular
 485 termination of $\text{RO}_2\cdot$ likely plays an important role leading to higher abundance of carbonyl HOM-ON ($\text{C}_{10}\text{H}_{15}\text{NO}_x$)
 486 than hydroxy/hydroperoxy HOM-ON ($\text{C}_{10}\text{H}_{17}\text{NO}_x$).

487
 488 Table 1. Observed $\text{C}_{10}\text{H}_{16}\text{NO}_x\cdot$ radicals (m) and their termination products, including carbonyl compounds (m-17),
 489 hydroxyl compounds (m-15), and hydroperoxy compounds (m+1). Their concentrations during period P1a are
 490 normalized to that of $\text{C}_{10}\text{H}_{15}\text{NO}_{10}$, which had the highest concentration among the ~~family-series~~families of 1N- C_{10}
 491 monomers. Their relative signal intensities during the P1a period are shown in the second line of each cell.

Peroxy radical	Carbonyl	Hydroxy	Hydroperoxy
m	m-17	m-15	m+1
$\text{C}_{10}\text{H}_{16}\text{NO}_6\cdot$			
1.5 %			

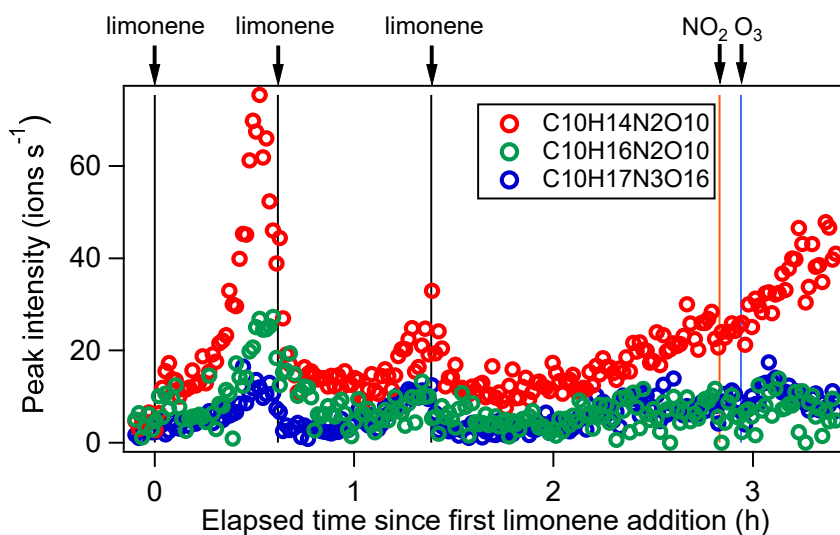
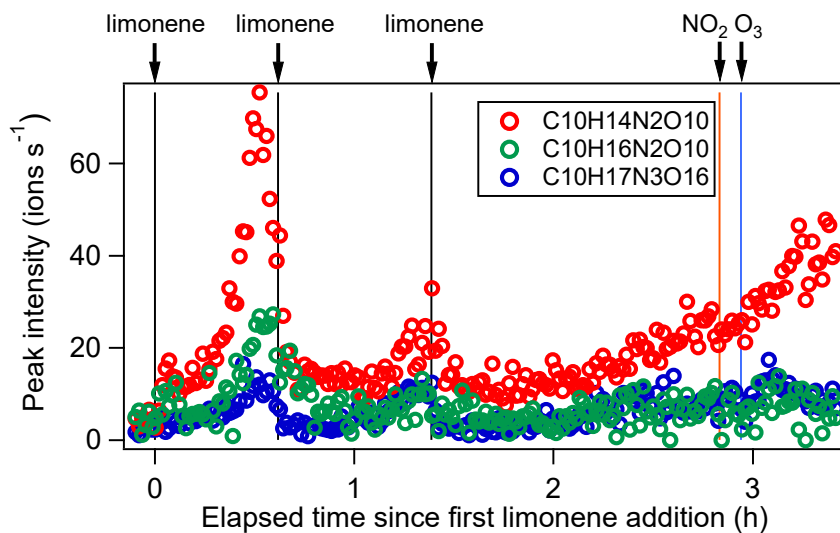
C ₁₀ H ₁₆ NO ₇ •			
2.0 %			
C ₁₀ H ₁₆ NO ₈ •	C ₁₀ H ₁₅ NO ₇		
6.7 %	8.0 %		
C ₁₀ H ₁₆ NO ₉ •	C ₁₀ H ₁₅ NO ₈	C ₁₀ H ₁₇ NO ₉	
6.0 %	25.2 %	3.7 %	
C ₁₀ H ₁₆ NO ₁₀ •	C ₁₀ H ₁₅ NO ₉	C ₁₀ H ₁₇ NO ₉	C ₁₀ H ₁₇ NO ₁₀
10.2 %	34.6 %	3.7 %	3.6 %
C ₁₀ H ₁₆ NO ₁₁ •	C ₁₀ H ₁₅ NO ₁₀	C ₁₀ H ₁₇ NO ₁₀	C ₁₀ H ₁₇ NO ₁₁
6.6 %	100.0 %	3.6 %	3.0 %
C ₁₀ H ₁₆ NO ₁₂ •	C ₁₀ H ₁₅ NO ₁₁	C ₁₀ H ₁₇ NO ₁₁	C ₁₀ H ₁₇ NO ₁₂
4.1 %	39.0 %	3.0 %	2.3 %
	C ₁₀ H ₁₅ NO ₁₂	C ₁₀ H ₁₇ NO ₁₂	C ₁₀ H ₁₇ NO ₁₃
	41.2 %	2.3 %	1.5 %
C ₁₀ H ₁₆ NO ₁₄ •	C ₁₀ H ₁₅ NO ₁₃	C ₁₀ H ₁₇ NO ₁₃	C ₁₀ H ₁₇ NO ₁₄
4.7 %	6.7 %	1.5 %	1.8 %
		C ₁₀ H ₁₇ NO ₁₄	
		1.8 %	

492

493 3.2.3 2N and 3N-C₁₀ monomers

494 C₁₀ monomers with 2 and 3 nitrogen atoms accounted for 27 % and 1 % of HOM monomers, respectively. They were
495 likely formed via the reaction of a second attack of NO₃ to the first-generation products ~~with the remaining double~~
496 ~~bond from limonene as~~ the 1N-C₁₀ closed-shell products formed via the reactions shown in Scheme 1a should contain
497 a remaining limonene C=C double bond. Typical 2N- and 3N-HOM showed a second-generation time profile (Fig.
498 4). For clarity, only periods P1 to P3 are shown. This time profile is consistent with the pathways with multiple NO₃
499 attacks. Scheme 2 shows possible formation pathways of 2N- and 3N-C₁₀ monomers. 2N-C₁₀ HOM were likely to be
500 formed from NO₃ oxidation of 1N-C₁₀ monomers (C₁₀H₁₅NO_x and C₁₀H₁₇NO_x), resulting in C₁₀H₁₅N₂O_x• and
501 C₁₀H₁₇N₂O_x• (Scheme 2a, 2b). While C₁₀H₁₅N₂O_x• (x=9-12) were observed, C₁₀H₁₇N₂O_x• could not be uniquely
502 identified because the peaks of the C₁₀H₁₇N₂O_x• and C₁₀H₁₅NO_x families are too close in the mass spectra to be
503 separated based on the resolution of our mass spectrometer. 3N-C₁₀ monomers, C₁₀H₁₇N₃O_x, were expected to be
504 formed from limonene via two steps of NO₃ oxidation to the double bonds and an addition of NO₂ to an RO₂ radical,
505 leading to a peroxyacetyl nitrate or peroxyacyl nitrate. NO₂ addition reactions may also contribute to the formation of 2N-
506 C₁₀ monomers. The addition of NO₂ to RO₂ radicals could occur either before (Scheme 2d) or after (Scheme 2c) the
507 second NO₃ attack.

508

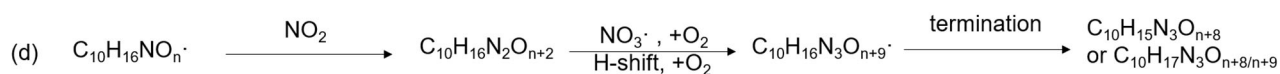
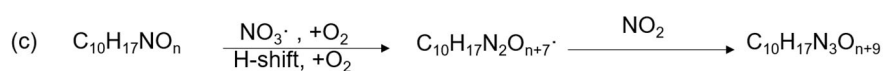
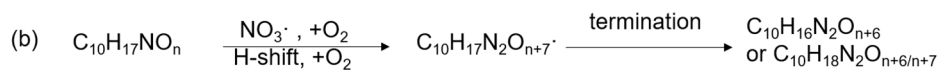
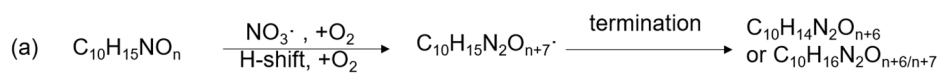


509

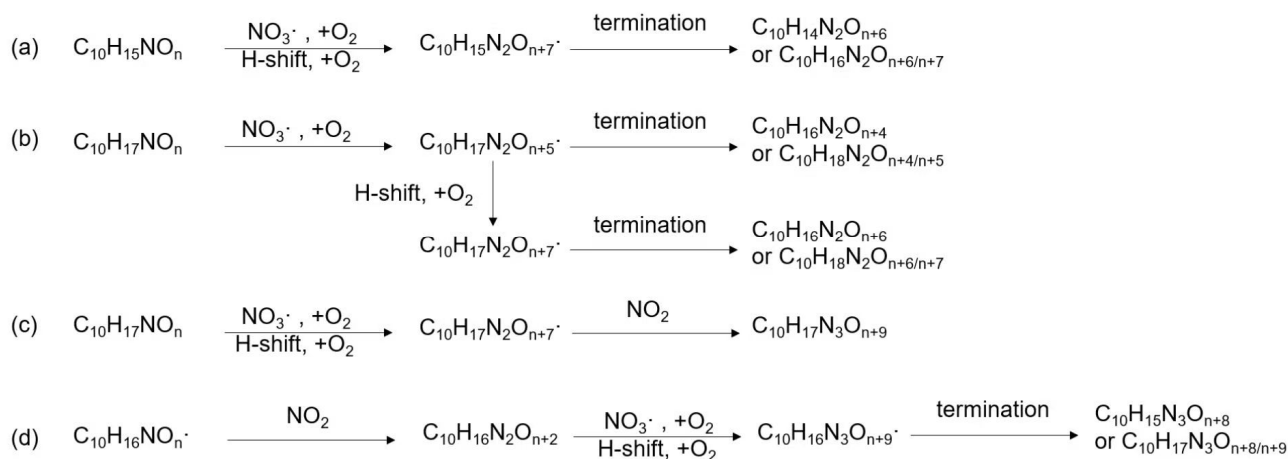
510

511 Figure 4. Time series of peak intensity of several monomers $C_{10}H_{14}N_2O_{10}$, $C_{10}H_{16}N_2O_{10}$ and $C_{10}H_{17}N_3O_{16}$ as the
 512 representatives of multiple N monomers during the periods P1-P3.

513



514



515

516 Scheme 2. Possible formation pathways of C₁₀-monomers containing 2 nitrogen atoms (a, b) and 3 nitrogen atoms
 517 (c, d). Termination denotes reactions of RO₂• with other RO₂• or HO₂• or unimolecular reactions, leading to closed-
 518 shell products.

519

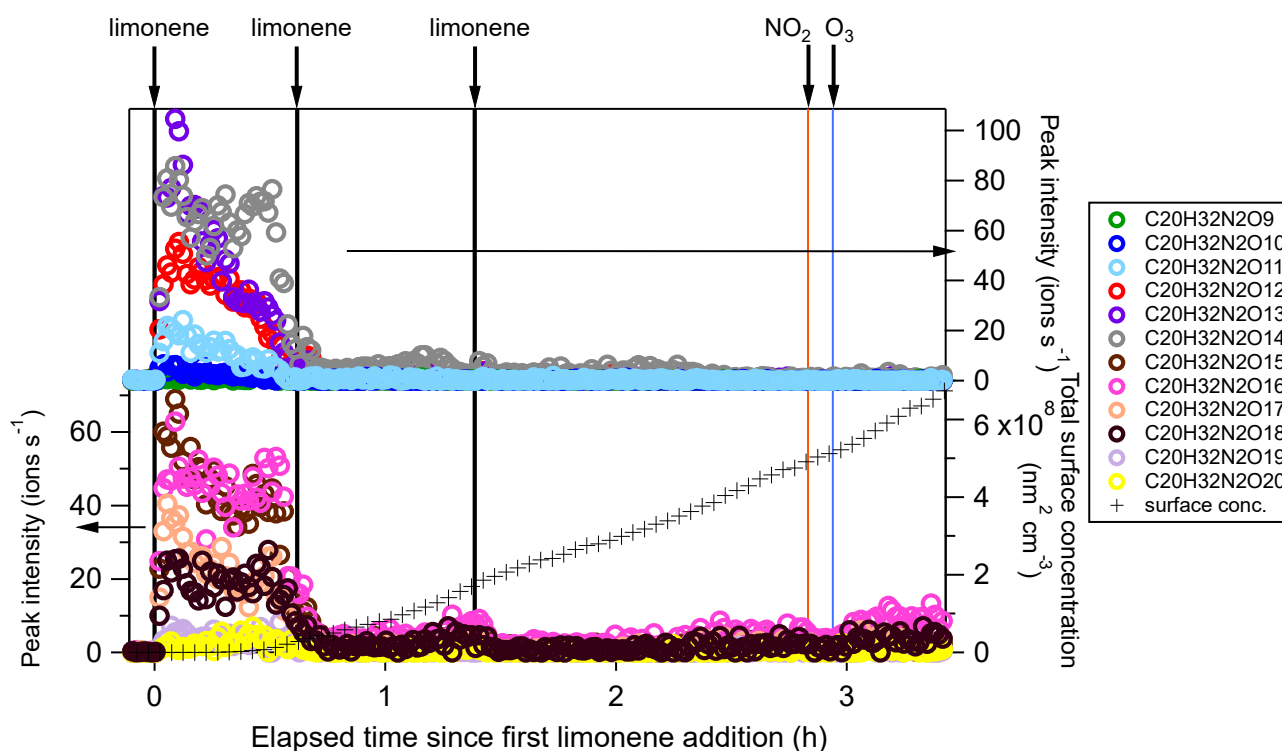
520 3.2.4 Formation pathways of C₁₀ monomers without N-atoms and monomers with less than 10 C-atoms

521 Besides C₁₀ products containing nitrogen atoms, HOM monomers without nitrogen atoms were also identified.
 522 Among these products, C₁₀H₁₄O_x (x=7-12) were the most prevalent family, which were also detected in limonene
 523 ozonolysis (Jokinen et al., 2015). The C₁₀H₁₄O_x family showed a time series typical of first-generation products (Fig.
 524 [S4S8](#)). C₁₀H₁₄O_x and C₁₀H₁₆O_x could be formed from limonene + NO₃ with C₁₀H₁₆NO_x• terminating their
 525 autoxidation by migration of the α-NO₃ H-atom, eliminating an NO₂ fragment (Scheme S2) (Novelli et al., 2021).
 526 Alternatively, these products could be formed via the reaction of O₃ with limonene (Scheme S2). ~~It~~ Either way,
 527 C₁₀H₁₄O_x and C₁₀H₁₆O_x were formed via first-generation pathways.

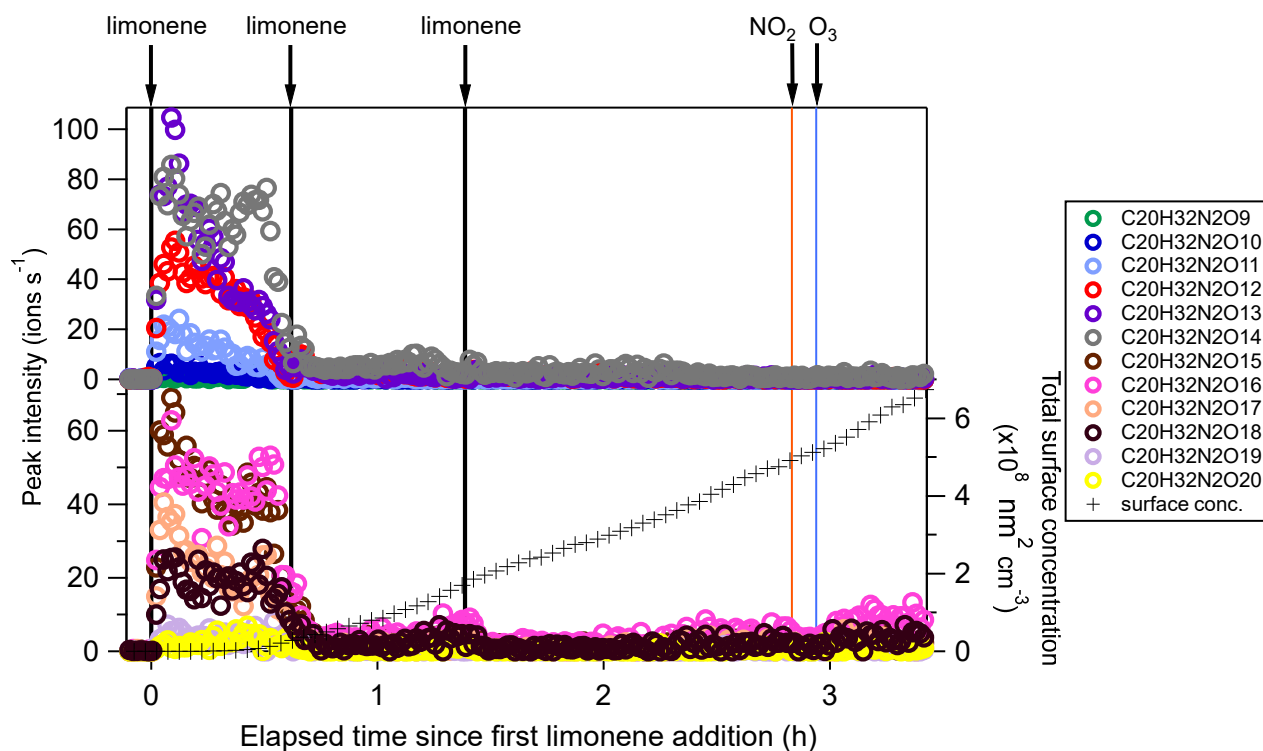
528 We also observed monomers with carbon atom number less than 10. During the P1a period, C₉ monomer families
 529 were the most abundant contributors to C<10 HOM monomers, followed by C₈ families. The majority of C₉
 530 monomers were C₉H₁₅NO_x (x=7-13) ([time series shown in Fig. S9](#)) and C₉H₁₃NO_x (x=8-14). The loss of one carbon
 531 atom may follow the mechanism shown in Scheme S3 (Fry et al., 2011; Bianchi et al., 2019). The major product
 532 family in C₈ monomers is C₈H₁₁NO_x (x=6, 7, 9-13). While during period P1a C₈H₁₁NO_x compounds could be hardly
 533 observed, their concentrations increased considerably in the later periods (Fig. [S6S10](#)). The gas-phase concentration
 534 of C₈H₁₁NO₇ was even the highest among all compounds in later periods (highest intensity signal in Fig. 2b). This is
 535 partly attributed to the relatively high volatility of C₈ compounds compared with C₁₀ HOM species and accretion
 536 products, which tend to condense on particles. The major family in C₇ monomers, C₇H₉NO_x (x=6-13), showed a time
 537 series pattern similar to C₈H₁₁NO_x compounds (Fig. [S7S11](#)). Such a time profile indicates that C₇ and C₈ products
 538 were likely a result of multi-generation gas-phase reactions.

539 3.3 Dimers and their formation

540 Among dimers, C₂₀ products were the most abundant, followed by C₁₉ products. Among C₂₀ and C₁₉ dimers, the most
 541 prevalent families included C₂₀H₃₂N₂O_x (x=9-20), C₂₀H₃₃N₃O_x (x=12-20), C₂₀H₃₁NO_x (x=10-15), C₂₀H₃₁N₃O_x
 542 (x=14-20), C₂₀H₃₄N₄O_x (x=15-20), and C₁₉H₃₀N₂O_x (x=10-18) (Fig. S8S5). The O/C ratio of dimers did not exceed
 543 one, while that of monomers was as high as two. This could be due to oxygen atom loss and participation of less
 544 oxygenated RO₂• in the dimer formation as discussed below. Time series of dimers also showed different
 545 patternsbehavior compared to monomers. For example, compounds of the C₂₀H₃₂N₂O_x family only reached a
 546 considerable peak intensity in period P1 and decreased rapidly, and thereafter, while the signal intensity in periods
 547 P2 to P6 were low (Fig. 5). Generally, other dimers showed similar patterns (Fig. S9-11), S12-S14), though the
 548 difference of their concentration between P2-P6 and P1 were not as large as for the C₂₀H₃₂N₂O_x family. The time
 549 when signals of several dimers (e.g. C₂₀H₃₂N₂O_x, C₂₀H₃₃N₃O_x, C₂₀H₃₄N₄O_x) dropped substantially matched the time
 550 of new particle formation (NPF) and the onset of particle growth, indicating that some dimers were likely to contribute
 551 toinvolved in the early growth of particles. Such a behavior is expected since dimers have a much lower volatility
 552 than monomers. This observation is consistent with the limonene + NO₃ laboratory study by Faxon et al. (2018) that
 553 found a significant fraction of HOM dimer derived from limonene + NO₃-in the particle phase.



554
555



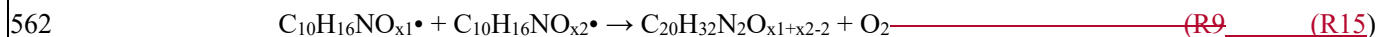
556

557 Figure 5. Time series of peak intensity of the $C_{20}H_{32}N_2O_x$ family compounds during the periods P1 to P3. The cross
 558 markers (lower right y-axis) indicate total particle surface concentration.

559

560 In general, $C_{20}H_{32}N_2O_x$ showed an overlaying time profile of first- and second-generation products (Fig. 5).

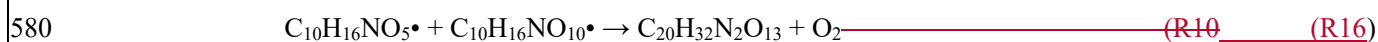
561 $C_{20}H_{32}N_2O_x$ were likely formed via the accretion reaction between two monomer $RO_2\cdot$ ($C_{10}H_{16}NO_x\cdot$):



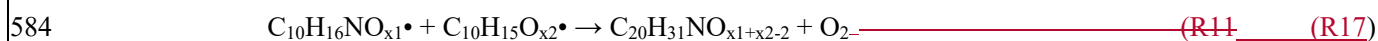
563 Since $C_{10}H_{16}NO_x\cdot$ can be first- or second-generation products, the resulting dimers $C_{20}H_{32}N_2O_x$ can also be first- or
 564 second-generation products. The time series showed show that $C_{20}H_{32}N_2O_x$ with less lower O number presented more
 565 of a first-generation product time profile (Fig. 5-). while the relative contribution of second-generation formation
 566 tended was observed to increase with oxygen number.

567 We compared the observed dimer formula with those expected based on accretion reactions of $HOM-RO_2\cdot$. X
 568 in the $C_{20}H_{32}N_2O_x$ observed was ≥ 9 ; however, according to the accretion mechanism and the observed $C_{10}H_{16}NO_x\cdot$
 569 ($x \geq 6$), x in $C_{20}H_{32}N_2O_x$ should be ≥ 10 ($6+6-2=10$). Moreover, as the most abundant $RO_2\cdot$ within the $C_{10}H_{16}NO_x\cdot$
 570 family was $C_{10}H_{16}NO_{10}\cdot$ (Table 1), the most abundant $C_{20}H_{32}N_2O_x$ was expected to would have an oxygen number of
 571 18 according to if they were exclusively formed by the accretion reaction mechanism of HOM $RO_2\cdot$. This contradicted
 572 the fact that the most abundant molecule among the $C_{20}H_{32}N_2O_x$ family was $C_{20}H_{32}N_2O_{13}$. The findings above could
 573 only be explained by the participation of less oxygenated $RO_2\cdot$ such as $C_{10}H_{16}NO_{5,6}\cdot$ in the accretion reaction (Berndt
 574 et al., 2018a; Berndt et al., 2018b; Mcfiggans et al., 2019). $C_{10}H_{16}NO_5\cdot$ was not detected in by our CI-API-TOF,
 575 which is attributed to the lower detection sensitivity of molecules with O number ≤ 5 in the NO_3^- -CIMS (Riva et al.,
 576 2019)-. Still, $C_{10}H_{16}NO_5\cdot$ is the first RO_2 radical formed in the limonene + NO_3 reaction (Scheme 1a-). so a high mass

577 flux has to pass through this RO₂•. If we assume that the abundance of C₁₀H₁₆NO₅• was high, and considering that
578 the concentration of C₁₀H₁₆NO₁₀• was the highest in the C₁₀H₁₆NO_x• family, their accretion reaction (~~R10~~R16) could
579 form C₂₀H₃₂N₂O₁₃ and justifysupport that C₂₀H₃₂N₂O₁₃ was the most abundant C₂₀ dimer product:



581 Time series of dimers with unequaldifferent numbers of N atoms were different, indicating different formation
582 pathways. For example, the C₂₀H₃₁NO_x family were mainly first-generation products (Fig. ~~S9~~S12), which may be
583 formed via the following reaction:



585 C₁₀H₁₅O_x• were first-generation radicals (Sect. 3.2.4), while C₁₀H₁₆NO_x• were mainly second-generation radicals.
586 C₁₀H₁₆NO_x• could also be formed via first-generation pathway as discussed above (Scheme 1a), but that was not
587 apparentborne out by the time profile, suggesting a fast termination of first-generation C₁₀H₁₆NO_x• radicals. Reaction
588 ~~R11~~R17 could be one of the termination pathways of first-generation C₁₀H₁₆NO_x• based on the first-generation time
589 profile of C₂₀H₃₁NO_x. In the study by Faxon et al. (2018), the formation of 1N-C₂₀ dimers was explained by a
590 mechanism involving two 1N-RO₂ radicals which produced HNO₃ as a by-product. However, C₁₀ RO₂ radicals
591 without nitrogen atoms were identified in our study, which provided a direct formation pathway of 1N-C₂₀ dimers
592 through ~~R11~~R17.

593 On the other hand, C₂₀H₃₃N₃O_x and C₂₀H₃₄N₄O_x were mainly second-generation products (Fig. ~~S10, 11~~S13, S14).
594 C₂₀H₃₃N₃O_x and C₂₀H₃₄N₄O_x were likely to be formed via NO₃ oxidation of dimers containing less nitrogen
595 atoms, and were thus second-generation products. The related radicals were also detected, such as C₂₀H₃₂N₃O_x•
596 (x=16-19) and C₂₀H₃₁N₂O_x• (x=13-16). Possible formation pathways of dominant oligomer families are displayed in
597 Table 2. We cannot exclude that the formation pathway of C₂₀H₃₃NO_x, C₂₀H₃₄N₄O_x and C₁₉H₃₁NO_x may also involve
598 limonene oxidation by OH• (Table 2), which can be formed in the ozonolysis of limonene as a minor pathway. In
599 addition, the high abundance of C₂₀H₃₁NO_x (x=10-15) among the dimers may be partly attributed to a contribution
600 of the reaction of limonene with O₃.

601 The initial drop of the products (dimers and monomers) in Fig. 1, Fig. S8, and Fig. S12 during P1 (the
602 characteristic time of the fastest decay was 15 min, 10 min, and 13 min, respectively) is attributed to the balance of
603 their sources via the reaction of limonene with NO₃, their wall loss, and their potential loss by the reaction with NO₃.
604 The characteristic time of the fastest decay of the HOM over the 2nd limonene addition in Fig. 1, 4, 5, S12, and S13
605 are 4-8 min. These decays can be explained by the wall loss rate (characteristic time ~8 min) and condensation sink
606 of vapor loss to particles according to the study of Kulmala et al. (2012) (characteristic time ~13 min). The
607 characteristic times of the fastest decay of the HOM at the end of P2 in Fig. S12 and S13 are 1.4-3.4 min, which can
608 also be well explained by the updated wall loss rate and condensation sink of vapor loss to particles at the end of P2
609 (characteristic time ~1.4 min).

610 In summary, HOM dimers are likely to be formed via accretion reactions of monomer RO₂•, and some dimers
611 can undergo secondary oxidation by NO₃. Some dimers were likely involved in the early growth of SOA particles.

612

613

Table 2. Major dimer and trimer families and their possible formation pathways.

Dimer/Trimer family	Possible formation pathways
$C_{20}H_{32}N_2O_x$	$C_{10}H_{16}NO_x\bullet + C_{10}H_{16}NO_x\bullet$
$C_{20}H_{33}N_3O_x / C_{20}H_{31}N_3O_x$	$C_{20}H_{32}N_2O_x + NO_3 + HO_2\bullet/RO_2\bullet$
$C_{20}H_{31}NO_x$	$C_{10}H_{16}NO_x\bullet + C_{10}H_{15}O_x\bullet$
$C_{20}H_{33}NO_x$	Unknown $C_{10}H_{16} + OH\bullet + C_{10}H_{16}NO_x\bullet$
$C_{20}H_{34}N_4O_x$	Unknown $(C_{10}H_{16}N_2O_x + OH\bullet) +$ $(C_{10}H_{16}N_2O_x + OH\bullet)$
$C_{19}H_{30}N_2O_x$	$C_{10}H_{16}NO_x\bullet + C_9H_{14}NO_x\bullet$
$C_{19}H_{31}N_3O_x$	$C_{19}H_{30}N_2O_x + NO_3 + HO_2\bullet/RO_2\bullet$
$C_{19}H_{29}NO_x$	$C_9H_{14}NO_x\bullet + C_{10}H_{15}O_x\bullet$
$C_{19}H_{31}NO_x$	Unknown $C_{10}H_{16} + OH\bullet + C_9H_{14}NO_x\bullet$
$C_{30}H_{48}N_4O_x$	$C_{20}H_{32}N_3O_x\bullet + C_{10}H_{16}NO_x\bullet$
$C_{30}H_{47}N_3O_x$	$C_{20}H_{31}N_2O_x\bullet + C_{10}H_{16}NO_x\bullet$

614

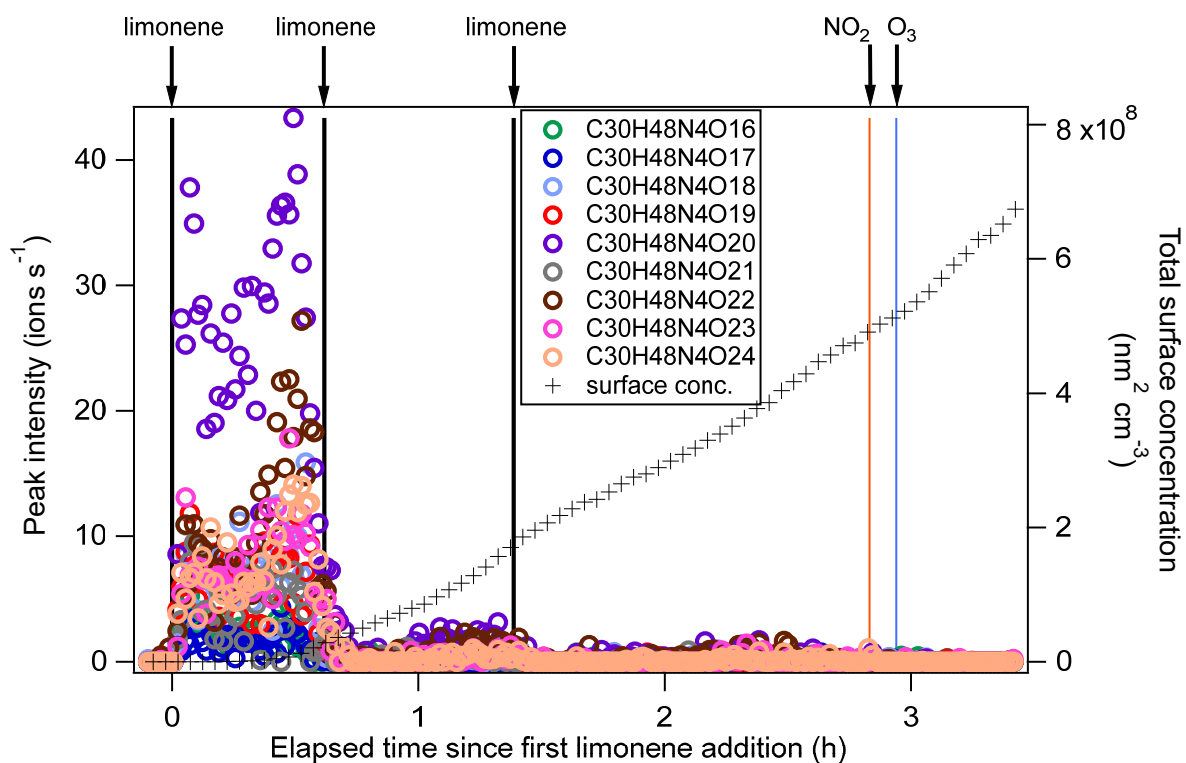
615 3.4 Trimers and their formation

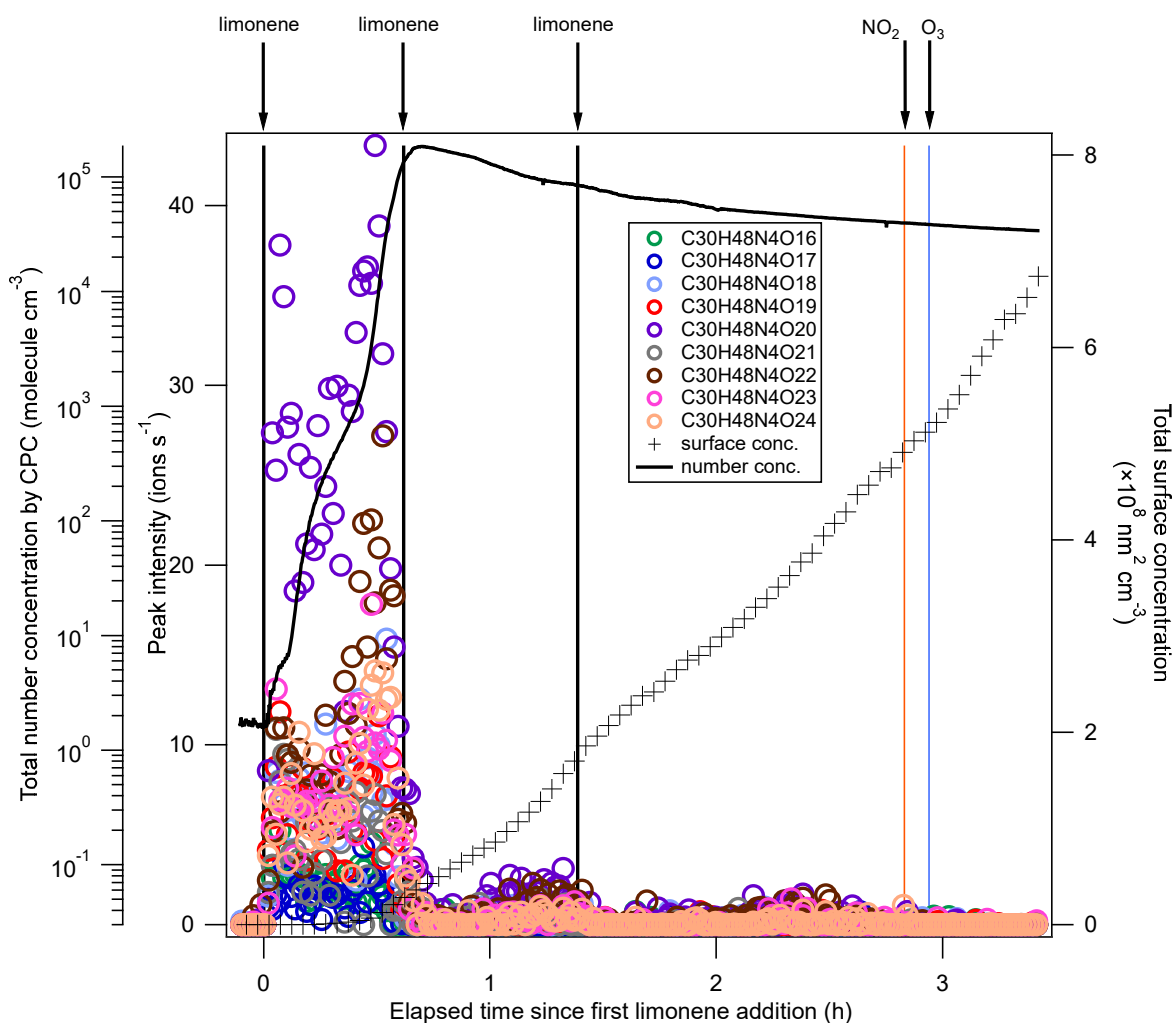
616 Trimers (C₂₆₋₃₀) were dominated by C₃₀ compounds (Fig. S12S6, Table S1). To the best of our knowledge, this is the
617 first study that identified gas-phase trimers in the limonene + NO₃ reaction. The O/C ratio of trimers were lower than
618 that of monomers and dimers, suggesting possible multiple accretion reactions in their formation pathways, which
619 lose 2 oxygen atoms in each reaction. As each accretion reaction terminates the peroxy radicals radical chain, the
620 observation of trimers also implies that some dimers could further react with NO₃, creating dimer RO₂•. The most
621 prevalent product families were C₃₀H₄₈N₄O_x (x=16-24) and C₃₀H₄₇N₃O_x (x=18,19,21,23,24), which were likely
622 formed via the most abundant monomer RO₂• radicals - C₁₀H₁₆NO_x• and the most abundant dimer RO₂ radicals -
623 C₂₀H₃₂N₃O_x• and C₂₀H₃₁N₂O_x•. Trimers from other monoterpenes + NO₃ have been observed in previous laboratory
624 studies. For example, C₃₀H₄₈N₄O₁₆ and C₃₀H₄₇N₃O₁₆ were observed in the mass spectra of α-pinene + NO₃ SOA by
625 Wu et al. (2021a), and C₃₀H₄₇N₃O₁₃ was identified in β-pinene + NO₃ SOA by Clafin and Ziemann (2018).

626 Similar to their precursors C₂₀H₃₂N₂O_x, C₃₀H₄₈N₄O_x showed negligible signal except in period P1, and presented
627 an overlaying time profile of first- and second-generation product pattern (Fig. 6). For comparison, gas-phase trimer
628 products were not observed in the β-pinene + NO₃ reaction (Shen et al., 2021), and the trimers observed in SOA from
629 β-pinene + NO₃ wereare likely formed via particle phase reactions (Clafin and Ziemann, 2018). An efficient gas-
630 phase trimer production via subsequent accretion reactions between peroxy radicals requires that the precursor dimer
631 has a high enough reactivity to create a dimer RO₂•, e.g. via NO₃ reaction to a double bond. This suggests that the
632 VOC containing at least two double bonds are likely more favorable to form trimers, which is consistent with our
633 previous findings that trimers were formed in the NO₃ reaction with isoprene which also contains two double bonds

634 (Zhao et al., 2021) while they were not observed in the reaction of NO_3 with β -pinene which contains only one double
635 bond (Shen et al., 2021).

636





638

639 Figure 6. Time series of peak intensity of the $C_{30}H_{48}N_4O_x$ family compounds during the periods P1 to P3. The solid
 640 black line refers to total number concentrations detected by CPC. The cross markers (right y-axis) indicate total
 641 particle surface concentration.

642

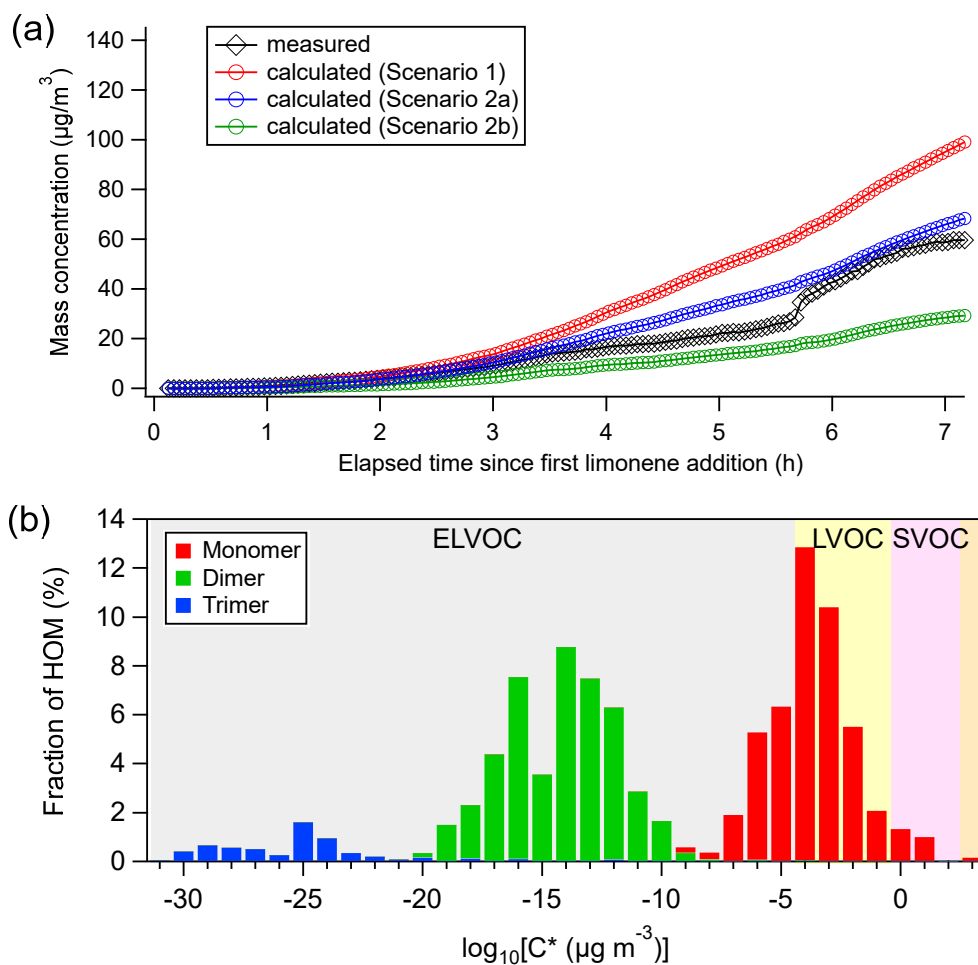
643 3.5 “Primary” incremental HOM yields

644 We chose period P1 for the calculation of HOM yields in order to minimize the influence of the condensational sink
 645 on HOM concentration. However, both first-generation and second-generation products existed in this period, as
 646 discussed in Sect. 3.2 through 3.4 and supported by the time-behavior of the total HOM concentration (Fig. [S13S15](#)).
 647 Period P1 can be roughly divided into three phases based on the trend-of-trends in HOM concentration. Shortly after
 648 the limonene injection, large quantities of HOM were produced (first-production phase) followed by a steady/balanced
 649 intermediate phase when HOM concentrations stopped increasing. After the intermediate phase, HOM concentrations
 650 began to increase again (second-production phase). The first-production phase overlapped with the time span where
 651 limonene, NO_3 and N_2O_5 concentrations decreased, implying the dominance of first-generation HOM production
 652 process. During the second production period, wall loss was compensated by second-generation HOM formation,
 653 leading to another rise of the total HOM concentrations. Therefore, we use the first-production phase to estimate

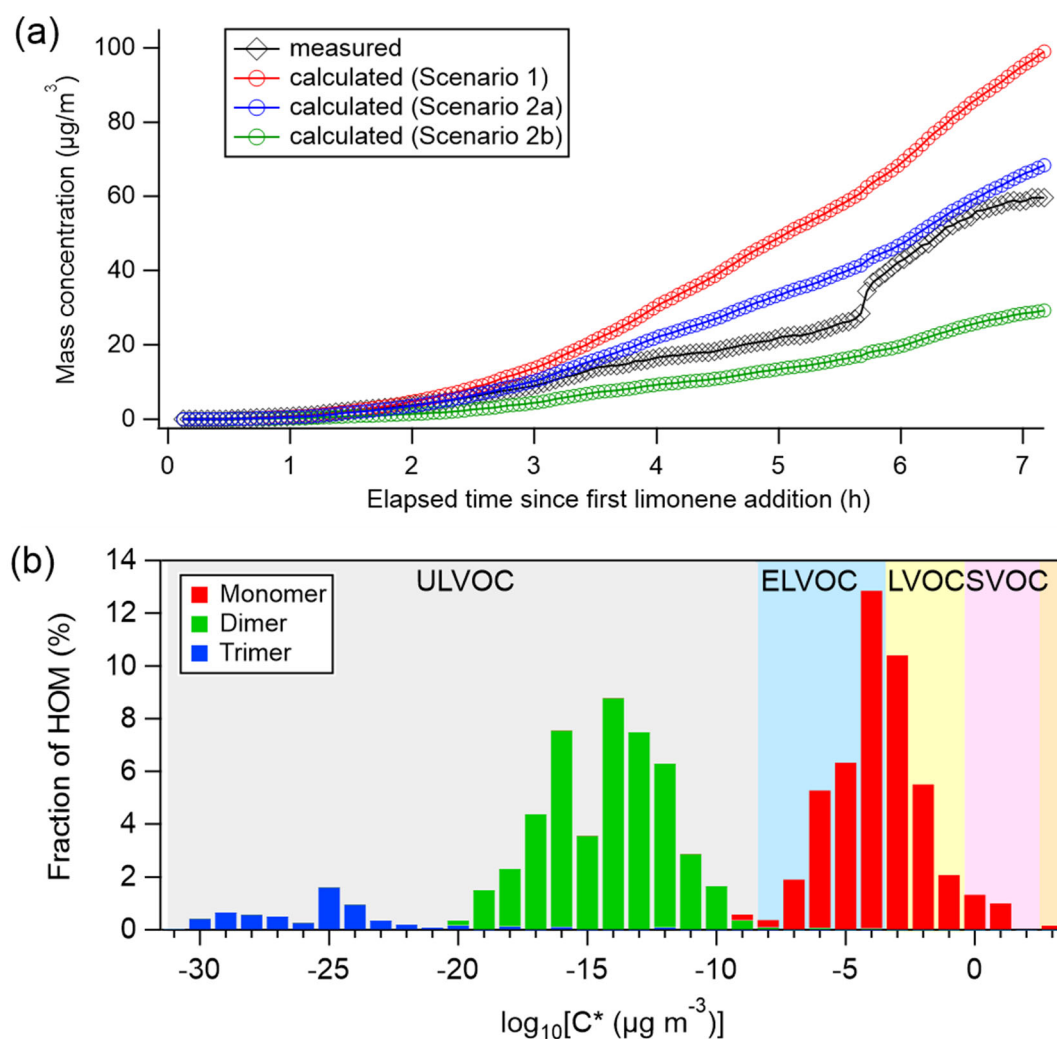
654 primary HOM production, determined over the first 3 min of the experiment. The calculated “primary” HOM molar
 655 yield is 1.5 %^{+1.7%}_{-0.7%}. This value is significantly lower than the HOM yield of 5 to 17 % in earlier limonene ozonolysis
 656 experiments (Ehn et al., 2014; Jokinen et al., 2015; Pagonis et al., 2019). It should be ~~noted~~emphasized that second-
 657 generation HOM₂ which contributed greatly to the limonene + NO₃ reaction system₂ is not included in this primary
 658 HOM yield.

659

660 3.6 Contribution of HOM to particle formation and growth



661



662

663 Figure 7. (a) Comparison of measured particle concentrations (black) ~~with~~against those predicted from
 664 condensation of measured HOM on aerosol particles, where red markers were calculated under Scenario 1, blue
 665 and green markers were calculated under Scenario 2 (only considering the condensation of ULVOC, ELVOC and
 666 LVOC)), with the volatility calculated using the method by Mohr et al. (2019) (Scenario 2a) and Peräkylä et al.
 667 (2020) (Scenario 2b) respectively. (b) HOM volatility distribution using formula provided by Mohr et al. (2019).
 668 Average concentrations of HOM in the P1 period were used to calculate the fraction of HOM.

669

670 We observed nucleation and growth of SOA particles in the limonene + NO₃ reaction. We calculated the contribution
 671 of HOM to SOA formation and particle growth and compared it to the measured particle growth (Fig. 7a). We
 672 assumed different scenarios of HOM uptake on aerosol particles, using the calculation ~~method~~methods described in
 673 the literature (Ehn et al., 2014; Seinfeld and Pandis, 2006; Nieminen et al., 2010). The assumption that all HOM
 674 irreversibly condense on the particles (Scenario 1) resulted in a strong overestimation of particle mass growth (red
 675 markers in Fig. 7a). Applying the ~~parameterizations~~parameterizations of Mohr et al. (2019) (Scenario 2a) or Peräkylä
 676 et al. (2020) (Scenario 2b) for classification and accounting only LVOC- and ULVOC/ELVOC-HOM for irreversible

677 uptake framed the observed values (blue and green markers in Fig. 7a). While Scenario 2a agreed quite well with the
678 observations and only slightly overestimated SOA ~~concentration~~concentrations after 7 h by +11%, Scenario 2b
679 underestimated the SOA concentration at the end by -53%. The agreement between the modeled and observed SOA
680 concentration suggests that HOM, ~~especially~~and particularly LVOC- and ULVOC/ELVOC-HOM play a major role
681 in ~~SOA~~growth of SOA particles in this study. According to This is consistent with the work by Faxon et al. (2018),
682 who found that many of the dimers are ELVOC ~~due to their partitioning behavior. This is consistent with, which is~~
683 also supported by our calculation result based on the method of Mohr et al. (2019).

684 ~~—— We observed nucleation and SOA growth in the limonene + NO₃ reaction.~~ Since neither SO₂ nor H₂SO₄
685 was added in our experiment, new particle formation (NPF) could be attributed to the nucleation initiated by HOM
686 of low volatility. HOM trimers with as many as 30 carbon atoms were identified in the early stage of this study, and
687 their sudden loss matched the ~~time when onset of~~ rapid formation of SOA ~~occurred~~. Trimers identified in our
688 experiment are classified as ULVOC/ELVOC, with much lower volatility than monomers and dimers (Fig. ~~7b~~7b).
689 Therefore, NPF in the current study can more likely be attributed to HOM trimers since they have the strongest
690 potential of initiating nucleation, although we cannot rule out some contributions of dimers in the NPF. In contrast,
691 in an earlier experiment investigating the NO₃-initiated oxidation of β-pinene also conducted in the SAPHIR chamber
692 under similar conditions, new particles were barely formed (<20 cm⁻³) (Shen et al., 2021). As already mentioned
693 above, no trimer HOM products were observed in that study, and only molecules with C≤20 were detected (Sect. ~~3.4~~).
694 Therefore, NPF in our study was likely attributed to HOM trimers since they have the strongest potential of initiating
695 nucleation due to their much lower volatility compared to monomers and dimers.3.4). Extremely low volatile organic
696 vapors formed in α-pinene ozonolysis have been shown to induce nucleation and drive initial particle growth in the
697 atmosphere (Tröstl et al., 2016; Kirkby et al., 2016). Since our experiment of NO₃ oxidation of limonene was
698 performed under near atmospheric conditions, such NPF events induced by the oxidation of limonene by NO₃ could
699 also occur in the ambient atmosphere. Although monoterpene concentrations in this study (0-0.92 ppbv) are higher
700 than in most ambient regions, they are still in the range of ambient concentrations (~0.01-1 ppbv) (e.g. Coggon et al.,
701 2021; Wang et al., 2022), especially for forested regions (e.g. Xu et al., 2015; Kontkanen et al., 2016; Janson, 1992).
702 Assuming that dimers react with NO₃ at a rate similar to limonene, and that they have a condensation sink similar to
703 H₂SO₄ (10⁻³-10⁻¹ s⁻¹) (Dada et al., 2020), the lifetime with respect to NO₃ at an NO₃ concentration of 5-300 ppt and
704 to condensation on particles are ~0.1-10 min and ~0.1-20 min, respectively. Therefore, although aerosols may
705 scavenge HOM dimers in the ambient atmosphere, dimers can still react with NO₃ at nighttime, forming trimers.
706 Such reactions are particularly important when the ambient aerosol concentration is low. Several field observations
707 have shown NPF events taking place at nighttime where biogenic emissions dominate (Kammer et al., 2018; Huang
708 et al., 2019). The work by Ortega et al. (2012) demonstrated an important role of monoterpene ~~ozonolysis~~ozonolysis
709 products in nocturnal NPF events in chamber experiments. In a previous laboratory study, limonene + NO₃ appears
710 more effective at initiating nucleation than the limonene + O₃ reaction (Fry et al., 2014), which supports that limonene
711 + NO₃ can play a significant role in nighttime nucleation. Our study suggests that NO₃ oxidation of limonene could

712 contribute to the nighttime NPF via HOM trimer formation. In contrast, we infer that NO₃ reactions with other
713 monoterpenes containing only one double bond such as α-pinene and β-pinene are less likely candidates for nighttime
714 NPF, because gas-phase trimers are not observed.

715

716 **4 Conclusion and implications**

717 HOM formation in the reaction of limonene with NO₃ was investigated in the SAPHIR chamber. About 280 gas-
718 phase HOM products were identified, including monomers (C₆₋₁₀, O₆₋₁₆, N₀₋₃), dimers (C₁₇₋₂₀, O₇₋₂₀, N₀₋₄) and trimers
719 (C₂₇₋₃₀, O₁₆₋₂₅, N₁₋₆). Nitrogen-containing products dominated the HOM, with compounds of the C₁₀H₁₅₋₁₇NO₆₋₁₄
720 series being the most prevalent. Dimers contributed 47 % in the early stage of the experiment when ~~new-particle~~
721 ~~formation (NPF) had not occurred yet, surface concentration was rather low (< 6×10⁴ nm² cm⁻³),~~ which was similar
722 to monomers (47 %). Tentative formation pathways of major families were proposed in this work based on their time-
723 dependent concentration profiles.

724 In HOM monomers, the abundance of carbonyl compounds significantly exceeded that of ~~hydroxyhydroxy~~ or
725 hydroperoxy compounds, indicating the significance of unimolecular termination of HOM-RO₂ radicals. Both RO₂•
726 autoxidation and alkoxy-peroxy pathways were found to be important in the formation of HOM monomers.
727 Monomers with 1 nitrogen atom (1N-monomers) contained both first- and second-generation products, which could
728 be formed via NO₃ oxidation of limonene and its first-generation products with the latter being more important.
729 Monomers with 2 nitrogen atoms were classified as second-generation products, which could be formed via NO₃
730 oxidation of the remaining C=C double bond of 1N-monomers.

731 Dimers showed both first- and second-generation time pattern. Dimers were mostly formed via accretion
732 reactions between monomer RO₂ radicals, resulting in a decrease in O/C ratio compared to monomers. The initial
733 less oxygenated RO₂• ~~such as C₁₀H₁₆O₅•, including the C₁₀H₁₆NO₅• radical that cannot be observed in our instrument,~~
734 likely played an important role in dimer formation based on the comparison of ~~measured dimers against~~ expected
735 dimer identity and concentrations according to accretion monomer RO₂• reactions ~~with measured ones.~~ Trimers were
736 likely formed via accretion reactions between monomer RO₂ and dimer RO₂ radicals ~~formed from secondary~~
737 ~~reactions of dimers with NO₃.~~ Trimer formation is ~~attributed~~ ~~thus linked~~ to the ~~presence of~~ two double bonds in
738 limonene, ~~of which~~ ~~can~~ ~~the~~ first ~~react~~ ~~reacts~~ with NO₃ leading to dimer products ~~with~~ ~~while the~~ remaining C=C double
739 bond, ~~thus providing provides a~~ reactive site for further oxidation ~~of the dimers~~ by NO₃, forming dimer RO₂ radicals.

740 ~~A “primary” HOM molar yield of 1.5 %^{+1.7%}_{-0.7%} in the limonene + NO₃ reaction was estimated, including only the~~
741 ~~first-generation HOM. Second-generation HOM contributed greatly to monomers, dimers and trimers, and hence the~~
742 ~~HOM yield we obtained is a lower limit of the total HOM yield, and is likewise much lower than the total HOM yield~~
743 ~~in the reaction of limonene with ozone (5 to 17 %) (Ehn et al., 2014; Jokinen et al., 2015; Pagonis et al., 2019).~~

744 NPF observed in this work was likely related to the trimer formation due to much lower volatility of trimers
745 compared to monomers and dimers. The SOA concentration in the limonene + NO₃ reaction could be explained by
746 the condensation of the HOM belonging to LVOC and ULVOC/ELVOC classes assuming irreversible uptake,

747 ~~suggesting the~~indicating an important role of HOM for ~~SOA-growth~~ of SOA particles in this reaction system.

748 A ~~“primary” HOM molar yield of 1.5 %^{+1.7%}_{-0.7%}~~ in the limonene + NO₃ reaction was estimated, which is much
749 ~~lower than the total HOM yield in the reaction of limonene with ozone (5 to 17 %)~~. It is worth noting that only first-
750 ~~generation HOM were taken into consideration in our calculation of HOM yield, while second-generation HOM~~
751 ~~contributed greatly to monomers, dimers and trimers, and hence the HOM yield we obtained is a lower limit of the~~
752 ~~total HOM yield.~~

753 To our knowledge, this work is the first identifying trimer products from the limonene + NO₃ reaction system,
754 suggesting that limonene + NO₃ is a possible crucial source of new particles formed in nighttime biogenic emission-
755 dominated areas (Kammer et al., 2018; Huang et al., 2019). Our work highlights the need to consider the role of
756 limonene + NO₃ in NPF in models simulating nighttime aerosols formation in biogenic-emission dominated areas,
757 especially with large limonene ~~emission~~emissions. In addition, comparison with the reactions of NO₃ with isoprene
758 (Zhao et al., 2021) and other monoterpenes (Shen et al., 2021) reveals a strong dependence of HOM products on the
759 molecular structure of the VOC species in NO₃-initiated chemistry.

760 The concentration of limonene and NO₃ in this study were on the order of few ppb and ~~~100~~a few to one hundred
761 ppt, respectively, which ~~is~~are similar to the ambient levels in rural and forest regions affected by anthropogenic
762 emissions (Brown and Stutz, 2012). The chemical lifetime of ~~NO₃RO₂•~~ was ~~on~~of the order of 50 to 500 s, which is
763 also similar to ambient conditions at nighttime (Fry et al., 2018). The RO₂• loss pathway in our study was dominated
764 by the reactions RO₂• + NO₃ and ~~of~~RO₂• + RO₂•, which is ~~representative~~relevant for the RO₂• fate in urban areas
765 and forested areas influenced by an urban plume at nighttime. However, in more pristine forested regions, the RO₂•
766 fate is mostly determined by RO₂• + HO₂ and RO₂• + RO₂•, as shown by Bates et al. (2022); for the example of a
767 Southeast US forest. As NO₃ concentration is generally enhanced with increased anthropogenic emissions, RO₂• +
768 NO₃ will become more important going from remote to urban areas. Therefore, the HOM products and their formation
769 process in our study are ~~representative~~relevant for rural and forested regions influenced by anthropogenic
770 ~~plume~~plumes and ambient urban regions with high volatile commercial products emissions as limonene is a typical
771 component of volatile chemical products (VCP) (Nazaroff and Weschler, 2004). In these regions, HOM from
772 monoterpene + NO₃ reactions can be major components of nighttime SOA. As nitrooxy-RO₂ fate can strongly affect
773 the oxidation product distribution and SOA yield as shown for the reaction of α -pinene with NO₃ (Bates et al., 2022),
774 more studies of HOM formation by NO₃ at various RO₂• fates are needed to be representative of various environment
775 including (remote) forested regions.

776 This study also highlights the important role of second-generation chemistry in HOM formation, which needs
777 to be further investigated and should be included in chemical mechanism used in numerical models. Additional work
778 is also needed to investigate the role of different HOM formed via NO₃-initiated BVOC oxidation reactions in NPF
779 and ~~SOA-growth~~ of SOA particles in order to better constrain the climatic and environmental effects of BVOC + NO₃
780 chemistry.

781

782 Acknowledgement

783 Y. Guo, H. Shen, H. Luo, and D. Zhao would like to thank the funding support of Science and Technology
784 Commission of Shanghai Municipality (No. 20230711400), National Natural Science Foundation of China (No.
785 41875145), and Shanghai International Science and Technology Partnership Project (No. 21230780200). Sungah
786 Kang, Astrid Kiendler-Scharr, and Thomas F. Mentel acknowledge the support by the EU Project FORCeS (grant
787 agreement no. 821205).

788 **References**

- 789 Ayres, B. R., Allen, H. M., Draper, D. C., Brown, S. S., Wild, R. J., Jimenez, J. L., Day, D. A., Campuzano-Jost, P., Hu, W.,
790 de Gouw, J., Koss, A., Cohen, R. C., Duffey, K. C., Romer, P., Baumann, K., Edgerton, E., Takahama, S., Thornton,
791 J. A., Lee, B. H., Lopez-Hilfiker, F. D., Mohr, C., Wennberg, P. O., Nguyen, T. B., Teng, A., Goldstein, A. H.,
792 Olson, K., and Fry, J. L.: Organic nitrate aerosol formation via NO_3 + biogenic volatile organic compounds in the
793 southeastern United States, *Atmos. Chem. Phys.*, 15, 13377-13392, 10.5194/acp-15-13377-2015, 2015.
- 794 Bates, K. H., Burke, G. J. P., Cope, J. D., and Nguyen, T. B.: Secondary organic aerosol and organic nitrogen yields from
795 the nitrate radical (NO_3) oxidation of alpha-pinene from various RO_2 fates, *Atmos. Chem. Phys.*, 22, 1467-1482,
796 10.5194/acp-22-1467-2022, 2022.
- 797 Beaver, M. R., Clair, J. M. S., Paulot, F., Spencer, K. M., Crouse, J. D., LaFranchi, B. W., Min, K. E., Pusede, S. E.,
798 Wooldridge, P. J., Schade, G. W., Park, C., Cohen, R. C., and Wennberg, P. O.: Importance of biogenic precursors
799 to the budget of organic nitrates: observations of multifunctional organic nitrates by CIMS and TD-LIF during
800 BEARPEX 2009, *Atmos. Chem. Phys.*, 12, 5773-5785, 10.5194/acp-12-5773-2012, 2012.
- 801 Bell, D. M., Wu, C., Bertrand, A., Graham, E., Schoonbaert, J., Giannoukos, S., Baltensperger, U., Prevot, A. S. H., Riipinen,
802 I., El Haddad, I., and Mohr, C.: Particle-phase processing of α -pinene NO_3 secondary organic aerosol in the dark,
803 *Atmos. Chem. Phys. Discuss.*, 2021, 1-28, 10.5194/acp-2021-379, 2021.
- 804 Berkemeier, T., Takeuchi, M., Eris, G., and Ng, N. L.: Kinetic modeling of formation and evaporation of secondary organic
805 aerosol from NO_3 oxidation of pure and mixed monoterpenes, *Atmos. Chem. Phys.*, 20, 15513-15535,
806 10.5194/acp-20-15513-2020, 2020.
- 807 Berndt, T., Mender, B., Scholz, W., Fischer, L., Herrmann, H., Kulmala, M., and Hansel, A.: Accretion Product Formation
808 from Ozonolysis and OH Radical Reaction of α -Pinene: Mechanistic Insight and the Influence of Isoprene and
809 Ethylene, *Environ. Sci. Technol.*, 52, 11069-11077, 10.1021/acs.est.8b02210, 2018a.
- 810 Berndt, T., Scholz, W., Mentler, B., Fischer, L., Herrmann, H., Kulmala, M., and Hansel, A.: Accretion Product Formation
811 from Self- and Cross-Reactions of RO_2 Radicals in the Atmosphere, *Angew. Chem. Int. Edit.*, 57, 3820-3824,
812 10.1002/anie.201710989, 2018b.
- 813 Bianchi, F., Kurtén, T., Riva, M., Mohr, C., Rissanen, M. P., Roldin, P., Berndt, T., Crouse, J. D., Wennberg, P. O., Mentel,
814 T. F., Wildt, J., Junninen, H., Jokinen, T., Kulmala, M., Worsnop, D. R., Thornton, J. A., Donahue, N., Kjaergaard,
815 H. G., and Ehn, M.: Highly Oxygenated Organic Molecules (HOM) from Gas-Phase Autoxidation Involving
816 Peroxy Radicals: A Key Contributor to Atmospheric Aerosol, *Chem. Rev.*, 119, 3472-3509,
817 10.1021/acs.chemrev.8b00395, 2019.
- 818 Boyd, C. M., Nah, T., Xu, L., Berkemeier, T., and Ng, N. L.: Secondary Organic Aerosol (SOA) from Nitrate Radical
819 Oxidation of Monoterpenes: Effects of Temperature, Dilution, and Humidity on Aerosol Formation, Mixing, and
820 Evaporation, *Environ. Sci. Technol.*, 51, 7831-7841, 10.1021/acs.est.7b01460, 2017.
- 821 Boyd, C. M., Sanchez, J., Xu, L., Eugene, A. J., Nah, T., Tuet, W. Y., Guzman, M. I., and Ng, N. L.: Secondary organic
822 aerosol formation from the β -pinene+ NO_3 system: effect of humidity and peroxy radical fate, *Atmos. Chem. Phys.*,
823 15, 7497-7522, 10.5194/acp-15-7497-2015, 2015.
- 824 Brown, S. S. and Stutz, J.: Nighttime radical observations and chemistry, *Chem. Soc. Rev.*, 41, 6405-6447,
825 10.1039/c2cs35181a, 2012.
- 826 Carslaw, N., Mota, T., Jenkin, M. E., Barley, M. H., and McFiggans, G.: A significant role for nitrate and peroxide groups
827 on indoor secondary organic aerosol, *Environ. Sci. Technol.*, 46, 9290-9298, 10.1021/es301350x, 2012.
- 828 Chen, Y., Takeuchi, M., Nah, T., Xu, L., Canagaratna, M. R., Stark, H., Baumann, K., Canonaco, F., Prévôt, A. S. H., Huey,
829 L. G., Weber, R. J., and Ng, N. L.: Chemical characterization of secondary organic aerosol at a rural site in the
830 southeastern US: insights from simultaneous high-resolution time-of-flight aerosol mass spectrometer (HR-ToF-
831 AMS) and FIGAERO chemical ionization mass spectrometer (CIMS) measurements, *Atmos. Chem. Phys.*, 20,

832 8421-8440, 10.5194/acp-20-8421-2020, 2020.

833 Claflin, M. S. and Ziemann, P. J.: Identification and Quantitation of Aerosol Products of the Reaction of β -Pinene with NO_3
834 Radicals and Implications for Gas- and Particle-Phase Reaction Mechanisms, *J. Phys. Chem. A*, 122, 3640-3652,
835 10.1021/acs.jpca.8b00692, 2018.

836 Clausen, P. A., Wilkins, C. K., Wolkoff, P., and Nielsen, G. D.: Chemical and biological evaluation of a reaction mixture
837 of R-(+)-limonene/ozone - Formation of strong airway irritants, *Environ. Int.*, 26, 511-522, 10.1016/s0160-
838 4120(01)00035-6, 2001.

839 Coggon, M. M., Gkatzelis, G. I., McDonald, B. C., Gilman, J. B., Schwantes, R. H., Abuhassan, N., Aikin, K. C., Arend,
840 M. F., Berkoff, T. A., Brown, S. S., Campos, T. L., Dickerson, R. R., Gronoff, G., Hurley, J. F., Isaacman-VanWertz,
841 G., Koss, A. R., Li, M., McKeen, S. A., Moshary, F., Peischl, J., Pospisilova, V., Ren, X., Wilson, A., Wu, Y.,
842 Trainer, M., and Warneke, C.: Volatile chemical product emissions enhance ozone and modulate urban chemistry,
843 *Proc. Nat. Acad. Sci. U.S.A.*, 118, 10.1073/pnas.2026653118, 2021.

844 Crounse, J. D., Nielsen, L. B., Jørgensen, S., Kjaergaard, H. G., and Wennberg, P. O.: Autoxidation of Organic Compounds
845 in the Atmosphere, *J. Phys. Chem. Lett.*, 4, 3513-3520, 10.1021/jz4019207, 2013.

846 Dada, L., Ylivinkka, I., Baalbaki, R., Li, C., Guo, Y., Yan, C., Yao, L., Sarnela, N., Jokinen, T., Daellenbach, K. R., Yin, R.,
847 Deng, C., Chu, B., Nieminen, T., Wang, Y., Lin, Z., Thakur, R. C., Kontkanen, J., Stolzenburg, D., Sipilä, M.,
848 Hussein, T., Paasonen, P., Bianchi, F., Salma, I., Weidinger, T., Pikridas, M., Sciare, J., Jiang, J., Liu, Y., Petäjä,
849 T., Kerminen, V.-M., and Kulmala, M.: Sources and sinks driving sulfuric acid concentrations in contrasting
850 environments: implications on proxy calculations, *Atmos. Chem. Phys.*, 20, 11747-11766, 10.5194/acp-20-11747-
851 2020, 2020.

852 Dam, M., Draper, D. C., Marsavin, A., Fry, J. L., and Smith, J. N.: Observations of gas-phase products from the nitrate-
853 radical-initiated oxidation of four monoterpenes, *Atmos. Chem. Phys.*, 22, 9017-9031, 10.5194/acp-22-9017-2022,
854 2022.

855 Donahue, N. M., Epstein, S. A., Pandis, S. N., and Robinson, A. L.: A two-dimensional volatility basis set: 1. organic-
856 aerosol mixing thermodynamics, *Atmos. Chem. Phys.*, 11, 3303-3318, 10.5194/acp-11-3303-2011, 2011.

857 Donahue, N. M., Kroll, J. H., Pandis, S. N., and Robinson, A. L.: A two-dimensional volatility basis set – Part 2: Diagnostics
858 of organic-aerosol evolution, *Atmos. Chem. Phys.*, 12, 615-634, 10.5194/acp-12-615-2012, 2012.

859 Ehn, M., Thornton, J. A., Kleist, E., Sipilä, M., Junninen, H., Pullinen, I., Springer, M., Rubach, F., Tillmann, R., Lee, B.,
860 Lopez-Hilfiker, F., Andres, S., Acir, I. H., Rissanen, M., Jokinen, T., Schobesberger, S., Kangasluoma, J.,
861 Kontkanen, J., Nieminen, T., Kurtén, T., Nielsen, L. B., Jørgensen, S., Kjaergaard, H. G., Canagaratna, M., Dal
862 Maso, M., Berndt, T., Petäjä, T., Wahner, A., Kerminen, V. M., Kulmala, M., Worsnop, D. R., Wildt, J., and Mentel,
863 T. F.: A large source of low-volatility secondary organic aerosol, *Nature*, 506, 476-485, 10.1038/nature13032,
864 2014.

865 Eisele, F. L. and Tanner, D. J.: Measurement of the gas phase concentration of H_2SO_4 and methane sulfonic acid and
866 estimates of H_2SO_4 production and loss in the atmosphere, *J. Geophys. Res.-Atmos.*, 98, 9001-9010,
867 10.1029/93jd00031, 1993.

868 Fan, Z. H., Liou, P., Weschler, C., Fiedler, N., Kipen, H., and Zhang, J. F.: Ozone-initiated reactions with mixtures of
869 volatile organic compounds under simulated indoor conditions, *Environ. Sci. Technol.*, 37, 1811-1821,
870 10.1021/es026231i, 2003.

871 Faxon, C., Hammes, J., Le Breton, M., Pathak, R. K., and Hallquist, M.: Characterization of organic nitrate constituents of
872 secondary organic aerosol (SOA) from nitrate-radical-initiated oxidation of limonene using high-resolution
873 chemical ionization mass spectrometry, *Atmos. Chem. Phys.*, 18, 5467-5481, 10.5194/acp-18-5467-2018, 2018.

874 Finlayson-Pitts, B. J. and Pitts, J. N.: Tropospheric air pollution: Ozone, airborne toxics, polycyclic aromatic hydrocarbons,
875 and particles, *Science*, 276, 1045-1052, 10.1126/science.276.5315.1045, 1997.

876 Fry, J. L., Draper, D. C., Barsanti, K. C., Smith, J. N., Ortega, J., Winkler, P. M., Lawler, M. J., Brown, S. S., Edwards, P.
877 M., Cohen, R. C., and Lee, L.: Secondary organic aerosol formation and organic nitrate yield from NO₃ oxidation
878 of biogenic hydrocarbons, *Environ. Sci. Technol.*, 48, 11944-11953, 10.1021/es502204x, 2014.

879 Fry, J. L., Kiendler-Scharr, A., Rollins, A. W., Wooldridge, P. J., Brown, S. S., Fuchs, H., Dubé, W., Mensah, A., dal Maso,
880 M., Tillmann, R., Dorn, H. P., Brauers, T., and Cohen, R. C.: Organic nitrate and secondary organic aerosol yield
881 from NO₃ oxidation of β-pinene evaluated using a gas-phase kinetics/aerosol partitioning model, *Atmos. Chem.
882 Phys.*, 9, 1431-1449, 10.5194/acp-9-1431-2009, 2009.

883 Fry, J. L., Kiendler-Scharr, A., Rollins, A. W., Brauers, T., Brown, S. S., Dorn, H. P., Dubé, W. P., Fuchs, H., Mensah, A.,
884 Rohrer, F., Tillmann, R., Wahner, A., Wooldridge, P. J., and Cohen, R. C.: SOA from limonene: role of NO₃ in its
885 generation and degradation, *Atmos. Chem. Phys.*, 11, 3879-3894, 10.5194/acp-11-3879-2011, 2011.

886 Fry, J. L., Draper, D. C., Zarzana, K. J., Campuzano-Jost, P., Day, D. A., Jimenez, J. L., Brown, S. S., Cohen, R. C., Kaser,
887 L., Hansel, A., Cappellin, L., Karl, T., Hodzic Roux, A., Turnipseed, A., Cantrell, C., Lefer, B. L., and Grossberg,
888 N.: Observations of gas- and aerosol-phase organic nitrates at BEACHON-RoMBAS 2011, *Atmos. Chem. Phys.*,
889 13, 8585-8605, 10.5194/acp-13-8585-2013, 2013.

890 Fry, J. L., Brown, S. S., Middlebrook, A. M., Edwards, P. M., Campuzano-Jost, P., Day, D. A., Jimenez, J. L., Allen, H. M.,
891 Ryerson, T. B., Pollack, I., Graus, M., Warneke, C., de Gouw, J. A., Brock, C. A., Gilman, J., Lerner, B. M., Dubé,
892 W. P., Liao, J., and Welti, A.: Secondary organic aerosol (SOA) yields from NO₃ radical + isoprene based on
893 nighttime aircraft power plant plume transects, *Atmos. Chem. Phys.*, 18, 11663-11682, 10.5194/acp-18-11663-
894 2018, 2018.

895 Fuchs, H., Hofzumahaus, A., Rohrer, F., Bohn, B., Brauers, T., Dorn, H. P., Häsel, R., Holland, F., Kaminski, M., Li, X.,
896 Lu, K., Nehr, S., Tillmann, R., Wegener, R., and Wahner, A.: Experimental evidence for efficient hydroxyl radical
897 regeneration in isoprene oxidation, *Nat. Geosci.*, 6, 1023-1026, 10.1038/ngeo1964, 2013.

898 Fuchs, N. A. and Sutugin, A. G.: *Topics in Current Aerosol Research (Part 2)*, Pergamon, New York, 1971.

899 Gkatzelis, G. I., Coggon, M. M., McDonald, B. C., Peischl, J., Aikin, K. C., Gilman, J. B., Trainer, M., and Warneke, C.:
900 Identifying Volatile Chemical Product Tracer Compounds in U.S. Cities, *Environ. Sci. Technol.*, 55, 188-199,
901 10.1021/acs.est.0c05467, 2021.

902 Guenther, A. B., Jiang, X., Heald, C. L., Sakulyanontvittaya, T., Duhl, T., Emmons, L. K., and Wang, X.: The Model of
903 Emissions of Gases and Aerosols from Nature version 2.1 (MEGAN2.1): an extended and updated framework for
904 modeling biogenic emissions, *Geosci. Model Dev.*, 5, 1471-1492, 10.5194/gmd-5-1471-2012, 2012.

905 Hallquist, M., Wängberg, I., Ljungström, E., Barnes, I., and Becker, K. H.: Aerosol and product yields from NO₃ radical-
906 initiated oxidation of selected monoterpenes, *Environ. Sci. Technol.*, 33, 553-559, 10.1021/es980292s, 1999.

907 Hallquist, M., Wenger, J. C., Baltensperger, U., Rudich, Y., Simpson, D., Claeys, M., Dommen, J., Donahue, N. M., George,
908 C., Goldstein, A. H., Hamilton, J. F., Herrmann, H., Hoffmann, T., Iinuma, Y., Jang, M., Jenkin, M. E., Jimenez,
909 J. L., Kiendler-Scharr, A., Maenhaut, W., McFiggans, G., Mentel, T. F., Monod, A., Prévôt, A. S. H., Seinfeld, J.
910 H., Surratt, J. D., Szmigielski, R., and Wildt, J.: The formation, properties and impact of secondary organic aerosol:
911 current and emerging issues, *Atmos. Chem. Phys.*, 9, 5155-5236, 10.5194/acp-9-5155-2009, 2009.

912 Huang, W., Saathoff, H., Shen, X., Ramisetty, R., Leisner, T., and Mohr, C.: Chemical Characterization of Highly
913 Functionalized Organonitrates Contributing to Night-Time Organic Aerosol Mass Loadings and Particle Growth,
914 *Environ. Sci. Technol.*, 53, 1165-1174, 10.1021/acs.est.8b05826, 2019.

915 Hyttinen, N., Kupiainen-Määttä, O., Rissanen, M. P., Muuronen, M., Ehn, M., and Kurtén, T.: Modeling the Charging of
916 Highly Oxidized Cyclohexene Ozonolysis Products Using Nitrate-Based Chemical Ionization, *J. Phys. Chem. A*,
917 119, 6339-6345, 10.1021/acs.jpca.5b01818, 2015.

918 Janson, R.: Monoterpene concentrations in and above a forest of scots pine, *J. Atmos. Chem.*, 14, 385-394,
919 10.1007/bf00115246, 1992.

920 Jenkin, M. E., Saunders, S. M., and Pilling, M. J.: The tropospheric degradation of volatile organic compounds: A protocol
 921 for mechanism development, *Atmos. Environ.*, 31, 81-104, 10.1016/s1352-2310(96)00105-7, 1997.

922 Jiang, L., Wang, W., and Xu, Y. S.: Theoretical investigation of the NO₃ radical addition to double bonds of limonene, *Int.*
 923 *J. Mol. Sci.*, 10, 3743-3754, 10.3390/ijms10093743, 2009.

924 Jokinen, T., Sipilä, M., Junninen, H., Ehn, M., Lönn, G., Hakala, J., Petäjä, T., Mauldin, R. L., Kulmala, M., and Worsnop,
 925 D. R.: Atmospheric sulphuric acid and neutral cluster measurements using CI-API-TOF, *Atmos. Chem. Phys.*, 12,
 926 4117-4125, 10.5194/acp-12-4117-2012, 2012.

927 Jokinen, T., Berndt, T., Makkonen, R., Kerminen, V. M., Junninen, H., Paasonen, P., Stratmann, F., Herrmann, H., Guenther,
 928 A. B., Worsnop, D. R., Kulmala, M., Ehn, M., and Sipilä, M.: Production of extremely low volatile organic
 929 compounds from biogenic emissions: Measured yields and atmospheric implications, *P. Natl. Acad. Sci. USA*,
 930 112, 7123-7128, 10.1073/pnas.1423977112, 2015.

931 Kammer, J., Perraudin, E., Flaud, P. M., Lamaud, E., Bonnefond, J. M., and Villenave, E.: Observation of nighttime new
 932 particle formation over the French Landes forest, *Sci. Total Environ.*, 621, 1084-1092,
 933 10.1016/j.scitotenv.2017.10.118, 2018.

934 Kirkby, J., Duplissy, J., Sengupta, K., Frege, C., Gordon, H., Williamson, C., Heinritzi, M., Simon, M., Yan, C., Almeida,
 935 J., Tröstl, J., Nieminen, T., Ortega, I. K., Wagner, R., Adamov, A., Amorim, A., Bernhammer, A. K., Bianchi, F.,
 936 Breitenlechner, M., Brilke, S., Chen, X., Craven, J., Dias, A., Ehrhart, S., Flagan, R. C., Franchin, A., Fuchs, C.,
 937 Guida, R., Hakala, J., Hoyle, C. R., Jokinen, T., Junninen, H., Kangasluoma, J., Kim, J., Krapf, M., Kürten, A.,
 938 Laaksonen, A., Lehtipalo, K., Makhmutov, V., Mathot, S., Molteni, U., Onnela, A., Peräkylä, O., Piel, F., Petäjä,
 939 T., Praplan, A. P., Pringle, K., Rap, A., Richards, N. A., Riipinen, I., Rissanen, M. P., Rondo, L., Sarnela, N.,
 940 Schobesberger, S., Scott, C. E., Seinfeld, J. H., Sipilä, M., Steiner, G., Stozhkov, Y., Stratmann, F., Tomé, A.,
 941 Virtanen, A., Vogel, A. L., Wagner, A. C., Wagner, P. E., Weingartner, E., Wimmer, D., Winkler, P. M., Ye, P.,
 942 Zhang, X., Hansel, A., Dommen, J., Donahue, N. M., Worsnop, D. R., Baltensperger, U., Kulmala, M., Carslaw,
 943 K. S., and Curtius, J.: Ion-induced nucleation of pure biogenic particles, *Nature*, 533, 521-526,
 944 10.1038/nature17953, 2016.

945 Klinger, L. F., Li, Q. J., Guenther, A. B., Greenberg, J. P., Baker, B., and Bai, J. H.: Assessment of volatile organic
 946 compound emissions from ecosystems of China, *J. Geophys. Res.-Atmos.*, 107, 10.1029/2001jd001076, 2002.

947 Kontkanen, J., Paasonen, P., Aalto, J., Bäck, J., Rantala, P., Petäjä, T., and Kulmala, M.: Simple proxies for estimating the
 948 concentrations of monoterpenes and their oxidation products at a boreal forest site, *Atmos. Chem. Phys.*, 16,
 949 13291-13307, 10.5194/acp-16-13291-2016, 2016.

950 Kulmala, M., Petäjä, T., Nieminen, T., Sipilä, M., Manninen, H. E., Lehtipalo, K., Dal Maso, M., Aalto, P. P., Junninen, H.,
 951 Paasonen, P., Riipinen, I., Lehtinen, K. E. J., Laaksonen, A., and Kerminen, V.-M.: Measurement of the nucleation
 952 of atmospheric aerosol particles, *Nat. Protoc.*, 7, 1651-1667, 10.1038/nprot.2012.091, 2012.

953 Kurtén, T., Møller, K. H., Nguyen, T. B., Schwantes, R. H., Misztal, P. K., Su, L., Wennberg, P. O., Fry, J. L., and Kjaergaard,
 954 H. G.: Alkoxy Radical Bond Scissions Explain the Anomalously Low Secondary Organic Aerosol and
 955 Organonitrate Yields From α -Pinene + NO₃, *J. Phys. Chem. Lett.*, 8, 2826-2834, 10.1021/acs.jpcclett.7b01038,
 956 2017.

957 Lee, B. H., Mohr, C., Lopez-Hilfiker, F. D., Lutz, A., Hallquist, M., Lee, L., Romer, P., Cohen, R. C., Iyer, S., Kurten, T.,
 958 Hu, W., Day, D. A., Campuzano-Jost, P., Jimenez, J. L., Xu, L., Ng, N. L., Guo, H., Weber, R. J., Wild, R. J.,
 959 Brown, S. S., Koss, A., de Gouw, J., Olson, K., Goldstein, A. H., Seco, R., Kim, S., McAvey, K., Shepson, P. B.,
 960 Starn, T., Baumann, K., Edgerton, E. S., Liu, J., Shilling, J. E., Miller, D. O., Brune, W., Schobesberger, S.,
 961 D'Ambro, E. L., and Thornton, J. A.: Highly functionalized organic nitrates in the southeast United States:
 962 Contribution to secondary organic aerosol and reactive nitrogen budgets, *P. Natl. Acad. Sci. USA*, 113, 1516-1521,
 963 10.1073/pnas.1508108113, 2016.

964 Liu, Y., Nie, W., Li, Y., Ge, D., Liu, C., Xu, Z., Chen, L., Wang, T., Wang, L., Sun, P., Qi, X., Wang, J., Xu, Z., Yuan, J.,
965 Yan, C., Zhang, Y., Huang, D., Wang, Z., Donahue, N. M., Worsnop, D., Chi, X., Ehn, M., and Ding, A.: Formation
966 of condensable organic vapors from anthropogenic and biogenic volatile organic compounds (VOCs) is strongly
967 perturbed by NO_x in eastern China, *Atmos. Chem. Phys.*, 21, 14789-14814, 10.5194/acp-21-14789-2021, 2021.

968 Massoli, P., Stark, H., Canagaratna, M. R., Krechmer, J. E., Xu, L., Ng, N. L., Mauldin, R. L., Yan, C., Kimmel, J., Misztal,
969 P. K., Jimenez, J. L., Jayne, J. T., and Worsnop, D. R.: Ambient Measurements of Highly Oxidized Gas-Phase
970 Molecules during the Southern Oxidant and Aerosol Study (SOAS) 2013, *ACS Earth Space Chem.*, 2, 653-672,
971 10.1021/acsearthspacechem.8b00028, 2018.

972 McDonald, B. C., de Gouw, J. A., Gilman, J. B., Jathar, S. H., Akherati, A., Cappa, C. D., Jimenez, J. L., Lee-Taylor, J.,
973 Hayes, P. L., McKeen, S. A., Cui, Y. Y., Kim, S.-W., Gentner, D. R., Isaacman-VanWertz, G., Goldstein, A. H.,
974 Harley, R. A., Frost, G. J., Roberts, J. M., Ryerson, T. B., and Trainer, M.: Volatile chemical products emerging as
975 largest petrochemical source of urban organic emissions, *Science*, 359, 760-764, 10.1126/science.aaq0524, 2018.

976 McFiggans, G., Mentel, T. F., Wildt, J., Pullinen, I., Kang, S., Kleist, E., Schmitt, S., Springer, M., Tillmann, R., Wu, C.,
977 Zhao, D. F., Hallquist, M., Faxon, C., Le Breton, M., Hallquist, A. M., Simpson, D., Bergström, R., Jenkin, M. E.,
978 Ehn, M., Thornton, J. A., Alfarra, M. R., Bannan, T. J., Percival, C. J., Priestley, M., Topping, D., and Kiendler-
979 Scharr, A.: Secondary organic aerosol reduced by mixture of atmospheric vapours, *Nature*, 565, 587-593,
980 10.1038/s41586-018-0871-y, 2019.

981 Mentel, T. F., Springer, M., Ehn, M., Kleist, E., Pullinen, I., Kurtén, T., Rissanen, M., Wahner, A., and Wildt, J.: Formation
982 of highly oxidized multifunctional compounds: autoxidation of peroxy radicals formed in the ozonolysis of
983 alkenes – deduced from structure–product relationships, *Atmos. Chem. Phys.*, 15, 6745-6765, 10.5194/acp-15-
984 6745-2015, 2015.

985 Mohr, C., Thornton, J. A., Heitto, A., Lopez-Hilfiker, F. D., Lutz, A., Riipinen, I., Hong, J., Donahue, N. M., Hallquist, M.,
986 Petäjä, T., Kulmala, M., and Yli-Juuti, T.: Molecular identification of organic vapors driving atmospheric
987 nanoparticle growth, *Nat. Commun.*, 10, 4442, <https://doi.org/10.1038/s41467-019-12473-2>, 2019.

988 Mutzel, A., Zhang, Y., Böge, O., Rodigast, M., Kolodziejczyk, A., Wang, X., and Herrmann, H.: Importance of secondary
989 organic aerosol formation of α -pinene, limonene, and m-cresol comparing day- and nighttime radical chemistry,
990 *Atmos. Chem. Phys.*, 21, 8479-8498, 10.5194/acp-21-8479-2021, 2021.

991 Nah, T., Sanchez, J., Boyd, C. M., and Ng, N. L.: Photochemical Aging of α -pinene and β -pinene Secondary Organic
992 Aerosol formed from Nitrate Radical Oxidation, *Environ. Sci. Technol.*, 50, 222-231, 10.1021/acs.est.5b04594,
993 2016.

994 Nazaroff, W. W. and Weschler, C. J.: Cleaning products and air fresheners: exposure to primary and secondary air pollutants,
995 *Atmos. Environ.*, 38, 2841-2865, 10.1016/j.atmosenv.2004.02.040, 2004.

996 Ng, N. L., Kwan, A. J., Surratt, J. D., Chan, A. W. H., Chhabra, P. S., Sorooshian, A., Pye, H. O. T., Crouse, J. D., Wennberg,
997 P. O., Flagan, R. C., and Seinfeld, J. H.: Secondary organic aerosol (SOA) formation from reaction of isoprene
998 with nitrate radicals (NO₃), *Atmos. Chem. Phys.*, 8, 4117-4140, 10.5194/acp-8-4117-2008, 2008.

999 Nie, W., Yan, C., Huang, D. D., Wang, Z., Liu, Y., Qiao, X., Guo, Y., Tian, L., Zheng, P., Xu, Z., Li, Y., Xu, Z., Qi, X., Sun,
1000 P., Wang, J., Zheng, F., Li, X., Yin, R., Dallenbach, K. R., Bianchi, F., Petäjä, T., Zhang, Y., Wang, M., Schervish,
1001 M., Wang, S., Qiao, L., Wang, Q., Zhou, M., Wang, H., Yu, C., Yao, D., Guo, H., Ye, P., Lee, S., Li, Y. J., Liu, Y.,
1002 Chi, X., Kerminen, V.-M., Ehn, M., Donahue, N. M., Wang, T., Huang, C., Kulmala, M., Worsnop, D., Jiang, J.,
1003 and Ding, A.: Secondary organic aerosol formed by condensing anthropogenic vapours over China's megacities,
1004 *Nat. Geosci.*, 15, 255-261, 10.1038/s41561-022-00922-5, 2022.

1005 Nieminen, T., Lehtinen, K. E. J., and Kulmala, M.: Sub-10 nm particle growth by vapor condensation – effects of vapor
1006 molecule size and particle thermal speed, *Atmos. Chem. Phys.*, 10, 9773-9779, 10.5194/acp-10-9773-2010, 2010.

1007 Novelli, A., Cho, C., Fuchs, H., Hofzumahaus, A., Rohrer, F., Tillmann, R., Kiendler-Scharr, A., Wahner, A., and Vereecken,

1008 L.: Experimental and theoretical study on the impact of a nitrate group on the chemistry of alkoxy radicals, *Phys.*
1009 *Chem. Chem. Phys.*, 23, 5474-5495, 10.1039/d0cp05555g, 2021.

1010 Ortega, I. K., Suni, T., Boy, M., Grönholm, T., Manninen, H. E., Nieminen, T., Ehn, M., Junninen, H., Hakola, H., Hellén,
1011 H., Valmari, T., Arvela, H., Zegelin, S., Hughes, D., Kitchen, M., Cleugh, H., Worsnop, D. R., Kulmala, M., and
1012 Kerminen, V. M.: New insights into nocturnal nucleation, *Atmos. Chem. Phys.*, 12, 4297-4312, 10.5194/acp-12-
1013 4297-2012, 2012.

1014 Pagonis, D., Algrim, L. B., Price, D. J., Day, D. A., Handschy, A. V., Stark, H., Miller, S. L., de Gouw, J. A., Jimenez, J. L.,
1015 and Ziemann, P. J.: Autoxidation of Limonene Emitted in a University Art Museum, *Environ. Sci. Tech. Let.*, 6,
1016 520-524, 10.1021/acs.estlett.9b00425, 2019.

1017 Peng, C., Wang, W., Li, K., Li, J., Zhou, L., Wang, L., and Ge, M.: The Optical Properties of Limonene Secondary Organic
1018 Aerosols: The Role of NO₃, OH, and O₃ in the Oxidation Processes, *J. Geophys. Res.-Atmos.*, 123, 3292-3303,
1019 <https://doi.org/10.1002/2017JD028090>, 2018.

1020 Peräkylä, O., Riva, M., Heikkinen, L., Quéléver, L., Roldin, P., and Ehn, M.: Experimental investigation into the volatilities
1021 of highly oxygenated organic molecules (HOMs), *Atmos. Chem. Phys.*, 20, 649-669, 10.5194/acp-20-649-2020,
1022 2020.

1023 Pullinen, I., Schmitt, S., Kang, S., Sarrafzadeh, M., Schlag, P., Andres, S., Kleist, E., Mentel, T. F., Rohrer, F., Springer, M.,
1024 Tillmann, R., Wildt, J., Wu, C., Zhao, D., Wahner, A., and Kiendler-Scharr, A.: Impact of NO_x on secondary
1025 organic aerosol (SOA) formation from α -pinene and β -pinene photooxidation: the role of highly oxygenated
1026 organic nitrates, *Atmos. Chem. Phys.*, 20, 10125-10147, 10.5194/acp-20-10125-2020, 2020.

1027 Pye, H. O. T., Chan, A. W. H., Barkley, M. P., and Seinfeld, J. H.: Global modeling of organic aerosol: the importance of
1028 reactive nitrogen (NO_x and NO₃), *Atmos. Chem. Phys.*, 10, 11261-11276, 10.5194/acp-10-11261-2010, 2010.

1029 Rissanen, M. P., Kurtén, T., Sipilä, M., Thornton, J. A., Kangasluoma, J., Sarnela, N., Junninen, H., Jørgensen, S., Schallhart,
1030 S., Kajos, M. K., Taipale, R., Springer, M., Mentel, T. F., Ruuskanen, T., Petäjä, T., Worsnop, D. R., Kjaergaard,
1031 H. G., and Ehn, M.: The formation of highly oxidized multifunctional products in the ozonolysis of cyclohexene,
1032 *J. Am. Chem. Soc.*, 136, 15596-15606, 10.1021/ja507146s, 2014.

1033 Riva, M., Rantala, P., Krechmer, J. E., Peräkylä, O., Zhang, Y., Heikkinen, L., Garmash, O., Yan, C., Kulmala, M., Worsnop,
1034 D., and Ehn, M.: Evaluating the performance of five different chemical ionization techniques for detecting gaseous
1035 oxygenated organic species, *Atmos. Meas. Tech.*, 12, 2403-2421, 10.5194/amt-12-2403-2019, 2019.

1036 Rohrer, F., Bohn, B., Brauers, T., Brüning, D., Johnen, F. J., Wahner, A., and Kleffmann, J.: Characterisation of the
1037 photolytic HONO-source in the atmosphere simulation chamber SAPHIR, *Atmos. Chem. Phys.*, 5, 2189-2201,
1038 10.5194/acp-5-2189-2005, 2005.

1039 Rollins, A. W., Browne, E. C., Min, K.-E., Pusede, S. E., Wooldridge, P. J., Gentner, D. R., Goldstein, A. H., Liu, S., Day,
1040 D. A., Russell, L. M., and Cohen, R. C.: Evidence for NO_x control over nighttime SOA formation, *Science*, 337,
1041 1210-1212, 10.1126/science.1221520, 2012.

1042 Rollins, A. W., Kiendler-Scharr, A., Fry, J. L., Brauers, T., Brown, S. S., Dorn, H. P., Dubé, W. P., Fuchs, H., Mensah, A.,
1043 Mentel, T. F., Rohrer, F., Tillmann, R., Wegener, R., Wooldridge, P. J., and Cohen, R. C.: Isoprene oxidation by
1044 nitrate radical: alkyl nitrate and secondary organic aerosol yields, *Atmos. Chem. Phys.*, 9, 6685-6703,
1045 10.5194/acp-9-6685-2009, 2009.

1046 Saunders, S. M., Jenkin, M. E., Derwent, R. G., and Pilling, M. J.: Protocol for the development of the Master Chemical
1047 Mechanism, MCM v3 (Part A): tropospheric degradation of non-aromatic volatile organic compounds, *Atmos.*
1048 *Chem. Phys.*, 3, 161-180, 2003a.

1049 Saunders, S. M., Jenkin, M. E., Derwent, R. G., and Pilling, M. J.: Protocol for the development of the Master Chemical
1050 Mechanism, MCM v3 (Part A): tropospheric degradation of non-aromatic volatile organic compounds, *Atmos.*
1051 *Chem. Phys.*, 3, 161-180, 10.5194/acp-3-161-2003, 2003b.

- 1052 Schervish, M. and Donahue, N. M.: Peroxy radical chemistry and the volatility basis set, *Atmos. Chem. Phys.*, 20, 1183-
1053 1199, 10.5194/acp-20-1183-2020, 2020.
- 1054 Seinfeld, J. H. and Pandis, S. N.: *Atmospheric Chemistry and Physics: From Air Pollution to Climate Change*, 2nd ed,
1055 Wiley, John & Sons, New York, 2006.
- 1056 Shen, H., Zhao, D., Pullinen, I., Kang, S., Vereecken, L., Fuchs, H., Acir, I.-H., Tillmann, R., Rohrer, F., Wildt, J., Kiendler-
1057 Scharr, A., Wahner, A., and Mentel, T. F.: Highly Oxygenated Organic Nitrates Formed from NO₃ Radical-Initiated
1058 Oxidation of β -Pinene, *Environ. Sci. Technol.*, 10.1021/acs.est.1c03978, 2021.
- 1059 Shrivastava, M., Cappa, C. D., Fan, J., Goldstein, A. H., Guenther, A. B., Jimenez, J. L., Kuang, C., Laskin, A., Martin, S.
1060 T., Ng, N. L., Petäjä, T., Pierce, J. R., Rasch, P. J., Roldin, P., Seinfeld, J. H., Shilling, J., Smith, J. N., Thornton,
1061 J. A., Volkamer, R., Wang, J., Worsnop, D. R., Zaveri, R. A., Zelenyuk, A., and Zhang, Q.: Recent advances in
1062 understanding secondary organic aerosol: Implications for global climate forcing, *Rev. Geophys.*, 55, 509-559,
1063 10.1002/2016rg000540, 2017.
- 1064 Slade, J. H., de Perre, C., Lee, L., and Shepson, P. B.: Nitrate radical oxidation of γ -terpinene: hydroxy nitrate, total
1065 organic nitrate, and secondary organic aerosol yields, *Atmos. Chem. Phys.*, 17, 8635-8650, 10.5194/acp-17-8635-
1066 2017, 2017.
- 1067 Spittler, M., Barnes, I., Bejan, I., Brockmann, K. J., Benter, T., and Wirtz, K.: Reactions of NO₃ radicals with limonene and
1068 α -pinene: Product and SOA formation, *Atmos. Environ.*, 40, 116-127, 10.1016/j.atmosenv.2005.09.093, 2006.
- 1069 Takeuchi, M. and Ng, N. L.: Chemical composition and hydrolysis of organic nitrate aerosol formed from hydroxyl and
1070 nitrate radical oxidation of α -pinene and β -pinene, *Atmos. Chem. Phys.*, 19, 12749-12766, 10.5194/acp-19-12749-
1071 2019, 2019.
- 1072 Tröstl, J., Chuang, W. K., Gordon, H., Heinritzi, M., Yan, C., Molteni, U., Ahlm, L., Frege, C., Bianchi, F., Wagner, R.,
1073 Simon, M., Lehtipalo, K., Williamson, C., Craven, J. S., Duplissy, J., Adamov, A., Almeida, J., Bernhammer, A.
1074 K., Breitenlechner, M., Brilke, S., Dias, A., Ehrhart, S., Flagan, R. C., Franchin, A., Fuchs, C., Guida, R., Gysel,
1075 M., Hansel, A., Hoyle, C. R., Jokinen, T., Junninen, H., Kangasluoma, J., Keskinen, H., Kim, J., Krapf, M., Kürten,
1076 A., Laaksonen, A., Lawler, M., Leiminger, M., Mathot, S., Möhler, O., Nieminen, T., Onnela, A., Petäjä, T., Piel,
1077 F. M., Miettinen, P., Rissanen, M. P., Rondo, L., Sarnela, N., Schobesberger, S., Sengupta, K., Sipilä, M., Smith,
1078 J. N., Steiner, G., Tomè, A., Virtanen, A., Wagner, A. C., Weingartner, E., Wimmer, D., Winkler, P. M., Ye, P.,
1079 Carslaw, K. S., Curtius, J., Dommen, J., Kirkby, J., Kulmala, M., Riipinen, I., Worsnop, D. R., Donahue, N. M.,
1080 and Baltensperger, U.: The role of low-volatility organic compounds in initial particle growth in the atmosphere,
1081 *Nature*, 533, 527-531, 10.1038/nature18271, 2016.
- 1082 Vereecken, L. and Nozière, B.: H migration in peroxy radicals under atmospheric conditions, *Atmos. Chem. Phys.*, 20,
1083 7429-7458, 10.5194/acp-20-7429-2020, 2020.
- 1084 Vereecken, L. and Peeters, J.: Decomposition of substituted alkoxy radicals-part I: a generalized structure-activity
1085 relationship for reaction barrier heights, *Phys. Chem. Chem. Phys.*, 11, 9062-9074, 10.1039/b909712k, 2009.
- 1086 Vereecken, L. and Peeters, J.: A structure-activity relationship for the rate coefficient of H-migration in substituted alkoxy
1087 radicals, *Phys. Chem. Chem. Phys.*, 12, 12608-12620, 10.1039/c0cp00387e, 2010.
- 1088 Wagner, N. L., Dubé, W. P., Washenfelder, R. A., Young, C. J., Pollack, I. B., Ryerson, T. B., and Brown, S. S.: Diode laser-
1089 based cavity ring-down instrument for NO₃, N₂O₅, NO, NO₂ and O₃ from aircraft, *Atmos. Meas. Tech.*, 4, 1227-
1090 1240, 10.5194/amt-4-1227-2011, 2011.
- 1091 Wang, H., Ma, X., Tan, Z., Wang, H., Chen, X., Chen, S., Gao, Y., Liu, Y., Liu, Y., Yang, X., Yuan, B., Zeng, L., Huang, C.,
1092 Lu, K., and and Zhang, Y.: Anthropogenic monoterpenes aggravating ozone pollution, *Natl. Sci. Rev.*, nwac103,
1093 10.1093/nsr/nwac103, 2022.
- 1094 Wang, S. and Pratt, K. A.: Molecular Halogens Above the Arctic Snowpack: Emissions, Diurnal Variations, and Recycling
1095 Mechanisms, *J. Geophys. Res.-Atmos.*, 122, 11991-12007, 10.1002/2017jd027175, 2017.

1096 Wu, C., Bell, D. M., Graham, E. L., Haslett, S., Riipinen, I., Baltensperger, U., Bertrand, A., Giannoukos, S., Schoonbaert,
1097 J., El Haddad, I., Prevot, A. S. H., Huang, W., and Mohr, C.: Photolytically induced changes in composition and
1098 volatility of biogenic secondary organic aerosol from nitrate radical oxidation during night-to-day transition,
1099 *Atmos. Chem. Phys.*, 21, 14907-14925, 10.5194/acp-21-14907-2021, 2021a.

1100 Wu, R., Vereecken, L., Tsiligiannis, E., Kang, S., Albrecht, S. R., Hantschke, L., Zhao, D., Novelli, A., Fuchs, H., Tillmann,
1101 R., Hohaus, T., Carlsson, P. T. M., Shenolikar, J., Bernard, F., Crowley, J. N., Fry, J. L., Brownwood, B., Thornton,
1102 J. A., Brown, S. S., Kiendler-Scharr, A., Wahner, A., Hallquist, M., and Mentel, T. F.: Molecular composition and
1103 volatility of multi-generation products formed from isoprene oxidation by nitrate radical, *Atmos. Chem. Phys.*,
1104 21, 10799-10824, 10.5194/acp-21-10799-2021, 2021b.

1105 Xu, L., Guo, H., Boyd, C. M., Klein, M., Bougiatioti, A., Cerully, K. M., Hite, J. R., Isaacman-VanWertz, G., Kreisberg,
1106 N. M., Knote, C., Olson, K., Koss, A., Goldstein, A. H., Hering, S. V., de Gouw, J., Baumann, K., Lee, S.-H.,
1107 Nenes, A., Weber, R. J., and Ng, N. L.: Effects of anthropogenic emissions on aerosol formation from isoprene
1108 and monoterpenes in the southeastern United States, *P. Natl. Acad. Sci. USA*, 112, 37-42,
1109 10.1073/pnas.1417609112, 2015.

1110 Yan, C., Nie, W., Äijälä, M., Rissanen, M. P., Canagaratna, M. R., Massoli, P., Junninen, H., Jokinen, T., Sarnela, N., Häme,
1111 S. A. K., Schobesberger, S., Canonaco, F., Yao, L., Prévôt, A. S. H., Petäjä, T., Kulmala, M., Sipilä, M., Worsnop,
1112 D. R., and Ehn, M.: Source characterization of highly oxidized multifunctional compounds in a boreal forest
1113 environment using positive matrix factorization, *Atmos. Chem. Phys.*, 16, 12715-12731, 10.5194/acp-16-12715-
1114 2016, 2016.

1115 Zhang, H., Yee, L. D., Lee, B. H., Curtis, M. P., Worton, D. R., Isaacman-VanWertz, G., Offenberg, J. H., Lewandowski,
1116 M., Kleindienst, T. E., Beaver, M. R., Holder, A. L., Lonneman, W. A., Docherty, K. S., Jaoui, M., Pye, H. O. T.,
1117 Hu, W., Day, D. A., Campuzano-Jost, P., Jimenez, J. L., Guo, H., Weber, R. J., de Gouw, J., Koss, A. R., Edgerton,
1118 E. S., Brune, W., Mohr, C., Lopez-Hilfiker, F. D., Lutz, A., Kreisberg, N. M., Spielman, S. R., Hering, S. V.,
1119 Wilson, K. R., Thornton, J. A., and Goldstein, A. H.: Monoterpenes are the largest source of summertime organic
1120 aerosol in the southeastern United States, *P. Natl. Acad. Sci. USA*, 115, 2038-2043, 10.1073/pnas.1717513115,
1121 2018.

1122 Zhao, D., Pullinen, I., Fuchs, H., Schrade, S., Wu, R., Acir, I.-H., Tillmann, R., Rohrer, F., Wildt, J., Guo, Y., Kiendler-
1123 Scharr, A., Wahner, A., Kang, S., Vereecken, L., and Mentel, T. F.: Highly oxygenated organic molecule (HOM)
1124 formation in the isoprene oxidation by NO₃ radical, *Atmos. Chem. Phys.*, 21, 9681-9704, 10.5194/acp-21-9681-
1125 2021, 2021.

1126 Zhao, D., Schmitt, S. H., Wang, M., Acir, I.-H., Tillmann, R., Tan, Z., Novelli, A., Fuchs, H., Pullinen, I., Wegener, R.,
1127 Rohrer, F., Wildt, J., Kiendler-Scharr, A., Wahner, A., and Mentel, T. F.: Effects of NO_x and SO₂ on the secondary
1128 organic aerosol formation from photooxidation of α -pinene and limonene, *Atmos. Chem. Phys.*, 18, 1611-1628,
1129 10.5194/acp-18-1611-2018, 2018.

1130 Zhao, D. F., Buchholz, A., Kortner, B., Schlag, P., Rubach, F., Kiendler-Scharr, A., Tillmann, R., Wahner, A., Flores, J. M.,
1131 Rudich, Y., Watne, Å. K., Hallquist, M., Wildt, J., and Mentel, T. F.: Size-dependent hygroscopicity parameter (κ)
1132 and chemical composition of secondary organic cloud condensation nuclei, *Geophys. Res. Lett.*, 42, 10920-10928,
1133 10.1002/2015gl066497, 2015a.

1134 Zhao, D. F., Kaminski, M., Schlag, P., Fuchs, H., Acir, I. H., Bohn, B., Häseler, R., Kiendler-Scharr, A., Rohrer, F., Tillmann,
1135 R., Wang, M. J., Wegener, R., Wildt, J., Wahner, A., and Mentel, T. F.: Secondary organic aerosol formation from
1136 hydroxyl radical oxidation and ozonolysis of monoterpenes, *Atmos. Chem. Phys.*, 15, 991-1012, 10.5194/acp-15-
1137 991-2015, 2015b.

1138 Zhou, L., Gierens, R., Sogachev, A., Mogensen, D., Ortega, J., Smith, J. N., Harley, P. C., Prenni, A. J., Levin, E. J. T.,
1139 Turnipseed, A., Rusanen, A., Smolander, S., Guenther, A. B., Kulmala, M., Karl, T., and Boy, M.: Contribution

1140 from biogenic organic compounds to particle growth during the 2010 BEACHON-ROCS campaign in a Colorado
1141 temperate needleleaf forest, *Atmos. Chem. Phys.*, 15, 8643-8656, 10.5194/acp-15-8643-2015, 2015.
1142 Ziemann, P. J. and Atkinson, R.: Kinetics, products, and mechanisms of secondary organic aerosol formation, *Chem. Soc.*
1143 *Rev.*, 41, 6582-6605, 10.1039/c2cs35122f, 2012.
1144

1 Supplement of

2 **Identification of highly oxygenated organic molecules and**
3 **their role in aerosol formation in the reaction of limonene**
4 **with nitrate radical**

5 Yindong Guo¹, Hongru Shen¹, Iida Pullinen^{2, a}, Hao Luo^{1,3}, Sungah Kang², Luc Vereecken², Hendrik
6 Fuchs², Mattias Hallquist⁴, Ismail-Hakki Acir^{2, b}, Ralf Tillmann², Franz Rohrer², Jürgen Wildt², Astrid
7 Kiendler-Scharr², Andreas Wahner², Defeng Zhao^{1,5,6*}, Thomas F. Mentel^{2*}

8 ¹Department of Atmospheric and Oceanic Sciences & Institute of Atmospheric Sciences, Fudan
9 University, 200438, Shanghai, China

10 ²Institute of Energy and Climate Research, IEK-8: Troposphere, Forschungszentrum Jülich [GmbH](#),
11 52425, Jülich, Germany

12 ³IRDR ICoE on Risk Interconnectivity and Governance on Weather/Climate Extremes Impact and
13 Public Health, Fudan University, Shanghai 200438, China

14 ⁴Department of Chemistry and Molecular biology, University of Gothenburg, Göteborg, 41258,
15 Sweden

16 ⁵Shanghai Frontiers Science Center of Atmosphere-Ocean Interaction, Fudan University, Shanghai
17 200438, China

18 ⁶Institute of Eco-Chongming (IEC), 20 Cuinia Rd., Chongming, Shanghai, 202162, China

19 ^a Now at: Department of Applied Physics, University of Eastern Finland, Kuopio, 70210, Finland.

20 ^b Now at: Institute of Nutrition and Food Sciences, University of Bonn, Bonn, 53115, Germany.

21 *Correspondence to:* Defeng Zhao (dfzhao@fudan.edu.cn), Thomas F. Mentel (t.mentel@fz-
22 juelich.de)

23

24 ~~In the supplement we describe the determination of the calibration coefficient of HOM, the~~
25 ~~estimation of SOA growth based on HOM condensation. In addition, more figures, tables and~~
26 ~~schemes are provided.~~

27

28

29

Content

30 **S1 Determination of the calibration coefficient**.....3

31 **S2 HOM condensation on SOA**.....5

32 **S3 Simulations based on the Master Chemical Mechanism (MCM)**7

33 **S4 Supplement figures, reaction schemes, and tables**89

34 **Figures S1 - S3, S5 - S15**89

35 **Reaction schemes S1 to S3**.....1716

36 **Tables S1 to S3**.....1917

37

38

39 S1 Determination of the calibration coefficient

40 A calibration coefficient was determined and used to convert peak intensity in CIMS to
41 concentrations. The calibration coefficient of H₂SO₄ can be applied to HOM because the ionization
42 efficiency of HOM and H₂SO₄ are close (Ehn et al., 2014; Pullinen et al., 2020). The concentration
43 of H₂SO₄ is given by:

$$44 \quad [H_2SO_4] = C \times I \quad (\text{Eq. S1})$$

45 where C is the calibration coefficient of H₂SO₄, I is the normalized count (nc, the peak area of an
46 ion divided by total ion signal of mass spectrum) of peak intensity. The detailed description of the
47 derivation of the calibration coefficient for H₂SO₄ in SAPHIR chamber can be found elsewhere
48 (Ehn et al., 2014; Pullinen et al., 2020; Zhao et al., 2021). In brief, H₂SO₄ was produced in the
49 chamber by OH•-initiated oxidation of SO₂. OH• were mainly generated from photolysis of HONO.
50 Concentrations of SO₂ and OH• were measured by laser induced fluorescence (LIF) (Fuchs et al.,
51 2012) and an SO₂ analyzer (Thermo System 43i). The concentration of H₂SO₄ is given by:

$$52 \quad d[H_2SO_4]/dt = k[SO_2][OH\bullet] - (k_{\text{wall}} + k_{\text{dil}})[H_2SO_4] \quad (\text{Eq. S2})$$

53 where [H₂SO₄], [SO₂], and [OH•] are concentrations, k is the rate constant of the reaction of SO₂ w
54 ith OH•, k_{wall} is the wall loss rate (6 × 10⁻⁴ s⁻¹) (Zhao et al., 2018), and k_{dil} is the dilution rate (1.5 × 1
55 0⁻⁵ s⁻¹).

56 C was determined to be 2.5 × 10¹⁰ molecule cm⁻³ nc⁻¹ for H₂SO₄. The uncertainty of C is -52
57 %/+101 % from the uncertainty of SO₂ concentration (~7 %), OH• concentration (~10 %), I (~10
58 %) and k (Δlogk = ±0.3) using error propagation (Zhao et al., 2021).

59 A relative transmission efficiency curve of the ¹⁵NO₃⁻-CIMS was measured with
60 perfluoropentanoic acid (C₄F₉COOH) in our previous study (Pullinen et al., 2020). A monotonous
61 decrease of the transmission function from 100 % to 86 % was determined within an m/z range of
62 62-791 Th. Thus, the uncertainty of the mass-independent transmission efficiency used when
63 applying the calibration coefficient of H₂SO₄ to HOM is determined to be -0 %/+14 %.

64 When the chamber was actively mixed, the wall loss is determined to be (2.2±0.2) × 10⁻³ s⁻¹.
65 We examined the decay of nitrated compounds such as C₁₀H₁₅NO₉₋₁₂ (volatility in the
66 LVOC/ELVOC range) and non-nitrated compounds such as C₁₀H₁₄O₈₋₁₁ in the reaction of limonene
67 with OH in the presence of NO, which all showed similar decay rates as shown below (Fig. S16).

68 The wall loss rate in SAPHIR chamber during active mixing is comparable to the chambers
69 such as those reported by Peräkylä et al. (2020) (lifetime ~400 s) and Krechmer et al. (2016)
70 (lifetime ~7 to 13 min). The time for complete mixing is ~1 min (Fuchs et al., 2013) when the fan
71 was on, which was further confirmed using measured VOC concentrations. We would like to note
72 that the SAPHIR chamber is much larger than the chambers in the cited studies above (270 m³ vs a
73 few m³) and also the chamber is running in batch mode instead of the continuous flow mode used
74 for many other chambers for HOM studies such as the COALA chamber (Peräkylä et al., 2020) or
75 our JPAC chamber (Ehn et al., 2014; Pullinen et al., 2020). The large volume and batch running

76 mode may result in a thicker boundary layer of the chamber wall, which delays vapor wall
77 deposition.
78
79

80 S2 HOM condensation on SOA

81 Estimation of HOM condensation on SOA was based on measurement of HOM concentration and
 82 particle surface concentration, and the assumption that all HOM colliding with the surface of
 83 particles led to a net and irreversible uptake. Collision rate of a gas phase HOM species with
 84 particles of all size is given by:

$$85 \quad K = \gamma \frac{\pi}{4} (d_p + d_v)^2 (\bar{c}_p^2 + \bar{c}_v^2)^{\frac{1}{2}} \cdot C_v \quad (\text{Eq. S3})$$

86 where d_p and d_v are the diameters of the particle and molecule, and \bar{c}_p and \bar{c}_v are the average
 87 thermal speeds of the particle and the HOM species, respectively. C_v represents measured HOM
 88 molecule concentration. The coefficient γ is given by:

$$89 \quad \gamma = \frac{4}{3} Kn \beta_m \quad (\text{Eq. S4})$$

90 where Kn is the Knudsen number and β_m is the correction factor in the transition regime according
 91 to the Fuchs-Sutugin approach (Seinfeld and Pandis, 2006). Then, particle growth rate as
 92 represented in mass concentration (GR_m) can be described as:

$$93$$

$$94 \quad GR_m = \frac{dM}{dt} = \rho_p \frac{dV_p}{dt} = \rho_p K \frac{m_v}{\rho_v} = \frac{\pi}{4} \gamma \frac{\rho_p}{\rho_v} (d_p + d_v)^2 (\bar{c}_p^2 + \bar{c}_v^2)^{\frac{1}{2}} \cdot m_v C_v$$

$$95 \quad = \frac{\pi}{4} \gamma \frac{\rho_p}{\rho_v} (d_p + d_v)^2 \left(\frac{8kT}{\pi} \right)^{\frac{1}{2}} \left(\frac{1}{m_p} + \frac{1}{m_v} \right)^{\frac{1}{2}} \cdot m_v C_v \quad (\text{Eq. S5})$$

96
 97 where M is the particle mass concentration ($\mu\text{g}/\text{m}^3$), t is time, V_p is the particle volume, T is
 98 temperature, m_p and m_v are the exact mass of particle and vapour, respectively. Omitting the $\frac{1}{m_p}$
 99 term (much smaller than $\frac{1}{m_v}$) (Ehn et al., 2014) and the d_v term (small compared to d_p) in Eq. 4,
 100 one can get

$$101 \quad GR_m = \frac{1}{4} \gamma \frac{\rho_p}{\rho_v} S_p \left(\frac{8kT}{\pi m_v} \right)^{\frac{1}{2}} \cdot m_v C_v \quad (\text{Eq. S6})$$

102 where S_p is the particle surface concentration measured by SMPS. The calculation of γ using Eq.
 103 S4 was taken from previous studies (Lehtinen and Kulmala, 2003; Seinfeld and Pandis, 2006).
 104 Multiplying the calculated particle mass growth rate by time interval gives the particle growth in
 105 each time interval.

106 The wall loss and dilution loss rates of the particles are obtained from a later period of the
 107 experiment when particle mass ceased to grow and the change in particle mass was only due to the
 108 wall loss and dilution. During this period the loss rate of the total particle mass concentration (TM)
 109 was obtained through linear fit of $\ln(TM)$ to t when:

$$110 \quad \ln(TM_{t_n}) = \ln(TM_{t_0}) - (k_{wall} + k_{dil})(t_n - t_0) \quad (\text{Eq. S7})$$

111 Herein $\ln(TM)$ decreased linearly over time at constant geometric mean of the particle diameter,
112 which suggests no noticeable evaporation loss. The wall loss was independently determined from
113 the particle number concentration, which showed values consistent with method using mass
114 concentration. The value of particle wall loss rate in this experiment k_{wall} was determined to be
115 $3.6 \times 10^{-5} \text{ s}^{-1}$.

116

| 117

118 S3 Simulations based on the Master Chemical Mechanism (MCM)

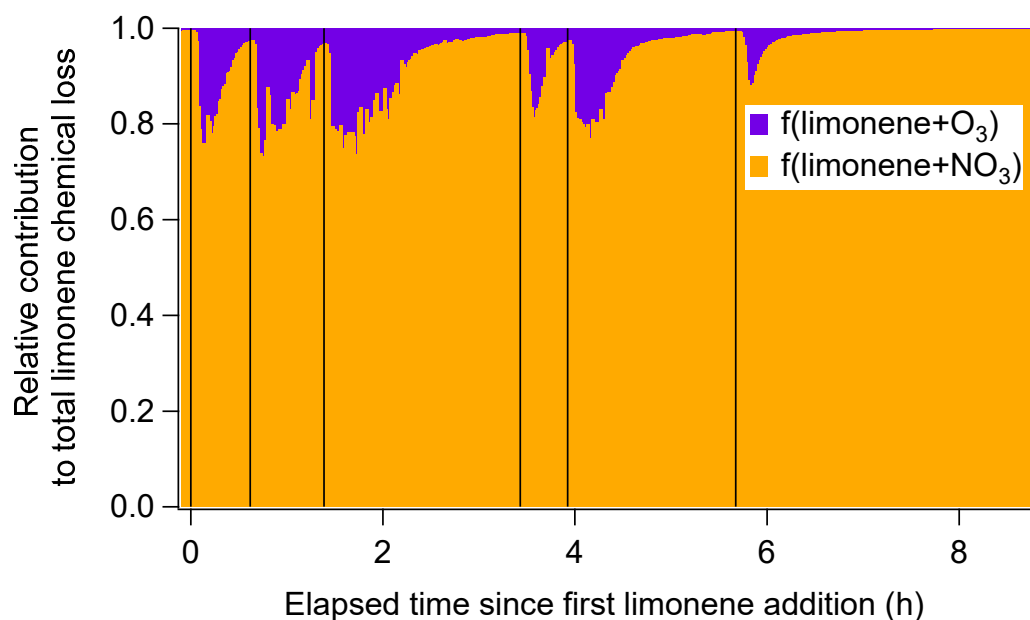
119 Besides simulations of the RO₂• loss pathway (Sect. 2.5), we conducted several simulations
120 including concentrations of NO₃, N₂O₅, limonene and RO₂• (Fig. S4) based on MCM v3.3.1
121 (<http://mcm.york.ac.uk/>) using iChamber, an open-source program
122 (<https://sites.google.com/view/wangsiyuan/models?authuser=0>) (Wang and Pratt, 2017)S3.

123 The modeled concentration of NO₃, N₂O₅ and limonene by MCM generally match the behavior
124 of measured concentrations (Fig. S4 a~c). The overestimated limonene concentrations can be
125 attributed to the absence of a temperature-dependence of the rate constant for the reaction of
126 limonene with NO₃. RO₂• concentrations showed 1st-generation trend (Fig. S4d). The reaction rate
127 (k×limonene×NO₃) was highest at every injection of limonene (Fig. S4e). As for oxidation products,
128 the second time of NO₃ attack to organic nitrate with a C=C double bond is not included in MCM,
129 so the simulation of the closed-shell products does not present 1st or 2nd generation product patterns
130 as we have observed in CIMS. But we are able to observe several good simulation of 1st and 2nd
131 generation RO₂• (Fig. S4f,g). For example, the “NLIMALO2” (Fig. S4g) showed a typical time
132 series of 2nd generation RO₂•, which is formed via NO₃ attack of a 1st-generation carbonyl product
133 which does not contain N atom according to the MCM mechanism.

134

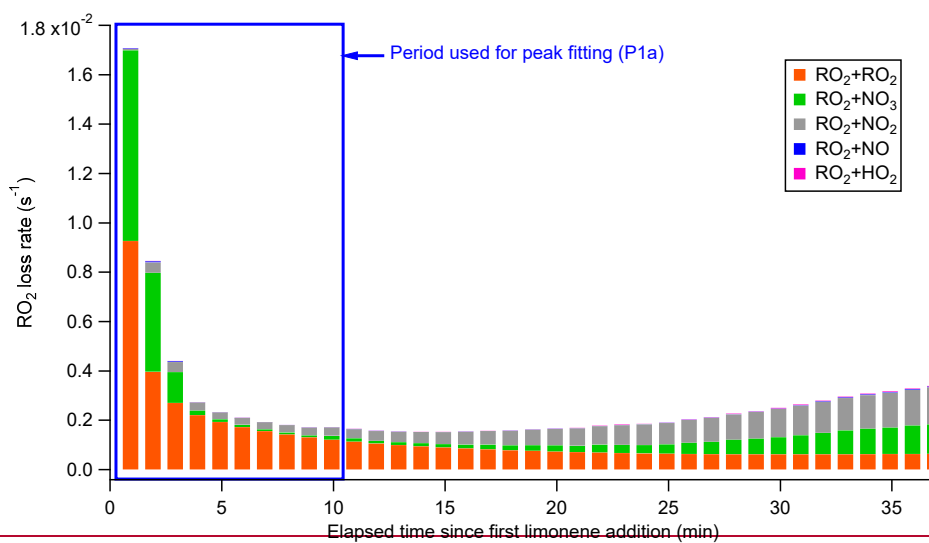
135 **S4** Supplement figures, reaction schemes, and tables

136 **Figures S1 - S13**, **S5 - S15**



137
138 Figure S1. Contribution of NO_3 and O_3 oxidation pathways of limonene to chemical loss of
139 limonene presented as fractions during the experiment. Black vertical lines indicate time for six
140 limonene additions into the chamber.

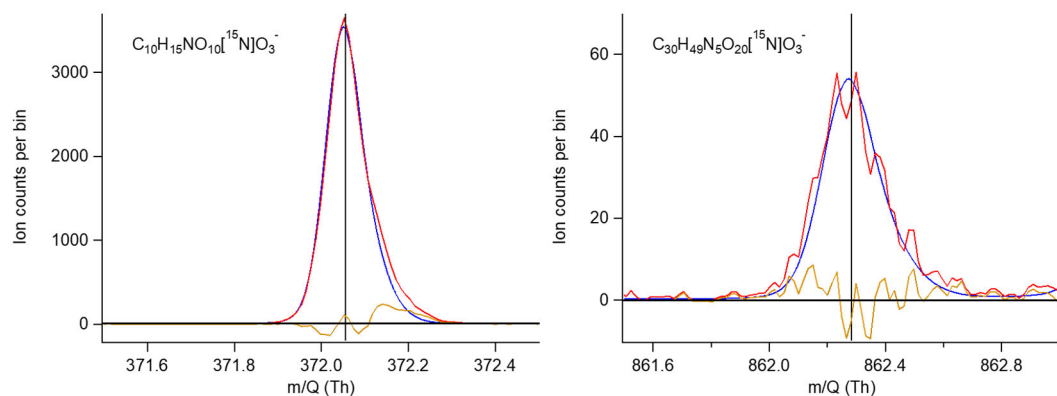
141



142

143 **Figure**

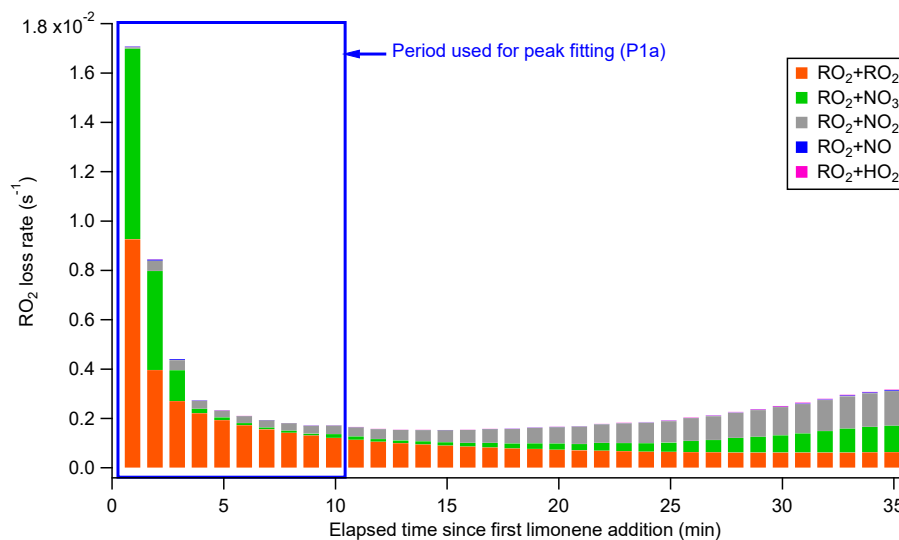
S2.



144

145 Figure S2. Examples of high-resolution peak fitting of HOM containing 1 N atom (left panel) and
 146 5 N atoms (right panel). Red lines are the mass spectrum, blue and orange lines show the sum of the
 147 isotopic contributions and the fitted peaks, and the residuals, respectively. The black vertical lines
 148 denote the exact mass of the fitted peaks.

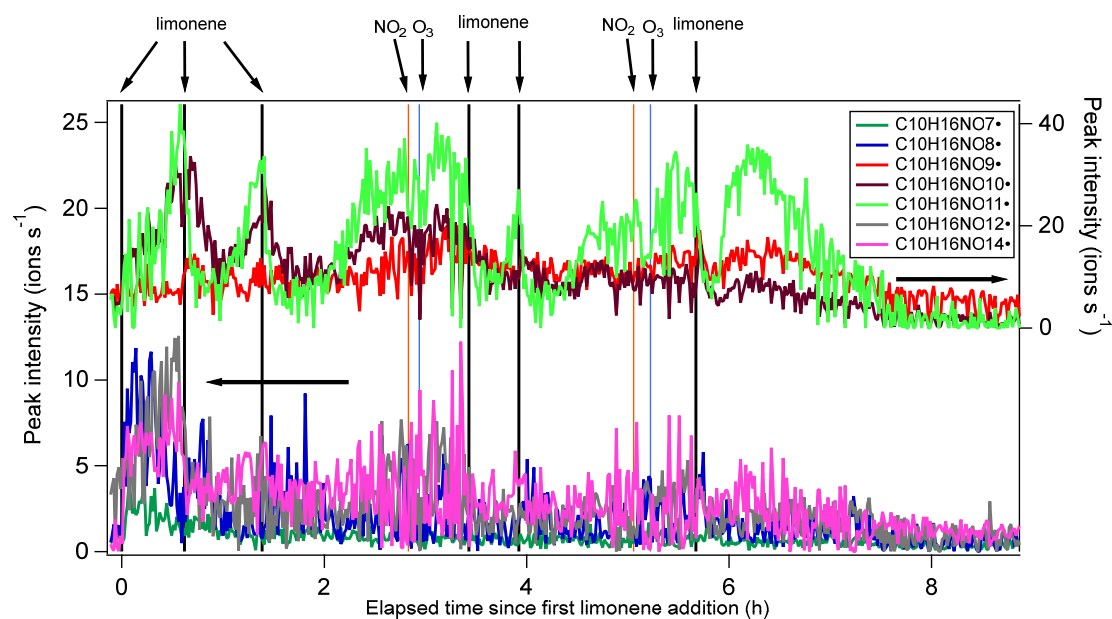
149



150

151 Figure S3. RO₂• loss rate based on bimolecular reactions with RO₂•, NO₃, NO₂, NO and HO₂• (color
 152 bars) during the first limonene addition period (P1). Blue rectangle denotes the first 10 min of the
 153 reaction time (P1a), which is the time period used for peak fitting.

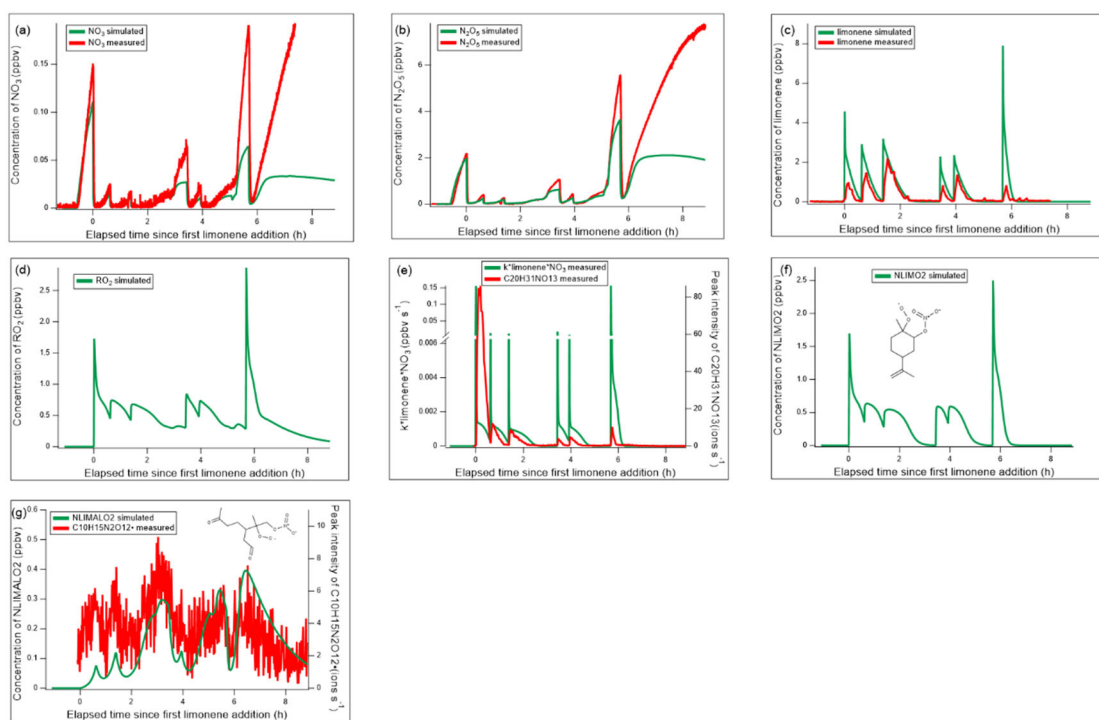
154



155

156

Figure S3.



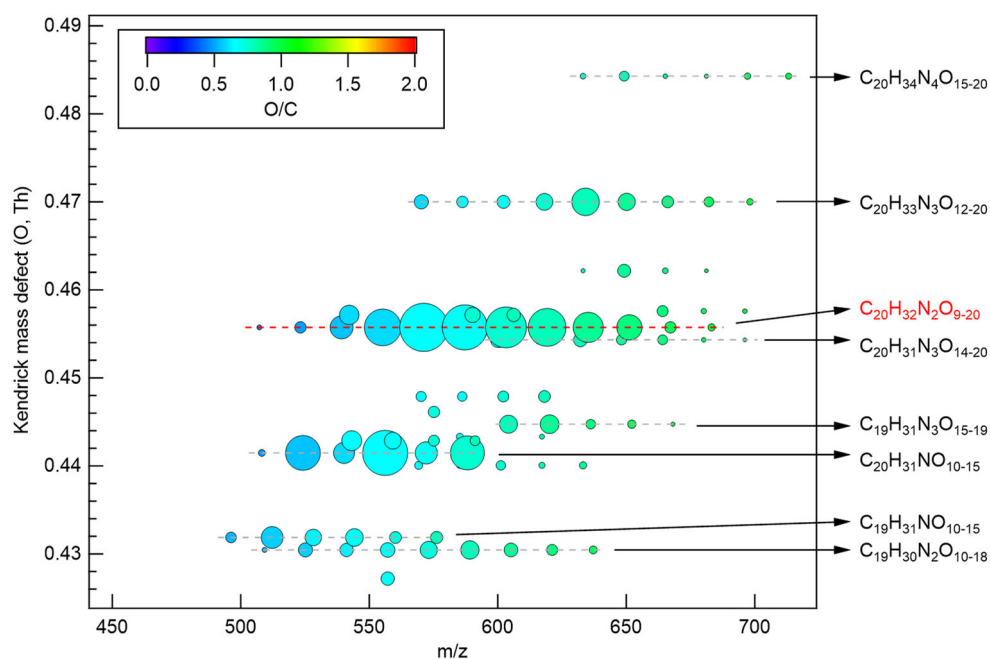
157

158 Figure S4. Simulation results of limonene + NO₃ gas-phase chemistry based on MCM v3.3.1 using
 159 iChamber model. The whole period of experiment was simulated, at measured T and RH, and
 160 additions of limonene, NO₂ and O₃ were included as initial conditions according to the experimental
 161 procedure. (a)~(c): Comparison of simulated (green trace) and measured (red trace) concentrations
 162 of (a) NO₃, (b) N₂O₅ and (c) limonene. (d)~(g): Simulated concentrations of (d) total RO₂• included
 163 in the limonene + NO₃ gas-phase chemistry in MCM v3.3.1, (e) reaction rate of limonene with NO₃
 164 (coefficient k×limonene×NO₃), compared with a measured 1st-generation HOM product
 165 C₂₀H₃₁NO₁₃; (f) “NLIMO2”, an example of 1st-generation C₁₀ RO₂•, and (g) “NLIMALO2”, an
 166 example of 2nd-generation C₁₀ RO₂•, compared with a measured 2nd-generation HOM RO₂•.

167 $C_{10}H_{15}N_2O_{12}^{\bullet}$.

168

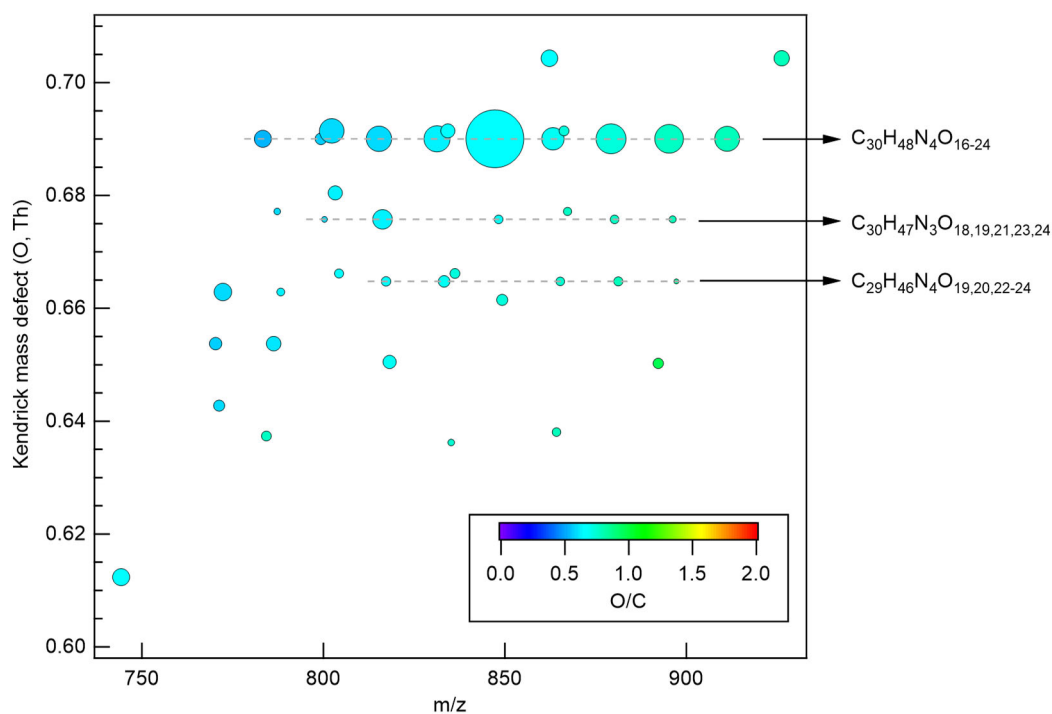
169



170

171 **Figure S5.** Kendrick mass defect plot (O atom-based) of major dimer products. The area of the
172 circles is proportional to the average intensity of each compound during the P1a period. The color
173 denotes O/C ratio. Dashed lines indicate major product families that were identified.

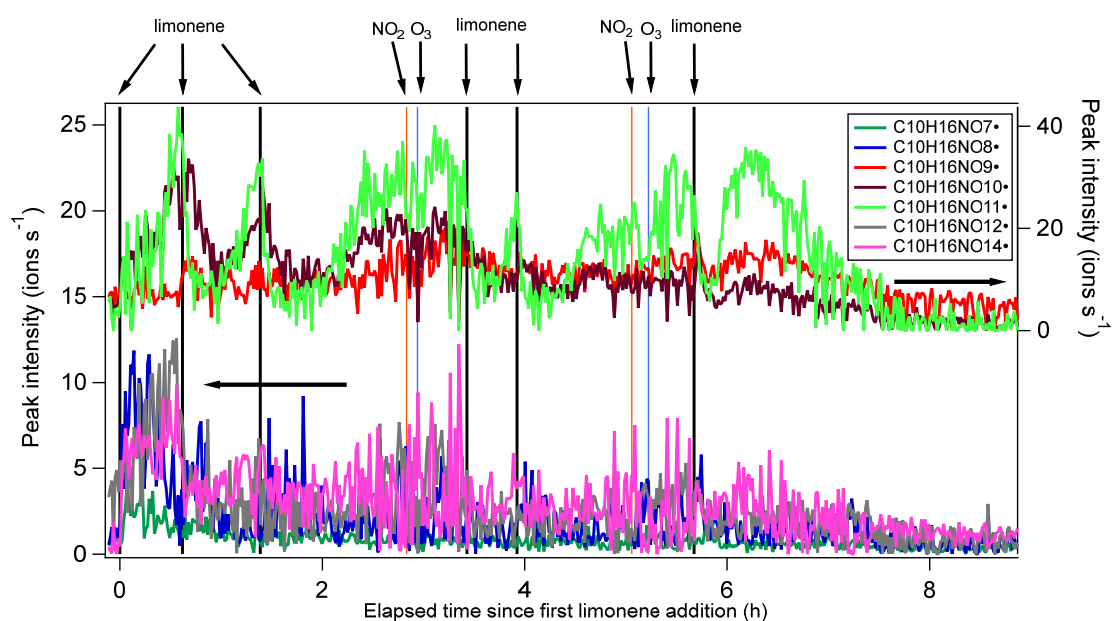
174



175

176 **Figure S6.** Kendrick mass defect plot (O-atom-based) of trimers. The area of the circles is

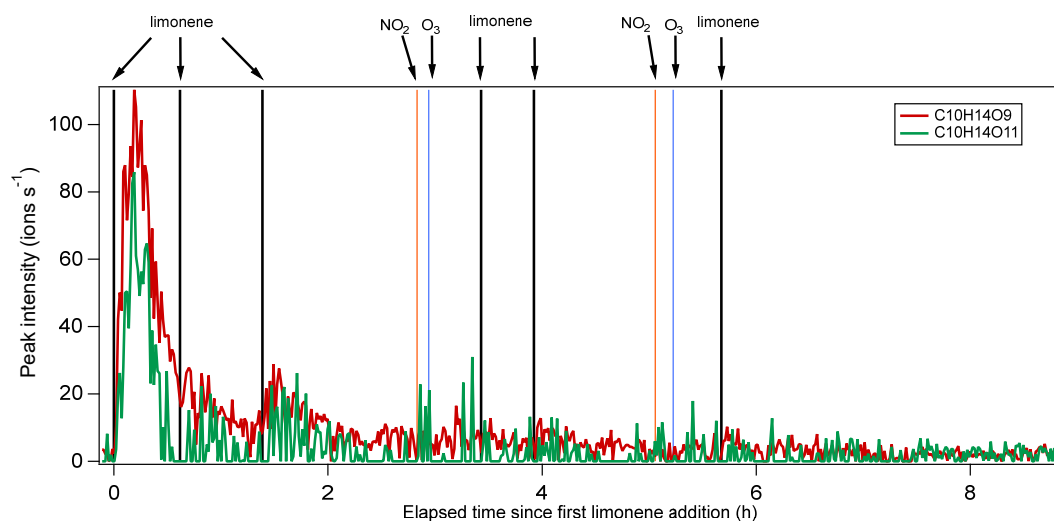
177 proportional to the average intensity of each compound during the P1a period. The color denotes
178 O/C ratio. Dashed lines indicate major product families that were identified.
179



180

181 **Figure S7.** Time series of peak intensity of the $C_{10}H_{16}NO_x\bullet$ family during the whole experimental
182 period. The vertical black, red and blue lines represent the time of limonene, NO_2 and O_3 additions,
183 respectively.

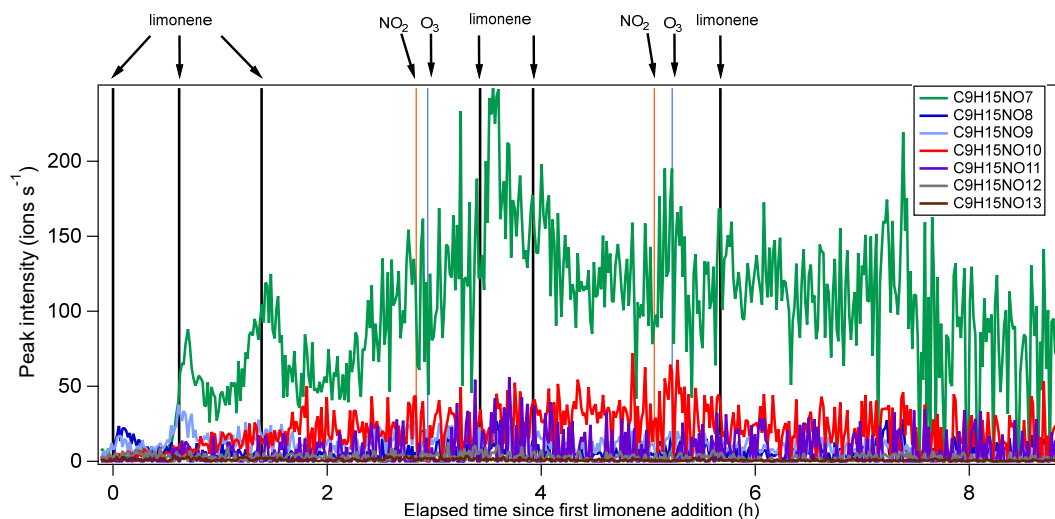
184



185

186 **Figure S4S8.** Time series of peak intensity of two representatives of the $C_{10}H_{14}O_x$ family during the
187 whole experimental period. The vertical black, red and blue lines represent the time of limonene,
188 NO_2 and O_3 additions, respectively.

189

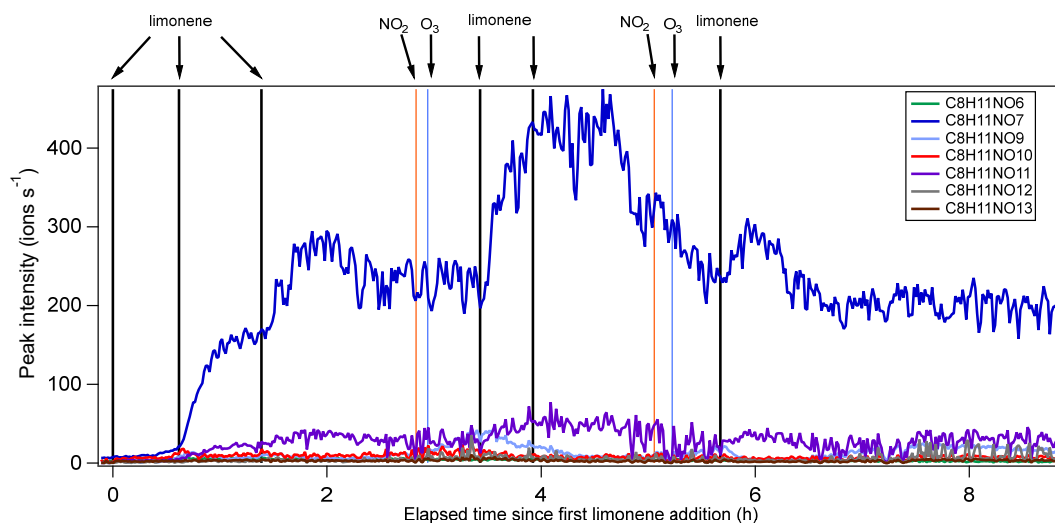


190

191 Figure [S5S9](#). Time series of peak intensity of the $C_9H_{15}NO_x$ family during the whole experimental
 192 period. The vertical black, red and blue lines represent the time of limonene, NO_2 and O_3 additions,
 193 respectively.

194

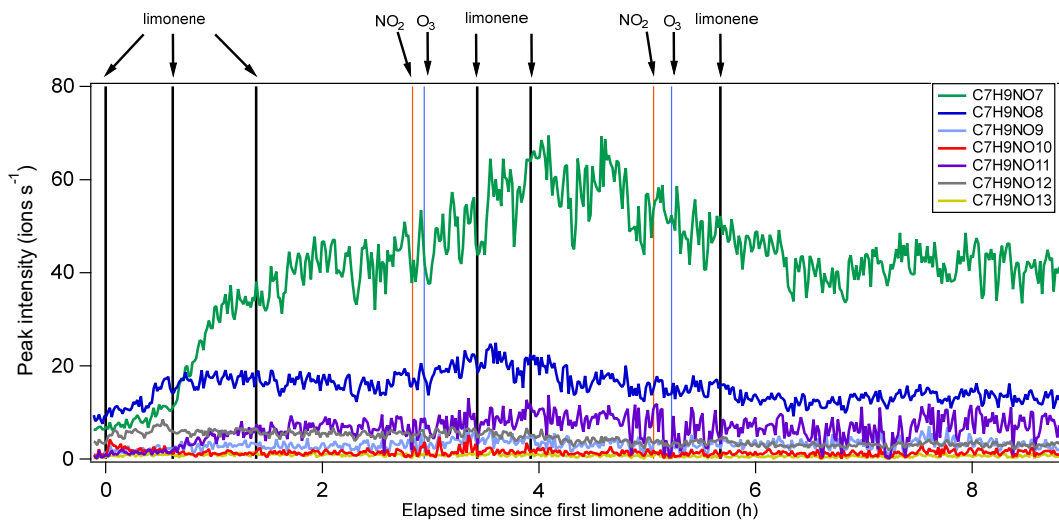
195



196

197 Figure [S6S10](#). Time series of peak intensity of the $C_8H_{11}NO_x$ family during the whole experimental
 198 period. The vertical black, red and blue lines represent the time of limonene, NO_2 and O_3 additions,
 199 respectively.

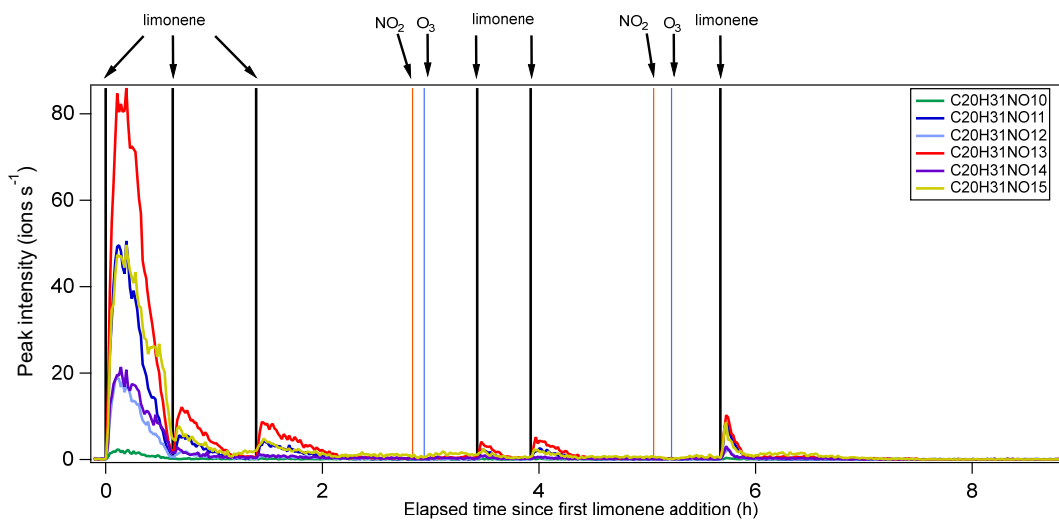
200



201

202 Figure S7S11. Time series of peak intensity of the $C_7H_9NO_x$ family during the whole experimental
 203 period. The vertical black, red and blue lines represent the time of limonene, NO_2 and O_3 additions,
 204 respectively.

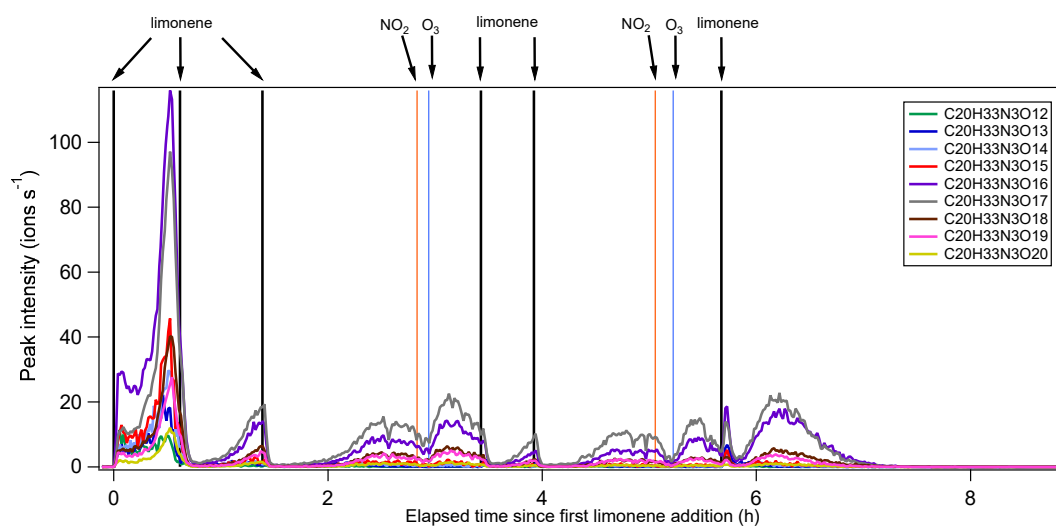
205



206

207 Figure S12. Time series of peak intensity of the $C_{20}H_{31}NO_x$ family during the whole experimental
 208 period. The vertical black, red and blue lines represent the time of limonene, NO_2 and O_3 additions,
 209 respectively.

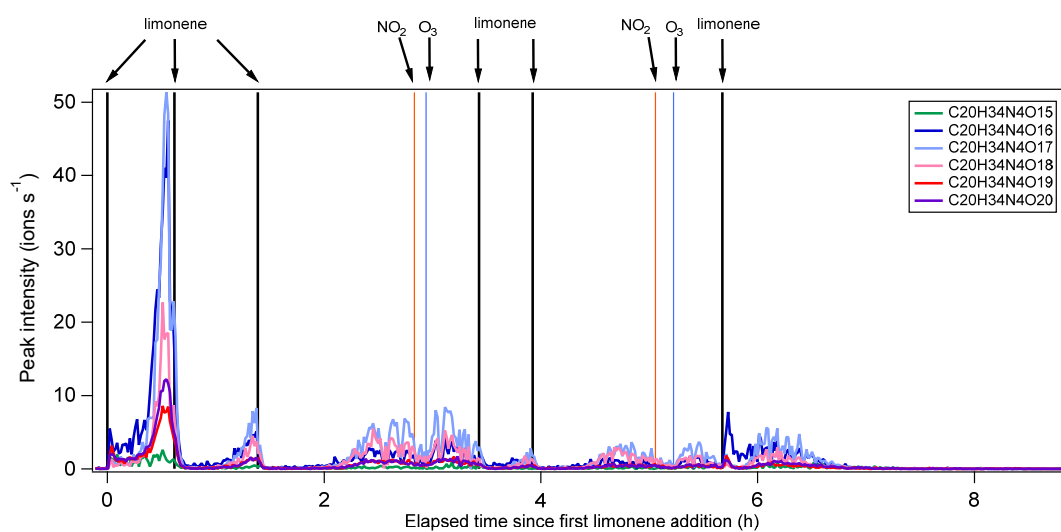
210



211

212 Figure S13. Time series of peak intensity of the $C_{20}H_{33}N_3O_x$ family during the whole experimental
 213 period. The vertical black, red and blue lines represent the time of limonene, NO_2 and O_3 additions,
 214 respectively.

215

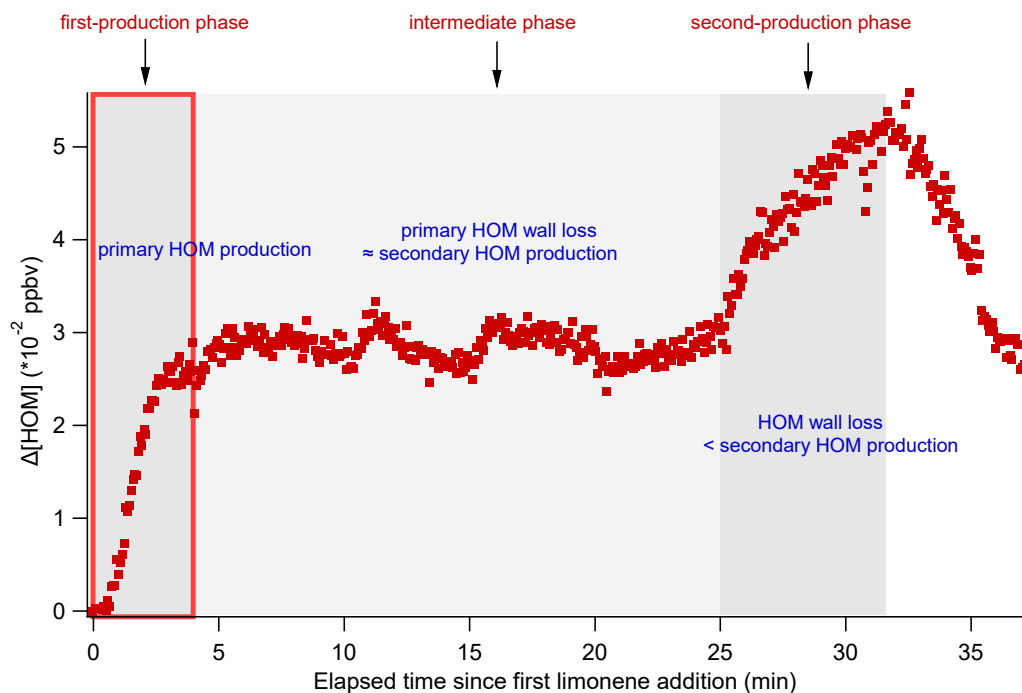


216

217 Figure S14. Time series of peak intensity of the $C_{20}H_{34}N_4O_x$ family during the whole experimental
 218 period. The vertical black, red and blue lines represent the time of limonene, NO_2 and O_3 additions,
 219 respectively.

220

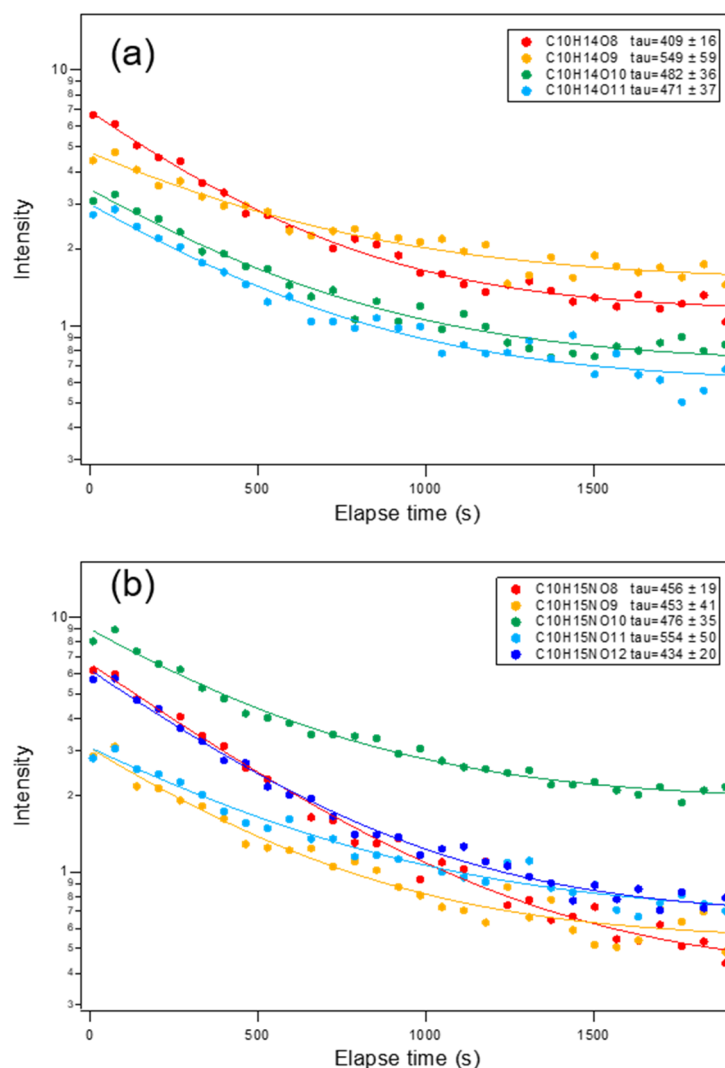
221



222

223 Figure S15. HOM concentration over time in the first limonene addition period- (P1). The HOM
 224 concentration underwent a period of rapid increase (first-production phase), followed by an
 225 intermediate phase where it remained constant and a second phase of increase afterwards (second-
 226 production phase). In the first-production phase, primary HOM production contributed most to the
 227 HOM increase, while in the intermediate phase and the second-production phase, wall loss and
 228 secondary HOM production increased in importance.

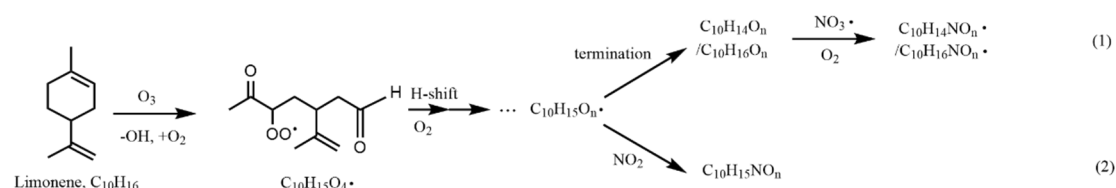
229



230
231
232
233
234
235

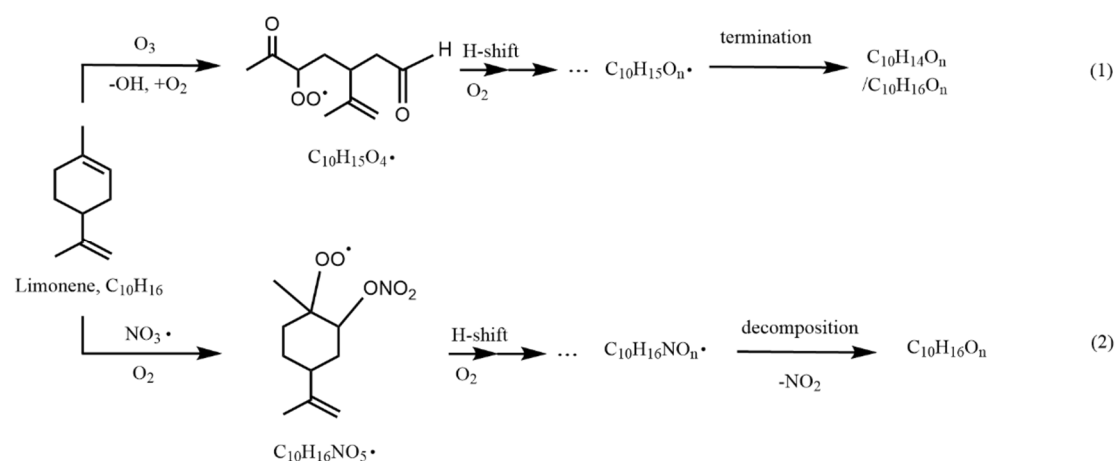
Figure S16. Decay of HOM C₁₀H₁₄O₈₋₁₁ (a) and C₁₀H₁₅NO₉₋₁₂ (b) due to wall loss during active mixing in SAPHIR chamber. The lifetimes (tau) of wall loss of each species are listed in the legend (s).

236 **Reaction schemes S1 to S3**



238 Scheme S1. The possible formation pathways towards the production of 1N-C₁₀ HOM RO₂ radicals
239 (C₁₀H₁₆NO_x•) and stable products C₁₀H₁₅NO_x initiated by O₃ oxidation of limonene (Mentel et al.,
240 2015).

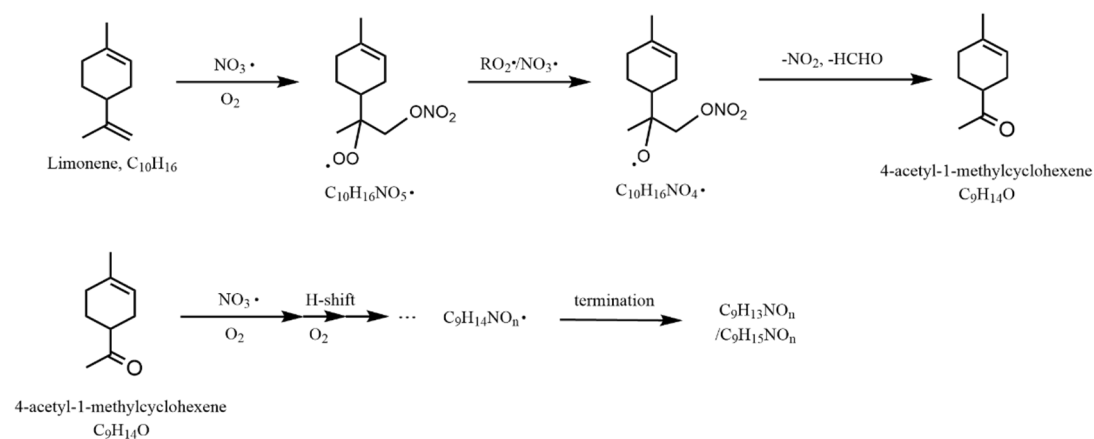
241



242

243 Scheme S2. Possible formation pathways of C₁₀ monomers without nitrogen atoms.

244



245

246 Scheme S3. Example scheme for C₉H₁₃NO_x and C₉H₁₅NO_x formation from limonene; the depicted
247 reactions may not be the dominant pathways.

248

249

251 Table S1. Peak list from limonene + NO₃ experiment.

m/z	Detected ion formula	Parent molecule formula
268.0077	C ₆ H ₇ NO ₇ [¹⁵ N]O ₃ ⁻	C ₆ H ₇ NO ₇
284.0026	C ₆ H ₇ NO ₈ [¹⁵ N]O ₃ ⁻	C ₆ H ₇ NO ₈
284.9866	C ₆ H ₆ O ₉ [¹⁵ N]O ₃ ⁻	C ₆ H ₆ O ₉
302.0131	C ₆ H ₉ NO ₉ [¹⁵ N]O ₃ ⁻	C ₆ H ₉ NO ₉
312.9927	C ₆ H ₆ N ₂ O ₉ [¹⁵ N]O ₃ ⁻	C ₆ H ₆ N ₂ O ₉
333.0189	C ₆ H ₁₀ N ₂ O ₁₀ [¹⁵ N]O ₃ ⁻	C ₆ H ₁₀ N ₂ O ₁₀
280.0077	C ₇ H ₇ NO ₇ [¹⁵ N]O ₃ ⁻	C ₇ H ₇ NO ₇
282.0233	C ₇ H ₉ NO ₇ [¹⁵ N]O ₃ ⁻	C ₇ H ₉ NO ₇
283.0073	C ₇ H ₈ O ₈ [¹⁵ N]O ₃ ⁻	C ₇ H ₈ O ₈
284.0390	C ₇ H ₁₁ NO ₇ [¹⁵ N]O ₃ ⁻	C ₇ H ₁₁ NO ₇
297.0104	C ₇ H ₈ NO ₈ [¹⁵ N]O ₃ ⁻	C ₇ H ₈ NO ₈
311.0135	C ₇ H ₈ N ₂ O ₈ [¹⁵ N]O ₃ ⁻	C ₇ H ₈ N ₂ O ₈
314.0131	C ₇ H ₉ NO ₉ [¹⁵ N]O ₃ ⁻	C ₇ H ₉ NO ₉
315.0210	C ₇ H ₁₀ NO ₉ [¹⁵ N]O ₃ ⁻	C ₇ H ₁₀ NO ₉
316.0288	C ₇ H ₁₁ NO ₉ [¹⁵ N]O ₃ ⁻	C ₇ H ₁₁ NO ₉
330.0080	C ₇ H ₉ NO ₁₀ [¹⁵ N]O ₃ ⁻	C ₇ H ₉ NO ₁₀
332.0237	C ₇ H ₁₁ NO ₁₀ [¹⁵ N]O ₃ ⁻	C ₇ H ₁₁ NO ₁₀
343.0033	C ₇ H ₈ N ₂ O ₁₀ [¹⁵ N]O ₃ ⁻	C ₇ H ₈ N ₂ O ₁₀
346.0030	C ₇ H ₉ NO ₁₁ [¹⁵ N]O ₃ ⁻	C ₇ H ₉ NO ₁₁
347.0108	C ₇ H ₁₀ NO ₁₁ [¹⁵ N]O ₃ ⁻	C ₇ H ₁₀ NO ₁₁
358.9982	C ₇ H ₈ N ₂ O ₁₁ [¹⁵ N]O ₃ ⁻	C ₇ H ₈ N ₂ O ₁₁
374.9931	C ₇ H ₈ N ₂ O ₁₂ [¹⁵ N]O ₃ ⁻	C ₇ H ₈ N ₂ O ₁₂
390.9880	C ₇ H ₈ N ₂ O ₁₃ [¹⁵ N]O ₃ ⁻	C ₇ H ₈ N ₂ O ₁₃
406.9830	C ₇ H ₈ N ₂ O ₁₄ [¹⁵ N]O ₃ ⁻	C ₇ H ₈ N ₂ O ₁₄
408.9986	C ₇ H ₁₀ N ₂ O ₁₄ [¹⁵ N]O ₃ ⁻	C ₇ H ₁₀ N ₂ O ₁₄
280.0440	C ₈ H ₁₁ NO ₆ [¹⁵ N]O ₃ ⁻	C ₈ H ₁₁ NO ₆
283.0437	C ₈ H ₁₂ O ₇ [¹⁵ N]O ₃ ⁻	C ₈ H ₁₂ O ₇
296.0390	C ₈ H ₁₁ NO ₇ [¹⁵ N]O ₃ ⁻	C ₈ H ₁₁ NO ₇
297.0468	C ₈ H ₁₂ NO ₇ [¹⁵ N]O ₃ ⁻	C ₈ H ₁₂ NO ₇
312.0339	C ₈ H ₁₁ NO ₈ [¹⁵ N]O ₃ ⁻	C ₈ H ₁₁ NO ₈
313.0417	C ₈ H ₁₂ NO ₈ [¹⁵ N]O ₃ ⁻	C ₈ H ₁₂ NO ₈
314.0495	C ₈ H ₁₃ NO ₈ [¹⁵ N]O ₃ ⁻	C ₈ H ₁₃ NO ₈
316.0652	C ₈ H ₁₅ NO ₈ [¹⁵ N]O ₃ ⁻	C ₈ H ₁₅ NO ₈
325.0291	C ₈ H ₁₀ N ₂ O ₈ [¹⁵ N]O ₃ ⁻	C ₈ H ₁₀ N ₂ O ₈
328.0288	C ₈ H ₁₁ NO ₉ [¹⁵ N]O ₃ ⁻	C ₈ H ₁₁ NO ₉
329.0366	C ₈ H ₁₂ NO ₉ [¹⁵ N]O ₃ ⁻	C ₈ H ₁₂ NO ₉
330.0444	C ₈ H ₁₃ NO ₉ [¹⁵ N]O ₃ ⁻	C ₈ H ₁₃ NO ₉
344.0237	C ₈ H ₁₁ NO ₁₀ [¹⁵ N]O ₃ ⁻	C ₈ H ₁₁ NO ₁₀
345.0315	C ₈ H ₁₂ NO ₁₀ [¹⁵ N]O ₃ ⁻	C ₈ H ₁₂ NO ₁₀
346.0393	C ₈ H ₁₃ NO ₁₀ [¹⁵ N]O ₃ ⁻	C ₈ H ₁₃ NO ₁₀
360.0186	C ₈ H ₁₁ NO ₁₁ [¹⁵ N]O ₃ ⁻	C ₈ H ₁₁ NO ₁₁

361.0264	$C_8H_{12}NO_{11}[^{15}N]O_3^-$	$C_8H_{12}NO_{11}$
376.0135	$C_8H_{11}NO_{12}[^{15}N]O_3^-$	$C_8H_{11}NO_{12}$
377.0214	$C_8H_{12}NO_{12}[^{15}N]O_3^-$	$C_8H_{12}NO_{12}$
392.0084	$C_8H_{11}NO_{13}[^{15}N]O_3^-$	$C_8H_{11}NO_{13}$
420.9986	$C_8H_{10}N_2O_{14}[^{15}N]O_3^-$	$C_8H_{10}N_2O_{14}$
297.0832	$C_9H_{16}NO_6[^{15}N]O_3^-$	$C_9H_{16}NO_6$
311.0624	$C_9H_{14}NO_7[^{15}N]O_3^-$	$C_9H_{14}NO_7$
312.0703	$C_9H_{15}NO_7[^{15}N]O_3^-$	$C_9H_{15}NO_7$
324.0577	$C_9H_{13}N_2O_7[^{15}N]O_3^-$	$C_9H_{13}N_2O_7$
326.0495	$C_9H_{13}NO_8[^{15}N]O_3^-$	$C_9H_{13}NO_8$
327.0573	$C_9H_{14}NO_8[^{15}N]O_3^-$	$C_9H_{14}NO_8$
328.0652	$C_9H_{15}NO_8[^{15}N]O_3^-$	$C_9H_{15}NO_8$
329.0730	$C_9H_{16}NO_8[^{15}N]O_3^-$	$C_9H_{16}NO_8$
342.0444	$C_9H_{13}NO_9[^{15}N]O_3^-$	$C_9H_{13}NO_9$
343.0523	$C_9H_{14}NO_9[^{15}N]O_3^-$	$C_9H_{14}NO_9$
344.0601	$C_9H_{15}NO_9[^{15}N]O_3^-$	$C_9H_{15}NO_9$
358.0393	$C_9H_{13}NO_{10}[^{15}N]O_3^-$	$C_9H_{13}NO_{10}$
359.0472	$C_9H_{14}NO_{10}[^{15}N]O_3^-$	$C_9H_{14}NO_{10}$
360.0550	$C_9H_{15}NO_{10}[^{15}N]O_3^-$	$C_9H_{15}NO_{10}$
370.0268	$C_9H_{11}N_2O_{10}[^{15}N]O_3^-$	$C_9H_{11}N_2O_{10}$
371.0346	$C_9H_{12}N_2O_{10}[^{15}N]O_3^-$	$C_9H_{12}N_2O_{10}$
374.0343	$C_9H_{13}NO_{11}[^{15}N]O_3^-$	$C_9H_{13}NO_{11}$
375.0421	$C_9H_{14}NO_{11}[^{15}N]O_3^-$	$C_9H_{14}NO_{11}$
376.0499	$C_9H_{15}NO_{11}[^{15}N]O_3^-$	$C_9H_{15}NO_{11}$
390.0292	$C_9H_{13}NO_{12}[^{15}N]O_3^-$	$C_9H_{13}NO_{12}$
391.0370	$C_9H_{14}NO_{12}[^{15}N]O_3^-$	$C_9H_{14}NO_{12}$
392.0448	$C_9H_{15}NO_{12}[^{15}N]O_3^-$	$C_9H_{15}NO_{12}$
403.0244	$C_9H_{12}N_2O_{12}[^{15}N]O_3^-$	$C_9H_{12}N_2O_{12}$
405.0401	$C_9H_{14}N_2O_{12}[^{15}N]O_3^-$	$C_9H_{14}N_2O_{12}$
406.0241	$C_9H_{13}NO_{13}[^{15}N]O_3^-$	$C_9H_{13}NO_{13}$
407.0319	$C_9H_{14}NO_{13}[^{15}N]O_3^-$	$C_9H_{14}NO_{13}$
408.0397	$C_9H_{15}NO_{13}[^{15}N]O_3^-$	$C_9H_{15}NO_{13}$
422.0190	$C_9H_{13}NO_{14}[^{15}N]O_3^-$	$C_9H_{13}NO_{14}$
423.0268	$C_9H_{14}NO_{14}[^{15}N]O_3^-$	$C_9H_{14}NO_{14}$
309.0594	$C_{10}H_{14}O_7[^{15}N]O_3^-$	$C_{10}H_{14}O_7$
309.0832	$C_{10}H_{16}NO_6[^{15}N]O_3^-$	$C_{10}H_{16}NO_6$
311.0750	$C_{10}H_{16}O_7[^{15}N]O_3^-$	$C_{10}H_{16}O_7$
324.0703	$C_{10}H_{15}NO_7[^{15}N]O_3^-$	$C_{10}H_{15}NO_7$
325.0543	$C_{10}H_{14}O_8[^{15}N]O_3^-$	$C_{10}H_{14}O_8$
325.0781	$C_{10}H_{16}NO_7[^{15}N]O_3^-$	$C_{10}H_{16}NO_7$
327.0699	$C_{10}H_{16}O_8[^{15}N]O_3^-$	$C_{10}H_{16}O_8$
340.0652	$C_{10}H_{15}NO_8[^{15}N]O_3^-$	$C_{10}H_{15}NO_8$
341.0492	$C_{10}H_{14}O_9[^{15}N]O_3^-$	$C_{10}H_{14}O_9$
341.0730	$C_{10}H_{16}NO_8[^{15}N]O_3^-$	$C_{10}H_{16}NO_8$
342.0570	$C_{10}H_{15}O_9[^{15}N]O_3^-$	$C_{10}H_{15}O_9$
343.0648	$C_{10}H_{16}O_9[^{15}N]O_3^-$	$C_{10}H_{16}O_9$

356.0601	$C_{10}H_{15}NO_9[^{15}N]O_3^-$	$C_{10}H_{15}NO_9$
357.0441	$C_{10}H_{14}O_{10}[^{15}N]O_3^-$	$C_{10}H_{14}O_{10}$
357.0679	$C_{10}H_{16}NO_9[^{15}N]O_3^-$	$C_{10}H_{16}NO_9$
358.0519	$C_{10}H_{15}O_{10}[^{15}N]O_3^-$	$C_{10}H_{15}O_{10}$
358.0757	$C_{10}H_{17}NO_9[^{15}N]O_3^-$	$C_{10}H_{17}NO_9$
359.0597	$C_{10}H_{16}O_{10}[^{15}N]O_3^-$	$C_{10}H_{16}O_{10}$
371.0710	$C_{10}H_{16}N_2O_9[^{15}N]O_3^-$	$C_{10}H_{16}N_2O_9$
372.0550	$C_{10}H_{15}NO_{10}[^{15}N]O_3^-$	$C_{10}H_{15}NO_{10}$
373.0390	$C_{10}H_{14}O_{11}[^{15}N]O_3^-$	$C_{10}H_{14}O_{11}$
373.0628	$C_{10}H_{16}NO_{10}[^{15}N]O_3^-$	$C_{10}H_{16}NO_{10}$
374.0468	$C_{10}H_{15}O_{11}[^{15}N]O_3^-$	$C_{10}H_{15}O_{11}$
374.0706	$C_{10}H_{17}NO_{10}[^{15}N]O_3^-$	$C_{10}H_{17}NO_{10}$
375.0547	$C_{10}H_{16}O_{11}[^{15}N]O_3^-$	$C_{10}H_{16}O_{11}$
385.0502	$C_{10}H_{14}N_2O_{10}[^{15}N]O_3^-$	$C_{10}H_{14}N_2O_{10}$
386.0581	$C_{10}H_{15}N_2O_{10}[^{15}N]O_3^-$	$C_{10}H_{15}N_2O_{10}$
387.0659	$C_{10}H_{16}N_2O_{10}[^{15}N]O_3^-$	$C_{10}H_{16}N_2O_{10}$
388.0499	$C_{10}H_{15}NO_{11}[^{15}N]O_3^-$	$C_{10}H_{15}NO_{11}$
389.0339	$C_{10}H_{14}O_{12}[^{15}N]O_3^-$	$C_{10}H_{14}O_{12}$
389.0577	$C_{10}H_{16}NO_{11}[^{15}N]O_3^-$	$C_{10}H_{16}NO_{11}$
390.0418	$C_{10}H_{15}O_{12}[^{15}N]O_3^-$	$C_{10}H_{15}O_{12}$
390.0656	$C_{10}H_{17}NO_{11}[^{15}N]O_3^-$	$C_{10}H_{17}NO_{11}$
391.0734	$C_{10}H_{18}NO_{11}[^{15}N]O_3^-$	$C_{10}H_{18}NO_{11}$
402.0530	$C_{10}H_{15}N_2O_{11}[^{15}N]O_3^-$	$C_{10}H_{15}N_2O_{11}$
403.0608	$C_{10}H_{16}N_2O_{11}[^{15}N]O_3^-$	$C_{10}H_{16}N_2O_{11}$
404.0448	$C_{10}H_{15}NO_{12}[^{15}N]O_3^-$	$C_{10}H_{15}NO_{12}$
405.0527	$C_{10}H_{16}NO_{12}[^{15}N]O_3^-$	$C_{10}H_{16}NO_{12}$
406.0605	$C_{10}H_{17}NO_{12}[^{15}N]O_3^-$	$C_{10}H_{17}NO_{12}$
417.0401	$C_{10}H_{14}N_2O_{12}[^{15}N]O_3^-$	$C_{10}H_{14}N_2O_{12}$
418.0479	$C_{10}H_{15}N_2O_{12}[^{15}N]O_3^-$	$C_{10}H_{15}N_2O_{12}$
420.0397	$C_{10}H_{15}NO_{13}[^{15}N]O_3^-$	$C_{10}H_{15}NO_{13}$
420.0636	$C_{10}H_{17}N_2O_{12}[^{15}N]O_3^-$	$C_{10}H_{17}N_2O_{12}$
422.0554	$C_{10}H_{17}NO_{13}[^{15}N]O_3^-$	$C_{10}H_{17}NO_{13}$
433.0350	$C_{10}H_{14}N_2O_{13}[^{15}N]O_3^-$	$C_{10}H_{14}N_2O_{13}$
434.0666	$C_{10}H_{17}N_3O_{12}[^{15}N]O_3^-$	$C_{10}H_{17}N_3O_{12}$
435.0506	$C_{10}H_{16}N_2O_{13}[^{15}N]O_3^-$	$C_{10}H_{16}N_2O_{13}$
437.0425	$C_{10}H_{16}NO_{14}[^{15}N]O_3^-$	$C_{10}H_{16}NO_{14}$
437.0663	$C_{10}H_{18}N_2O_{13}[^{15}N]O_3^-$	$C_{10}H_{18}N_2O_{13}$
438.0503	$C_{10}H_{17}NO_{14}[^{15}N]O_3^-$	$C_{10}H_{17}NO_{14}$
451.0456	$C_{10}H_{16}N_2O_{14}[^{15}N]O_3^-$	$C_{10}H_{16}N_2O_{14}$
453.0612	$C_{10}H_{18}N_2O_{14}[^{15}N]O_3^-$	$C_{10}H_{18}N_2O_{14}$
466.0565	$C_{10}H_{17}N_3O_{14}[^{15}N]O_3^-$	$C_{10}H_{17}N_3O_{14}$
467.0405	$C_{10}H_{16}N_2O_{15}[^{15}N]O_3^-$	$C_{10}H_{16}N_2O_{15}$
482.0514	$C_{10}H_{17}N_3O_{15}[^{15}N]O_3^-$	$C_{10}H_{17}N_3O_{15}$
498.0463	$C_{10}H_{17}N_3O_{16}[^{15}N]O_3^-$	$C_{10}H_{17}N_3O_{16}$
453.1618	$C_{17}H_{28}NO_9[^{15}N]O_3^-$	$C_{17}H_{28}NO_9$
467.1649	$C_{17}H_{28}N_2O_9[^{15}N]O_3^-$	$C_{17}H_{28}N_2O_9$

500.1387	$C_{17}H_{27}NO_{12}[^{15}N]O_3^-$	$C_{17}H_{27}NO_{12}$
513.1340	$C_{17}H_{26}N_2O_{12}[^{15}N]O_3^-$	$C_{17}H_{26}N_2O_{12}$
531.1445	$C_{17}H_{28}N_2O_{13}[^{15}N]O_3^-$	$C_{17}H_{28}N_2O_{13}$
545.1238	$C_{17}H_{26}N_2O_{14}[^{15}N]O_3^-$	$C_{17}H_{26}N_2O_{14}$
548.1235	$C_{17}H_{27}NO_{15}[^{15}N]O_3^-$	$C_{17}H_{27}NO_{15}$
449.1907	$C_{18}H_{30}N_2O_7[^{15}N]O_3^-$	$C_{18}H_{30}N_2O_7$
480.1489	$C_{18}H_{27}NO_{10}[^{15}N]O_3^-$	$C_{18}H_{27}NO_{10}$
511.1547	$C_{18}H_{28}N_2O_{11}[^{15}N]O_3^-$	$C_{18}H_{28}N_2O_{11}$
527.1496	$C_{18}H_{28}N_2O_{12}[^{15}N]O_3^-$	$C_{18}H_{28}N_2O_{12}$
529.1415	$C_{18}H_{28}NO_{13}[^{15}N]O_3^-$	$C_{18}H_{28}NO_{13}$
558.1554	$C_{18}H_{29}N_3O_{13}[^{15}N]O_3^-$	$C_{18}H_{29}N_3O_{13}$
562.1391	$C_{18}H_{29}NO_{15}[^{15}N]O_3^-$	$C_{18}H_{29}NO_{15}$
574.1504	$C_{18}H_{29}N_3O_{14}[^{15}N]O_3^-$	$C_{18}H_{29}N_3O_{14}$
494.1645	$C_{19}H_{29}NO_{10}[^{15}N]O_3^-$	$C_{19}H_{29}NO_{10}$
496.1802	$C_{19}H_{31}NO_{10}[^{15}N]O_3^-$	$C_{19}H_{31}NO_{10}$
509.1754	$C_{19}H_{30}N_2O_{10}[^{15}N]O_3^-$	$C_{19}H_{30}N_2O_{10}$
510.1595	$C_{19}H_{29}NO_{11}[^{15}N]O_3^-$	$C_{19}H_{29}NO_{11}$
512.1751	$C_{19}H_{31}NO_{11}[^{15}N]O_3^-$	$C_{19}H_{31}NO_{11}$
525.1704	$C_{19}H_{30}N_2O_{11}[^{15}N]O_3^-$	$C_{19}H_{30}N_2O_{11}$
526.1544	$C_{19}H_{29}NO_{12}[^{15}N]O_3^-$	$C_{19}H_{29}NO_{12}$
528.1700	$C_{19}H_{31}NO_{12}[^{15}N]O_3^-$	$C_{19}H_{31}NO_{12}$
541.1653	$C_{19}H_{30}N_2O_{12}[^{15}N]O_3^-$	$C_{19}H_{30}N_2O_{12}$
542.1493	$C_{19}H_{29}NO_{13}[^{15}N]O_3^-$	$C_{19}H_{29}NO_{13}$
544.1649	$C_{19}H_{31}NO_{13}[^{15}N]O_3^-$	$C_{19}H_{31}NO_{13}$
557.1602	$C_{19}H_{30}N_2O_{13}[^{15}N]O_3^-$	$C_{19}H_{30}N_2O_{13}$
560.1599	$C_{19}H_{31}NO_{14}[^{15}N]O_3^-$	$C_{19}H_{31}NO_{14}$
573.1551	$C_{19}H_{30}N_2O_{14}[^{15}N]O_3^-$	$C_{19}H_{30}N_2O_{14}$
575.1708	$C_{19}H_{32}N_2O_{14}[^{15}N]O_3^-$	$C_{19}H_{32}N_2O_{14}$
576.1548	$C_{19}H_{31}NO_{15}[^{15}N]O_3^-$	$C_{19}H_{31}NO_{15}$
577.1388	$C_{19}H_{30}O_{16}[^{15}N]O_3^-$	$C_{19}H_{30}O_{16}$
585.1663	$C_{19}H_{30}N_4O_{13}[^{15}N]O_3^-$	$C_{19}H_{30}N_4O_{13}$
589.1500	$C_{19}H_{30}N_2O_{15}[^{15}N]O_3^-$	$C_{19}H_{30}N_2O_{15}$
604.1609	$C_{19}H_{31}N_3O_{15}[^{15}N]O_3^-$	$C_{19}H_{31}N_3O_{15}$
605.1449	$C_{19}H_{30}N_2O_{16}[^{15}N]O_3^-$	$C_{19}H_{30}N_2O_{16}$
607.1368	$C_{19}H_{30}NO_{17}[^{15}N]O_3^-$	$C_{19}H_{30}NO_{17}$
617.1562	$C_{19}H_{30}N_4O_{15}[^{15}N]O_3^-$	$C_{19}H_{30}N_4O_{15}$
620.1558	$C_{19}H_{31}N_3O_{16}[^{15}N]O_3^-$	$C_{19}H_{31}N_3O_{16}$
621.1398	$C_{19}H_{30}N_2O_{17}[^{15}N]O_3^-$	$C_{19}H_{30}N_2O_{17}$
636.1507	$C_{19}H_{31}N_3O_{17}[^{15}N]O_3^-$	$C_{19}H_{31}N_3O_{17}$
637.1348	$C_{19}H_{30}N_2O_{18}[^{15}N]O_3^-$	$C_{19}H_{30}N_2O_{18}$
652.1457	$C_{19}H_{31}N_3O_{18}[^{15}N]O_3^-$	$C_{19}H_{31}N_3O_{18}$
664.1569	$C_{19}H_{31}N_5O_{17}[^{15}N]O_3^-$	$C_{19}H_{31}N_5O_{17}$
668.1406	$C_{19}H_{31}N_3O_{19}[^{15}N]O_3^-$	$C_{19}H_{31}N_3O_{19}$
680.1518	$C_{19}H_{31}N_5O_{18}[^{15}N]O_3^-$	$C_{19}H_{31}N_5O_{18}$
696.1467	$C_{19}H_{31}N_5O_{19}[^{15}N]O_3^-$	$C_{19}H_{31}N_5O_{19}$
507.1962	$C_{20}H_{32}N_2O_9[^{15}N]O_3^-$	$C_{20}H_{32}N_2O_9$

508.1802	$C_{20}H_{31}NO_{10}[^{15}N]O_3^-$	$C_{20}H_{31}NO_{10}$
523.1911	$C_{20}H_{32}N_2O_{10}[^{15}N]O_3^-$	$C_{20}H_{32}N_2O_{10}$
524.1751	$C_{20}H_{31}NO_{11}[^{15}N]O_3^-$	$C_{20}H_{31}NO_{11}$
539.1860	$C_{20}H_{32}N_2O_{11}[^{15}N]O_3^-$	$C_{20}H_{32}N_2O_{11}$
540.1700	$C_{20}H_{31}NO_{12}[^{15}N]O_3^-$	$C_{20}H_{31}NO_{12}$
542.1857	$C_{20}H_{33}NO_{12}[^{15}N]O_3^-$	$C_{20}H_{33}NO_{12}$
543.1697	$C_{20}H_{32}O_{13}[^{15}N]O_3^-$	$C_{20}H_{32}O_{13}$
553.1653	$C_{20}H_{30}N_2O_{12}[^{15}N]O_3^-$	$C_{20}H_{30}N_2O_{12}$
555.1809	$C_{20}H_{32}N_2O_{12}[^{15}N]O_3^-$	$C_{20}H_{32}N_2O_{12}$
556.1649	$C_{20}H_{31}NO_{13}[^{15}N]O_3^-$	$C_{20}H_{31}NO_{13}$
557.1490	$C_{20}H_{30}O_{14}[^{15}N]O_3^-$	$C_{20}H_{30}O_{14}$
559.1646	$C_{20}H_{32}O_{14}[^{15}N]O_3^-$	$C_{20}H_{32}O_{14}$
569.1602	$C_{20}H_{30}N_2O_{13}[^{15}N]O_3^-$	$C_{20}H_{30}N_2O_{13}$
570.1680	$C_{20}H_{31}N_2O_{13}[^{15}N]O_3^-$	$C_{20}H_{31}N_2O_{13}$
570.1918	$C_{20}H_{33}N_3O_{12}[^{15}N]O_3^-$	$C_{20}H_{33}N_3O_{12}$
571.1758	$C_{20}H_{32}N_2O_{13}[^{15}N]O_3^-$	$C_{20}H_{32}N_2O_{13}$
572.1599	$C_{20}H_{31}NO_{14}[^{15}N]O_3^-$	$C_{20}H_{31}NO_{14}$
575.1595	$C_{20}H_{32}O_{15}[^{15}N]O_3^-$	$C_{20}H_{32}O_{15}$
585.1551	$C_{20}H_{30}N_2O_{14}[^{15}N]O_3^-$	$C_{20}H_{30}N_2O_{14}$
586.1629	$C_{20}H_{31}N_2O_{14}[^{15}N]O_3^-$	$C_{20}H_{31}N_2O_{14}$
586.1867	$C_{20}H_{33}N_3O_{13}[^{15}N]O_3^-$	$C_{20}H_{33}N_3O_{13}$
587.1708	$C_{20}H_{32}N_2O_{14}[^{15}N]O_3^-$	$C_{20}H_{32}N_2O_{14}$
588.1548	$C_{20}H_{31}NO_{15}[^{15}N]O_3^-$	$C_{20}H_{31}NO_{15}$
590.1704	$C_{20}H_{33}NO_{15}[^{15}N]O_3^-$	$C_{20}H_{33}NO_{15}$
591.1544	$C_{20}H_{32}O_{16}[^{15}N]O_3^-$	$C_{20}H_{32}O_{16}$
600.1660	$C_{20}H_{31}N_3O_{14}[^{15}N]O_3^-$	$C_{20}H_{31}N_3O_{14}$
601.1500	$C_{20}H_{30}N_2O_{15}[^{15}N]O_3^-$	$C_{20}H_{30}N_2O_{15}$
602.1578	$C_{20}H_{31}N_2O_{15}[^{15}N]O_3^-$	$C_{20}H_{31}N_2O_{15}$
602.1817	$C_{20}H_{33}N_3O_{14}[^{15}N]O_3^-$	$C_{20}H_{33}N_3O_{14}$
603.1657	$C_{20}H_{32}N_2O_{15}[^{15}N]O_3^-$	$C_{20}H_{32}N_2O_{15}$
606.1653	$C_{20}H_{33}NO_{16}[^{15}N]O_3^-$	$C_{20}H_{33}NO_{16}$
616.1609	$C_{20}H_{31}N_3O_{15}[^{15}N]O_3^-$	$C_{20}H_{31}N_3O_{15}$
617.1449	$C_{20}H_{30}N_2O_{16}[^{15}N]O_3^-$	$C_{20}H_{30}N_2O_{16}$
618.1528	$C_{20}H_{31}N_2O_{16}[^{15}N]O_3^-$	$C_{20}H_{31}N_2O_{16}$
618.1766	$C_{20}H_{33}N_3O_{15}[^{15}N]O_3^-$	$C_{20}H_{33}N_3O_{15}$
619.1606	$C_{20}H_{32}N_2O_{16}[^{15}N]O_3^-$	$C_{20}H_{32}N_2O_{16}$
632.1558	$C_{20}H_{31}N_3O_{16}[^{15}N]O_3^-$	$C_{20}H_{31}N_3O_{16}$
633.1398	$C_{20}H_{30}N_2O_{17}[^{15}N]O_3^-$	$C_{20}H_{30}N_2O_{17}$
633.1637	$C_{20}H_{32}N_3O_{16}[^{15}N]O_3^-$	$C_{20}H_{32}N_3O_{16}$
633.1875	$C_{20}H_{34}N_4O_{15}[^{15}N]O_3^-$	$C_{20}H_{34}N_4O_{15}$
634.1715	$C_{20}H_{33}N_3O_{16}[^{15}N]O_3^-$	$C_{20}H_{33}N_3O_{16}$
635.1555	$C_{20}H_{32}N_2O_{17}[^{15}N]O_3^-$	$C_{20}H_{32}N_2O_{17}$
648.1507	$C_{20}H_{31}N_3O_{17}[^{15}N]O_3^-$	$C_{20}H_{31}N_3O_{17}$
649.1586	$C_{20}H_{32}N_3O_{17}[^{15}N]O_3^-$	$C_{20}H_{32}N_3O_{17}$
649.1824	$C_{20}H_{34}N_4O_{16}[^{15}N]O_3^-$	$C_{20}H_{34}N_4O_{16}$
650.1664	$C_{20}H_{33}N_3O_{17}[^{15}N]O_3^-$	$C_{20}H_{33}N_3O_{17}$

651.1504	$C_{20}H_{32}N_2O_{18}[^{15}N]O_3^-$	$C_{20}H_{32}N_2O_{18}$
664.1457	$C_{20}H_{31}N_3O_{18}[^{15}N]O_3^-$	$C_{20}H_{31}N_3O_{18}$
665.1535	$C_{20}H_{32}N_3O_{18}[^{15}N]O_3^-$	$C_{20}H_{32}N_3O_{18}$
665.1773	$C_{20}H_{34}N_4O_{17}[^{15}N]O_3^-$	$C_{20}H_{34}N_4O_{17}$
666.1613	$C_{20}H_{33}N_3O_{18}[^{15}N]O_3^-$	$C_{20}H_{33}N_3O_{18}$
667.1453	$C_{20}H_{32}N_2O_{19}[^{15}N]O_3^-$	$C_{20}H_{32}N_2O_{19}$
680.1406	$C_{20}H_{31}N_3O_{19}[^{15}N]O_3^-$	$C_{20}H_{31}N_3O_{19}$
681.1484	$C_{20}H_{32}N_3O_{19}[^{15}N]O_3^-$	$C_{20}H_{32}N_3O_{19}$
681.1722	$C_{20}H_{34}N_4O_{18}[^{15}N]O_3^-$	$C_{20}H_{34}N_4O_{18}$
682.1562	$C_{20}H_{33}N_3O_{19}[^{15}N]O_3^-$	$C_{20}H_{33}N_3O_{19}$
683.1402	$C_{20}H_{32}N_2O_{20}[^{15}N]O_3^-$	$C_{20}H_{32}N_2O_{20}$
696.1355	$C_{20}H_{31}N_3O_{20}[^{15}N]O_3^-$	$C_{20}H_{31}N_3O_{20}$
697.1671	$C_{20}H_{34}N_4O_{19}[^{15}N]O_3^-$	$C_{20}H_{34}N_4O_{19}$
698.1511	$C_{20}H_{33}N_3O_{20}[^{15}N]O_3^-$	$C_{20}H_{33}N_3O_{20}$
713.1620	$C_{20}H_{34}N_4O_{20}[^{15}N]O_3^-$	$C_{20}H_{34}N_4O_{20}$
784.2607	$C_{26}H_{47}N_3O_{20}[^{15}N]O_3^-$	$C_{26}H_{47}N_3O_{20}$
892.2414	$C_{26}H_{47}N_5O_{25}[^{15}N]O_3^-$	$C_{26}H_{47}N_5O_{25}$
771.2668	$C_{27}H_{44}N_6O_{16}[^{15}N]O_3^-$	$C_{27}H_{44}N_6O_{16}$
727.2545	$C_{28}H_{44}N_2O_{16}[^{15}N]O_3^-$	$C_{28}H_{44}N_2O_{16}$
744.2334	$C_{28}H_{43}NO_{18}[^{15}N]O_3^-$	$C_{28}H_{43}NO_{18}$
770.2715	$C_{28}H_{45}N_5O_{16}[^{15}N]O_3^-$	$C_{28}H_{45}N_5O_{16}$
786.2664	$C_{28}H_{45}N_5O_{17}[^{15}N]O_3^-$	$C_{28}H_{45}N_5O_{17}$
864.2254	$C_{28}H_{43}N_5O_{22}[^{15}N]O_3^-$	$C_{28}H_{43}N_5O_{22}$
803.2818	$C_{29}H_{48}N_4O_{18}[^{15}N]O_3^-$	$C_{29}H_{48}N_4O_{18}$
804.2658	$C_{29}H_{47}N_3O_{19}[^{15}N]O_3^-$	$C_{29}H_{47}N_3O_{19}$
817.2610	$C_{29}H_{46}N_4O_{19}[^{15}N]O_3^-$	$C_{29}H_{46}N_4O_{19}$
818.2450	$C_{29}H_{45}N_3O_{20}[^{15}N]O_3^-$	$C_{29}H_{45}N_3O_{20}$
833.2559	$C_{29}H_{46}N_4O_{20}[^{15}N]O_3^-$	$C_{29}H_{46}N_4O_{20}$
835.2240	$C_{29}H_{44}N_2O_{22}[^{15}N]O_3^-$	$C_{29}H_{44}N_2O_{22}$
836.2556	$C_{29}H_{47}N_3O_{21}[^{15}N]O_3^-$	$C_{29}H_{47}N_3O_{21}$
865.2458	$C_{29}H_{46}N_4O_{22}[^{15}N]O_3^-$	$C_{29}H_{46}N_4O_{22}$
881.2407	$C_{29}H_{46}N_4O_{23}[^{15}N]O_3^-$	$C_{29}H_{46}N_4O_{23}$
897.2356	$C_{29}H_{46}N_4O_{24}[^{15}N]O_3^-$	$C_{29}H_{46}N_4O_{24}$
772.2647	$C_{30}H_{47}NO_{18}[^{15}N]O_3^-$	$C_{30}H_{47}NO_{18}$
783.2919	$C_{30}H_{48}N_4O_{16}[^{15}N]O_3^-$	$C_{30}H_{48}N_4O_{16}$
787.2756	$C_{30}H_{48}N_2O_{18}[^{15}N]O_3^-$	$C_{30}H_{48}N_2O_{18}$
788.2596	$C_{30}H_{47}NO_{19}[^{15}N]O_3^-$	$C_{30}H_{47}NO_{19}$
799.2868	$C_{30}H_{48}N_4O_{17}[^{15}N]O_3^-$	$C_{30}H_{48}N_4O_{17}$
800.2709	$C_{30}H_{47}N_3O_{18}[^{15}N]O_3^-$	$C_{30}H_{47}N_3O_{18}$
802.2865	$C_{30}H_{49}N_3O_{18}[^{15}N]O_3^-$	$C_{30}H_{49}N_3O_{18}$
815.2818	$C_{30}H_{48}N_4O_{18}[^{15}N]O_3^-$	$C_{30}H_{48}N_4O_{18}$
816.2658	$C_{30}H_{47}N_3O_{19}[^{15}N]O_3^-$	$C_{30}H_{47}N_3O_{19}$
831.2767	$C_{30}H_{48}N_4O_{19}[^{15}N]O_3^-$	$C_{30}H_{48}N_4O_{19}$
834.2763	$C_{30}H_{49}N_3O_{20}[^{15}N]O_3^-$	$C_{30}H_{49}N_3O_{20}$
847.2716	$C_{30}H_{48}N_4O_{20}[^{15}N]O_3^-$	$C_{30}H_{48}N_4O_{20}$
848.2556	$C_{30}H_{47}N_3O_{21}[^{15}N]O_3^-$	$C_{30}H_{47}N_3O_{21}$

849.2396	$C_{30}H_{46}N_2O_{22}[^{15}N]O_3^-$	$C_{30}H_{46}N_2O_{22}$
862.2825	$C_{30}H_{49}N_5O_{20}[^{15}N]O_3^-$	$C_{30}H_{49}N_5O_{20}$
863.2665	$C_{30}H_{48}N_4O_{21}[^{15}N]O_3^-$	$C_{30}H_{48}N_4O_{21}$
866.2662	$C_{30}H_{49}N_3O_{22}[^{15}N]O_3^-$	$C_{30}H_{49}N_3O_{22}$
867.2502	$C_{30}H_{48}N_2O_{23}[^{15}N]O_3^-$	$C_{30}H_{48}N_2O_{23}$
879.2614	$C_{30}H_{48}N_4O_{22}[^{15}N]O_3^-$	$C_{30}H_{48}N_4O_{22}$
880.2454	$C_{30}H_{47}N_3O_{23}[^{15}N]O_3^-$	$C_{30}H_{47}N_3O_{23}$
895.2563	$C_{30}H_{48}N_4O_{23}[^{15}N]O_3^-$	$C_{30}H_{48}N_4O_{23}$
896.2404	$C_{30}H_{47}N_3O_{24}[^{15}N]O_3^-$	$C_{30}H_{47}N_3O_{24}$
911.2513	$C_{30}H_{48}N_4O_{24}[^{15}N]O_3^-$	$C_{30}H_{48}N_4O_{24}$
926.2621	$C_{30}H_{49}N_5O_{24}[^{15}N]O_3^-$	$C_{30}H_{49}N_5O_{24}$

252

253

254 Table S2. Observed C₉H₁₄NO_x• radicals (m) and their termination products, including carbonyl
 255 compounds (m-17), hydroxyl compounds (m-15), and hydroperoxy compounds (m+1). Their
 256 concentrations during P1a period are normalized to that of C₉H₁₅NO₈, which had the highest
 257 concentration among the [family-series](#) families of 1N-C₉ monomers. Their relative intensities during
 258 the P1a period are shown on the second line in each cell.

Peroxy radical m	Carbonyl m-17	Hydroxy m-15	Hydroperoxy m+1
C ₉ H ₁₄ NO ₇ • 18.8 %			C ₉ H ₁₅ NO ₇ 19.3 %
C ₉ H ₁₄ NO ₈ • 27.9 %		C ₉ H ₁₅ NO ₇ 19.3 %	C ₉ H ₁₅ NO ₈ 100.0 %
C ₉ H ₁₄ NO ₉ • 20.7 %	C ₉ H ₁₃ NO ₈ 98.6 %	C ₉ H ₁₅ NO ₈ 100.0 %	C ₉ H ₁₅ NO ₉ 66.2 %
C ₉ H ₁₄ NO ₁₀ • 46.2 %	C ₉ H ₁₃ NO ₉ 56.9 %	C ₉ H ₁₅ NO ₉ 66.2 %	C ₉ H ₁₅ NO ₁₀ 30.9 %
C ₉ H ₁₄ NO ₁₁ • 12.4 %	C ₉ H ₁₃ NO ₁₀ 38.3 %	C ₉ H ₁₅ NO ₁₀ 30.9 %	C ₉ H ₁₅ NO ₁₁ 3.6 %
C ₉ H ₁₄ NO ₁₂ • 12.2 %	C ₉ H ₁₃ NO ₁₁ 14.5 %	C ₉ H ₁₅ NO ₁₁ 3.6 %	C ₉ H ₁₅ NO ₁₂ 23.9 %
C ₉ H ₁₄ NO ₁₃ • 9.7 %	C ₉ H ₁₃ NO ₁₂ 13.9 %	C ₉ H ₁₅ NO ₁₂ 23.9 %	C ₉ H ₁₅ NO ₁₃ 10.4 %
C ₉ H ₁₄ NO ₁₄ • 20.1 %	C ₉ H ₁₃ NO ₁₃ 10.0 %	C ₉ H ₁₅ NO ₁₃ 10.4 %	
	C ₉ H ₁₃ NO ₁₄ 8.9 %		

259

260

261 Table S3. Reaction rate constants (code named in the MCM) of every individual RO₂• bimolecular
 262 reaction used for estimating RO₂• fate according to MCM.

RO ₂ • species	Rate constant with the reactant below (cm ³ -molecule ⁻¹ -s ⁻¹)				
	HO ₂ •	NO	NO ₃ •	RO ₂ •	NO ₂
C732CO3	KAPHO2	KAPNO	KRO2NO3*1.74	1.00E-11	KFPAN
C622CO3	KAPHO2	KAPNO	KRO2NO3*1.74	1.00E-11	KFPAN
MACRO2	KRO2HO2*0.625	KRO2NO	KRO2NO3	9.20E-14	
NC826O2	KRO2HO2*0.859	KRO2NO	KRO2NO3	9.20E-14	
MMALANHYO2	KRO2HO2*0.706	KRO2NO	KRO2NO3	9.20E-14	
NORLIMO2	KRO2HO2*0.890	KRO2NO	KRO2NO3	9.20E-14	
C312COCO3	KAPHO2	KAPNO	KRO2NO3*1.74	1.00E-11	KFPAN
NLMKAO2	KRO2HO2*0.914	KRO2NO*0.760	KRO2NO3	9.20E-14	
C629O2	KRO2HO2*0.770	KRO2NO	KRO2NO3	9.20E-14	
C624CO3	KAPHO2	KAPNO	KRO2NO3*1.74	1.00E-11	KFPAN
C622O2	KRO2HO2*0.770	KRO2NO	KRO2NO3	1.30E-12	
C537O2	KRO2HO2*0.706	KRO2NO	KRO2NO3	8.80E-13	
NLIMALO2	KRO2HO2*0.914	KRO2NO	KRO2NO3	9.20E-14	
C531O2	KRO2HO2*0.706	KRO2NO	KRO2NO3	2.00E-12	
LMKAO2	KRO2HO2*0.914	KRO2NO	KRO2NO3	9.20E-14	
C533O2	KRO2HO2*0.706	KRO2NO	KRO2NO3	8.80E-13	
C816O2	KRO2HO2*0.859	KRO2NO	KRO2NO3	2.50E-13	
C517CO3	KAPHO2	KAPNO	KRO2NO3*1.74	1.00E-11	KFPAN
C626O2	KRO2HO2*0.770	KRO2NO	KRO2NO3	1.30E-12	
C535O2	KRO2HO2*0.706	KRO2NO	KRO2NO3	9.20E-14	
C731CO3	KAPHO2	KAPNO	KRO2NO3*1.74	1.00E-11	KFPAN
C626CO3	KAPHO2	KAPNO	KRO2NO3*1.74	1.00E-11	KFPAN
HMVKBO2	KRO2HO2*0.625	KRO2NO	KRO2NO3	8.80E-13	
C31CO3	KAPHO2	KAPNO	KRO2NO3*1.6	1.00E-11	KFPAN
C3MCOBBCO3	KAPHO2	KAPNO	KRO2NO3*1.74	1.00E-11	KFPAN
IECCO3	KAPHO2	KAPNO	KRO2NO3*1.74	1.00E-11	KFPAN
C732O2	KRO2HO2*0.859	KRO2NO	KRO2NO3	1.30E-12	
INCO2	KRO2HO2*0.706	KRO2NO	KRO2NO3	2.90E-12	
HPC52CO3	KAPHO2	KAPNO	KRO2NO3*1.6	1.00E-11	KFPAN
INCNCO3	KAPHO2	KAPNO	KRO2NO3*1.74	1.00E-11	KFPAN
C519CO3	KAPHO2	KAPNO	KRO2NO3*1.74	1.00E-11	KFPAN
C823CO3	KAPHO2	KAPNO	KRO2NO3*1.74	1.00E-11	KFPAN
C735O2	KRO2HO2*0.820	KRO2NO	KRO2NO3	9.20E-14	
MMALNACO3	KAPHO2	KAPNO	KRO2NO3*1.74	1.00E-11	KFPAN
HCOCO3	KAPHO2	KAPNO	KRO2NO3*1.74	1.00E-11	KFPAN
HCOCH2O2	KRO2HO2*0.387	KRO2NO	KRO2NO3	2.00E-12	
C923CO3	KAPHO2	KAPNO	KRO2NO3*1.74	1.00E-11	KFPAN
CONM2CO3	KAPHO2	KAPNO	KRO2NO3*1.74	1.00E-11	KFPAN
C518CO3	KAPHO2	KAPNO	KRO2NO3*1.74	1.00E-11	KFPAN
C822CO3	KAPHO2	KAPNO	KRO2NO3*1.74	1.00E-11	KFPAN
HOCH2CO3	KAPHO2	KAPNO	KRO2NO3*1.74	1.00E-11	KFPAN
CHOC3COCO3	KAPHO2	KAPNO	KRO2NO3*1.74	1.00E-11	KFPAN

C926O2	KRO2HO2*0.890	KRO2NO	KRO2NO3	9.20E-14	
C511CO3	KAPHO2	KAPNO	KRO2NO3*1.74	1.00E-11	KFPAN
C924O2	KRO2HO2*0.890	KRO2NO	KRO2NO3	8.80E-13	
C47CO3	KAPHO2	KAPNO	KRO2NO3*1.6	1.00E-11	KFPAN
C520O2	KRO2HO2*0.706	KRO2NO	KRO2NO3	9.20E-14	
C733O2	KRO2HO2*0.859	KRO2NO	KRO2NO3	8.80E-12	
LMKBO2	KRO2HO2*0.914	KRO2NO	KRO2NO3	8.80E-13	
MEKAO2	KRO2HO2*0.625	KRO2NO	KRO2NO3	2.00E-12	
C731O2	KRO2HO2*0.859	KRO2NO	KRO2NO3	1.30E-12	
INDHPCO3	KAPHO2	KAPNO	KRO2NO3*1.74	1.00E-11	KFPAN
CO23C4CO3	KAPHO2	KAPNO	KRO2NO3*1.74	1.00E-11	KFPAN
C823O2	KRO2HO2*0.859	KRO2NO	KRO2NO3	1.30E-12	
C730O2	KRO2HO2*0.820	KRO2NO	KRO2NO3	9.20E-14	
C734O2	KRO2HO2*0.859	KRO2NO	KRO2NO3	8.80E-12	
C527O2	KRO2HO2*0.706	KRO2NO	KRO2NO3	8.80E-13	
CH3COCO3	KAPHO2	KAPNO	KRO2NO3*1.74	1.00E-11	KFPAN
C57O2	KRO2HO2*0.706	KRO2NO	KRO2NO3	9.20E-14	
C824O2	KRO2HO2*0.859	KRO2NO	KRO2NO3	8.80E-12	
NC623O2	KRO2HO2*0.770	KRO2NO	KRO2NO3	8.80E-13	
HOCH2CH2O2	1.53D- 13*EXP(1300/TEMP)	KRO2NO	KRO2NO3	2*(KCH3O2*7.8 D- 14*EXP(1000/T EMP))@0.5	
INDO2	KRO2HO2*0.706	KRO2NO	KRO2NO3	8.80E-13	
CH3CO3	KAPHO2	7.5D- 12*EXP(290/TEMP)	4.00E-12	1.00E-11	KFPAN
CH3COCH2O2	1.36D- 13*EXP(1250/TEMP)	KRO2NO	KRO2NO3	2*(K298CH3O2* 8.0D-12)@0.5	
MACROHO2	KRO2HO2*0.625	KRO2NO	KRO2NO3	1.40E-12	
COHM2CO3	KAPHO2	KAPNO	KRO2NO3*1.74	1.00E-11	KFPAN
C821O2	KRO2HO2*0.859	KRO2NO	KRO2NO3	8.80E-13	
C58NO3CO3	KAPHO2	KAPNO	KRO2NO3*1.74	1.00E-11	KFPAN
C57NO3CO3	KAPHO2	KAPNO	KRO2NO3*1.74	1.00E-11	KFPAN
ISOPCO2	KRO2HO2*0.706	KRO2NO	KRO2NO3	2.00E-12	
MACRNCO3	KAPHO2	KAPNO	KRO2NO3*1.74	1.00E-11	KFPAN
C925O2	KRO2HO2*0.890	KRO2NO	KRO2NO3	9.20E-14	
C923O2	KRO2HO2*0.890	KRO2NO	KRO2NO3	1.32E-12	
C817CO3	KAPHO2	KAPNO	KRO2NO3*1.74	1.00E-11	KFPAN
HC4CCO3	KAPHO2	KAPNO	KRO2NO3*1.74	1.00E-11	KFPAN
LIMAO2	KRO2HO2*0.914	KRO2NO	KRO2NO3	9.20E-14	
HC4ACO3	KAPHO2	KAPNO	KRO2NO3*1.74	1.00E-11	KFPAN
C816CO3	KAPHO2	KAPNO	KRO2NO3*1.74	1.00E-11	KFPAN

C822O2	KRO2HO2*0.859	KRO2NO	KRO2NO3	1.30E-12	
C820O2	KRO2HO2*0.859	KRO2NO	KRO2NO3	9.20E-14	
INBINBCO3	KAPHO2	KAPNO	KRO2NO3*1.74	1.00E-11	KFPAN
C826O2	KRO2HO2*0.859	KRO2NO	KRO2NO3	9.20E-14	
LIMALBO2	KRO2HO2*0.914	KRO2NO	KRO2NO3	8.80E-13	
C57AO2	KRO2HO2*0.706	KRO2NO	KRO2NO3	8.80E-13	
LIMCO2	KRO2HO2*0.914	KRO2NO	KRO2NO3	9.20E-14	
C817O2	KRO2HO2*0.859	KRO2NO	KRO2NO3	1.30E-12	
NLIMO2	KRO2HO2*0.914	KRO2NO	KRO2NO3	9.20E-14	
NC728O2	KRO2HO2*0.770	KRO2NO	KRO2NO3	9.20E-14	
CHOC3COO2	KRO2HO2*0.625	KRO2NO	KRO2NO3	2.00E-12	
NC730O2	KRO2HO2*0.820	KRO2NO	KRO2NO3	9.20E-14	
C728O2	KRO2HO2*0.770	KRO2NO	KRO2NO3	9.20E-14	
LIMALO2	KRO2HO2*0.914	KRO2NO	KRO2NO3	9.20E-14	
C4M2ALOH02	KRO2HO2*0.706	KRO2NO	KRO2NO3	9.20E-14	
MACRNBCO3	KAPHO2	KAPNO	KRO2NO3*1.74	1.00E-11	KFPAN
HCOCH2CO3	KAPHO2	KAPNO	KRO2NO3*1.74	1.00E-11	KFPAN
C727O2	KRO2HO2*0.820	KRO2NO	KRO2NO3	8.80E-13	
C58O2	KRO2HO2*0.706	KRO2NO	KRO2NO3	9.20E-14	
C729CO3	KAPHO2	KAPNO	KRO2NO3*1.74	1.00E-11	KFPAN
MC3CODBCO3	KAPHO2	KAPNO	KRO2NO3*1.74	1.00E-11	KFPAN
HPC52O2	KRO2HO2*0.706	KRO2NO	KRO2NO3	9.20E-14	
HMVKBCO3	KAPHO2	KAPNO	KRO2NO3*1.74	1.00E-11	KFPAN
ISOPDO2	KRO2HO2*0.706	KRO2NO	KRO2NO3	2.90E-12	
C624O2	KRO2HO2*0.770	KRO2NO	KRO2NO3	2.50E-13	
C727CO3	KAPHO2	KAPNO	KRO2NO3*1.74	1.00E-11	KFPAN
INDHCO3	KAPHO2	KAPNO	KRO2NO3*1.74	1.00E-11	KFPAN
BIACETO2	KRO2HO2*0.625	KRO2NO	KRO2NO3	2.00E-12	
CISOPCO2	KRO2HO2*0.706	KRO2NO	KRO2NO3	2.00E-12	
LMLKAO2	KRO2HO2*0.914	KRO2NO	KRO2NO3	8.80E-13	
CO2H3CO3	KAPHO2	KAPNO	KRO2NO3*1.74	1.00E-11	KFPAN
LIMBO2	KRO2HO2*0.914	KRO2NO	KRO2NO3	8.80E-13	
CH3O2	3.8D- 13*EXP(780/TEMP)* (1-1/(1+498*EXP(- 1160/TEMP)))	2.3D- 12*EXP(360/TE MP)	1.2E-12	2*KCH3O2*RO 2*7.18*EXP(- 885/TEMP) 2*KCH3O2*RO 2*(1-7.18*EXP(- 885/TEMP))	KMT13
LIMALAO2	KRO2HO2*0.914	KRO2NO	KRO2NO3	8.80E-13	
C825O2	KRO2HO2*0.859	KRO2NO	KRO2NO3	8.80E-12	
CO2N3CO3	KAPHO2	KAPNO	KRO2NO3*1.74	1.00E-11	KFPAN
MACO3	KAPHO2	8.70D- 12*EXP(290/TE MP)	KRO2NO3*1.74	1.00E-11	KFPAN
INBINACO3	KAPHO2	KAPNO	KRO2NO3*1.74	1.00E-11	KFPAN

C58AO2	KRO2HO2*0.706	KRO2NO	KRO2NO3	8.80E-13	
C59O2	KRO2HO2*0.706	KRO2NO	KRO2NO3	9.20E-14	
CHOMOHCO3	KAPHO2	KAPNO	KRO2NO3*1.74	1.00E-11	KFPAN
C729O2	KRO2HO2*0.820	KRO2NO	KRO2NO3	1.30E-12	
CO25C6CO3	KAPHO2	KAPNO	KRO2NO3*1.74	1.00E-11	KFPAN
CO2C3CO3	KAPHO2	KAPNO	KRO2NO3*1.74	1.00E-11	KFPAN
HO1CO3C4O2	KRO2HO2*0.625	KRO2NO	KRO2NO3	2.00E-12	
MMALNBCO3	KAPHO2	KAPNO	KRO2NO3*1.74	1.00E-11	KFPAN
CHOCOCH2O2	KRO2HO2*0.520	KRO2NO	KRO2NO3	2.00E-12	
HOC2H4CO3	KAPHO2	KAPNO	KRO2NO3*1.74	1.00E-11	KFPAN
C628O2	KRO2HO2*0.770	KRO2NO	KRO2NO3	9.20E-14	
C623O2	KRO2HO2*0.770	KRO2NO	KRO2NO3	8.00E-13	
C625O2	KRO2HO2*0.770	KRO2NO	KRO2NO3	9.20E-14	
LMLKBO2	KRO2HO2*0.914	KRO2NO	KRO2NO3	8.80E-13	
C627O2	KRO2HO2*0.770	KRO2NO	KRO2NO3	2.50E-12	
C517O2	KRO2HO2*0.706	KRO2NO	KRO2NO3	1.30E-12	
C3MDIALO2	KRO2HO2*0.625	KRO2NO	KRO2NO3	9.20E-14	
C819O2	KRO2HO2	KRO2NO	KRO2NO3	9.20E-14	
CO2C4CO3	KAPHO2	KAPNO	KRO2NO3*1.74	1.00E-11	KFPAN
C534O2	KRO2HO2*0.706	KRO2NO	KRO2NO3	9.20E-14	
C818O2	KRO2HO2*0.859	KRO2NO	KRO2NO3	1.30E-12	
C511O2	KRO2HO2*0.706	KRO2NO	KRO2NO3	8.80E-13	
C519O2	KRO2HO2*0.706	KRO2NO	KRO2NO3	8.80E-13	

264 **References**

- 265 Ehn, M., Thornton, J. A., Kleist, E., Sipilä, M., Junninen, H., Pullinen, I., Springer, M., Rubach, F.,
266 Tillmann, R., Lee, B., Lopez-Hilfiker, F., Andres, S., Acir, I. H., Rissanen, M., Jokinen, T.,
267 Schobesberger, S., Kangasluoma, J., Kontkanen, J., Nieminen, T., Kurtén, T., Nielsen, L. B.,
268 Jørgensen, S., Kjaergaard, H. G., Canagaratna, M., Dal Maso, M., Berndt, T., Petäjä, T., Wahner,
269 A., Kerminen, V. M., Kulmala, M., Worsnop, D. R., Wildt, J., and Mentel, T. F.: A large source
270 of low-volatility secondary organic aerosol, *Nature*, 506, 476-485, 10.1038/nature13032, 2014.
- 271 Fuchs, H., Dorn, H. P., Bachner, M., Bohn, B., Brauers, T., Gomm, S., Hofzumahaus, A., Holland, F.,
272 Nehr, S., Rohrer, F., Tillmann, R., and Wahner, A.: Comparison of OH concentration
273 measurements by DOAS and LIF during SAPHIR chamber experiments at high OH reactivity
274 and low NO concentration, *Atmos. Meas. Tech.*, 5, 1611-1626, 10.5194/amt-5-1611-2012, 2012.
- 275 Fuchs, H., Hofzumahaus, A., Rohrer, F., Bohn, B., Brauers, T., Dorn, H. P., Häseler, R., Holland, F.,
276 Kaminski, M., Li, X., Lu, K., Nehr, S., Tillmann, R., Wegener, R., and Wahner, A.: Experimental
277 evidence for efficient hydroxyl radical regeneration in isoprene oxidation, *Nat. Geosci.*, 6, 1023-
278 1026, 10.1038/ngeo1964, 2013.
- 279 Krechmer, J. E., Pagonis, D., Ziemann, P. J., and Jimenez, J. L.: Quantification of Gas-Wall Partitioning
280 in Teflon Environmental Chambers Using Rapid Bursts of Low-Volatility Oxidized Species
281 Generated in Situ, *Environ. Sci. Technol.*, 50, 5757-5765, 10.1021/acs.est.6b00606, 2016.
- 282 Lehtinen, K. E. J. and Kulmala, M.: A model for particle formation and growth in the atmosphere with
283 molecular resolution in size, *Atmos. Chem. Phys.*, 3, 251-257, 10.5194/acp-3-251-2003, 2003.
- 284 Peräkylä, O., Riva, M., Heikkinen, L., Quéléver, L., Roldin, P., and Ehn, M.: Experimental investigation
285 into the volatilities of highly oxygenated organic molecules (HOMs), *Atmos. Chem. Phys.*, 20,
286 649-669, 10.5194/acp-20-649-2020, 2020.
- 287 Pullinen, I., Schmitt, S., Kang, S., Sarrafzadeh, M., Schlag, P., Andres, S., Kleist, E., Mentel, T. F., Rohrer,
288 F., Springer, M., Tillmann, R., Wildt, J., Wu, C., Zhao, D., Wahner, A., and Kiendler-Scharr, A.:
289 Impact of NO_x on secondary organic aerosol (SOA) formation from α -pinene and β -pinene
290 photooxidation: the role of highly oxygenated organic nitrates, *Atmos. Chem. Phys.*, 20, 10125-
291 10147, 10.5194/acp-20-10125-2020, 2020.
- 292 Seinfeld, J. H. and Pandis, S. N.: *Atmospheric Chemistry and Physics: From Air Pollution to Climate*
293 *Change*, 2nd ed, Wiley, John & Sons, New York, 2006.
- 294 Wang, S. and Pratt, K. A.: Molecular Halogens Above the Arctic Snowpack: Emissions, Diurnal
295 Variations, and Recycling Mechanisms, *J. Geophys. Res.-Atmos.*, 122, 11991-12007,
296 10.1002/2017jd027175, 2017.
- 297 Zhao, D., Pullinen, I., Fuchs, H., Schrade, S., Wu, R., Acir, I.-H., Tillmann, R., Rohrer, F., Wildt, J., Guo,
298 Y., Kiendler-Scharr, A., Wahner, A., Kang, S., Vereecken, L., and Mentel, T. F.: Highly
299 oxygenated organic molecule (HOM) formation in the isoprene oxidation by NO₃ radical,
300 *Atmos. Chem. Phys.*, 21, 9681-9704, 10.5194/acp-21-9681-2021, 2021.
- 301 Zhao, D., Schmitt, S. H., Wang, M., Acir, I.-H., Tillmann, R., Tan, Z., Novelli, A., Fuchs, H., Pullinen,
302 I., Wegener, R., Rohrer, F., Wildt, J., Kiendler-Scharr, A., Wahner, A., and Mentel, T. F.: Effects
303 of NO_x and SO₂ on the secondary organic aerosol formation from photooxidation of α -pinene
304 and limonene, *Atmos. Chem. Phys.*, 18, 1611-1628, 10.5194/acp-18-1611-2018, 2018.
- 305